# Characterization of the Neuroprotective Function of the TGF-ß Signaling Pathway in the Retina


DISSERTATION

zur Erlangung des Doktorgrades der Humanmedizin (Dr. med.)

der Naturwissenschaftlichen Fakultät III für

Biologie und Vorklinische Medizin der

Universität Regensburg

vorgelegt von

Stefaniya Konstantinova Boneva

aus Pazardzhik, Bulgarien

Regensburg, 2016

# Characterization of the Neuroprotective Function of the TGF-ß Signaling Pathway in the Retina


DISSERTATION

zur Erlangung des Doktorgrades der Humanmedizin (Dr. med.)

der Naturwissenschaftlichen Fakultät III für

Biologie und Vorklinische Medizin der

Universität Regensburg

vorgelegt von

Stefaniya Konstantinova Boneva

aus Pazardzhik, Bulgarien

Regensburg, 2016

Das Promotionsgesuch wurde eingereicht am:
9. November 2016

Diese Arbeit wurde angeleitet und betreut von
PD Dr. rer. nat., Dr. med. Barbara Braunger am
Lehrstuhl für Humananatomie und Embryologie der Universität Regensburg

Prüfungsausschuss:

Erstgutachter: PD Dr. rer. nat., Dr. med. Barbara Braunger
Zweitgutachter: Prof. Dr. med. Frank Schweda

Unterschrift: ……

# Table of Contents

# 1. Introduction

## 1.1 Aspects of the anatomy of the eye

The mammalian eye is constituted of the eye globe (Bulbus oculi) and various supportive and protective appendages (Welsch and Deller, 2010). The globe of the eye (Bulbus oculi) is composed of light-sensitive and light-refractive components. The cornea, the lens and the vitreous humor are counted among the light-refractive tissue elements, while the light-sensitive part of the eyeball is represented by the retina (Trepel, 2012). The eyeball is enclosing a cavity, filled with a transparent, gelatinous substance, named vitreous humor (Corpus vitreum). The eye globe itself represents a tissue coat of three layers (Figure 1): the external (Tunica fibrosa bulbi), the middle (Tunica vasculosa bulbi) and the inner (Tunica interna bulbi) layer (Welsch and Deller, 2010).

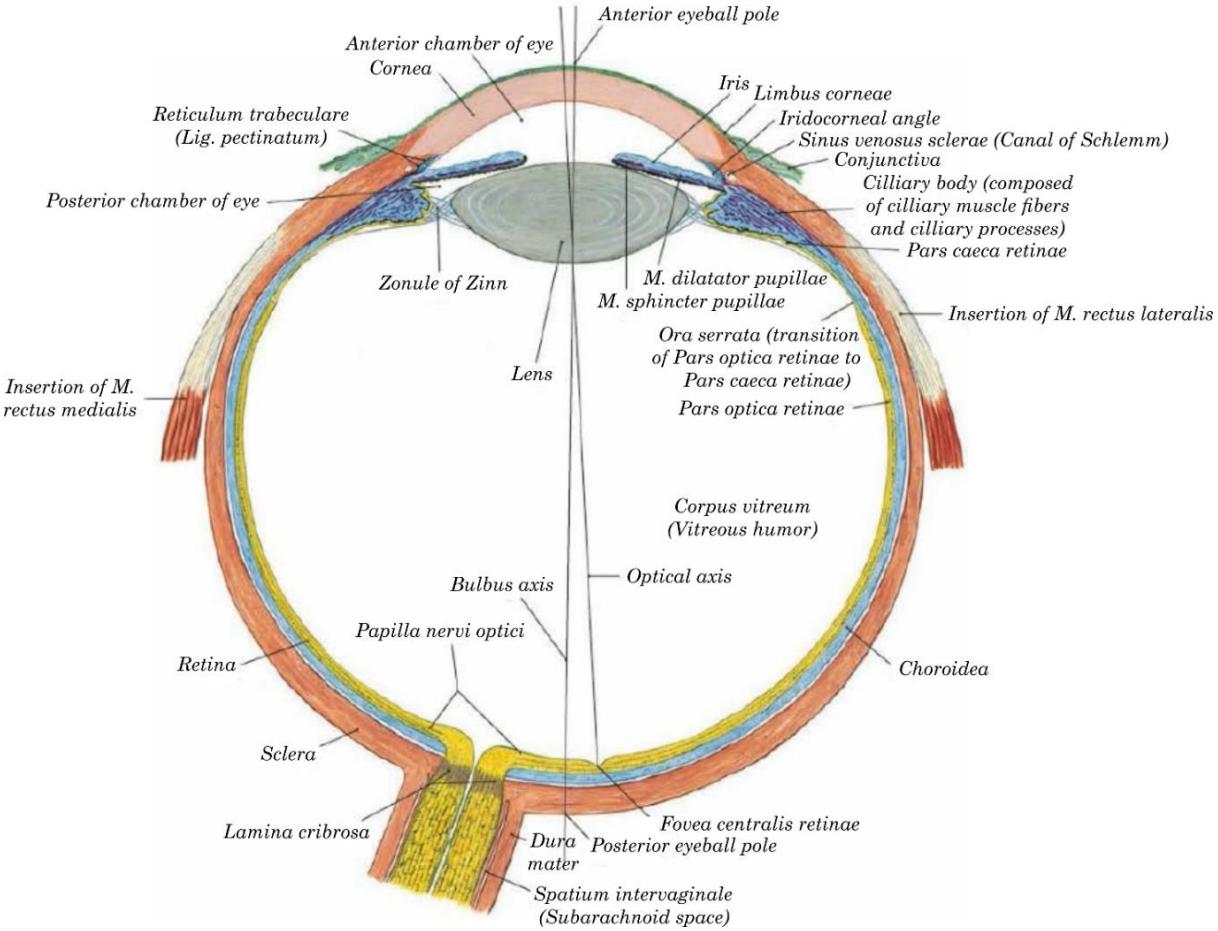


*Figure 1:* Horizontal section across the bulbus oculi
Modified after (Sobotta, 2013; Trepel, 2012)

Since the emphasis of this work is put on the elucidation of the TGF-ß signaling pathway in the retina, we focus on the innermost layer of the eyeball tunic in the following.

### 1.1.1 Internal layer of the eye tunic: the retina and the retinal pigment epithelium

#### 1.1.1.1 The retina

The retina, as the light-sensitive medium of the eye, is responsible for the conversion of the physical light impulse into a neuronal stimulus over a series of photochemical processes (Trepel, 2012). Within the inner layer of the eye tunic there are two distinguishable regions, which merge into each other at the Ora serrata (OS). The Pars optica consists of an outer Stratum pigmentosum and an internal Stratum nervosum. The anterior Pars caeca comprises a layer without photosensory cells ("caecus": Latin for "blind"), adjacent to the ciliary body (Pars ciliaris retinae) and the iris backplane (Pars iridica) (Figure 1) (Trepel, 2012). Although both Stratum nervosum and Stratum pigmentosum arise from the optic vesicle, these two tissue layers are quite different: the multilayered neural retina contains millions of neurons, interconnected through synapses, whereas the pigmented epithelium comprises just a single layer of non-neuronal, cuboidal cells, containing pigment-bearing melanin granules (Reh, 2012). Strata pigmentosum and nervosum exhibit an epithelium-like layered architecture, comprised of several distinct layers (Welsch and Deller, 2010). The "outermost" layer encompasses the outer and inner segments of the primary light-sensitive neurons: the rods, providing black-and-white vision, and the cones, capable of perceiving color vision. Their respective cell bodies are located in the outer nuclear layer (ONL) (Figure 2). Beneath them (in the direction towards the vitreous humor) follows the outer plexiform layer (OPL), that constitutes synapses between the neurons of the ONL and the neurons of the inner nuclear layer (INL). Within the INL are situated the cell bodies of the bipolar, amacrine and horizontal neurons. The inner plexiform layer (IPL) consists of synapses between the neurons of the INL and the retinal ganglion cells (RGCs). The adjacent layer is the retinal ganglion cell layer (GCL), the axons of which constitute the nerve fiber layer and project to neurons beyond the retina, within higher visual centers of the brain (Figure 2) (Trepel, 2012). The information streams, in its simplest and most direct flow, from the sensory cells, over the bipolar cells, to the cells in the GCL, which bundle their axons to form the optic nerve. Thus, rods and cones, bipolar cells and RGC represent the first three neurons of the visual pathway, connected in a fluent network by their processes (Welsch and Deller, 2010). The other retinal neurons, the horizontal and

amacrine cells, play an important role for contrast enhancement and motion detection (Trepel, 2012). The Müller glia cells contribute to the formation of the outer (OLM) and inner limiting membranes (ILM) (Magalhães and Coimbra, 1972). The outer limiting membrane is situated between the inner segments of the photoreceptors and the ONL, while the inner limiting membrane is located on top of the nerve fiber layer, next to the vitreous body (Figure 2).


*Figure 2:* Microscopic anatomy of the retina
The retina, in its light-sensitive area – the Pars optica, shows a complex layered architecture, resembling the functional arrangement in a fluent network of neurons, interconnected through synapses. Picture taken from (Welsch, 2005).

#### 1.1.1.1.1 Retinal ganglion cells (RGCs)

The ganglion cells constitute in their entirety the innermost retinal neuronal layer. These are typical multipolar nerve cells, containing large euchromatic nuclei and basophilic Nissl bodies within an organelle-rich cytoplasm (Mescher, Anthony L., Junqueira, Luiz Carlos Uchôa, 2010; Welsch and Deller, 2010). Both bipolar and amacrine cells release neurotransmitters at respective synaptic endings to the ganglion cells. The RGCs project their axons to the nerve fiber layer and finally form the optic nerve head in the central retina (Mescher, 2010). A subset of atypical ganglion cells is photoreceptive itself. They express the photopigment melanopsin that is involved in relaying the changes in light quantity and quality via respective axons of the retinohypothalamic tract to the suprachiasmatic nuclei of the hypothalamus. Thus, RGCs contribute to the control of the physiological circadian rhythms, pupillary light reflex and sleep (Schmidt et al., 2011).

#### 1.1.1.1.2 The inner nuclear layer (INL)

The perikarya of the bipolar cells are the main constituents of the inner nuclear layer (INL), besides the cell bodies of Müller glial cells, horizontal and amacrine cells. Bipolars extend their processes into the inner (IPL) and outer plexiform layers (OPL) and thus act as interneurons, transmitting photoreceptor signals to the RGCs (Welsch and Deller, 2010). Two types of bipolar cells may be distinguished by means of functional characteristics and due to the expression of two types of glutamate receptors: on- and off-bipolars. Upon light-mediated hyperpolarization of a photoreceptor, a respective on-bipolar cell would react with depolarization, since its metabotropic glutamate receptors (mGluR6) are stimulated. In response to photoreceptor hyperpolarization, the glutamate release at the ionotropic receptors (AMPA and kainate cation channels) of the off-bipolar cells is reduced, leading to a negative shifting of their membrane potential, i.e. hyperpolarization (Masland, 2012). Eventually, the information is relayed to the output neurons, the RGCs. This distinctly complex connectivity system within the retina is a major component of the visual perception.

Horizontal cells and amacrine cells also have their nuclei in the INL, while their processes spread horizontally in the plexiform layers and thus integrate and fine-tune photoreceptor signals over a wide area of the retina (Mescher, 2010).

The ramified Müller cells constitute the major supportive glial cells of the retina. Their nuclei lie in the INL, while their processes span the entire thickness of the retina (García and Vecino, 2003). Müller cells are the only non-neuronal cells that originate from retinal progenitor cells (Turner and Cepko, 1987), ensheathing all retinal neurons in the vertebrate retina (Bringmann et al., 2006). This tight developmental and morphological relationship is reflected by the multiple functions of the Müller cells, encompassing maintenance of retinal homeostasis and trophic support for the neurons via release of neuroprotective factors (Bringmann et al., 2006). However, aberrant function of the glia appears to contribute to certain pathological conditions, such as retinal degeneration (Jadhav et al., 2009). Their progress may be accelerated by reactive Müller cell gliosis, which involves the dysregulation of various neuron-supportive functions. Thus, impairments of any kind on this level must aggravate a present dysfunction of neurons by increasing their susceptibility to stressful stimuli in the diseased retina (Bringmann et al., 2006).

#### 1.1.1.1.3 The light-sensitive neurons of the outer nuclear layer (ONL)

The outer nuclear layer (ONL) represents the outermost layer of perikarya within the Stratum nervosum (Figure 3). Hence, incoming light has to penetrate all the layers in the front to reach the photoreceptors. These cells act as neurons, perceiving light sensory stimuli (= photoreceptors), i.e. as primary sensory cells (Trepel, 2012). Within the mammalian retina the outputs of the two distinct photoreceptor types, the rods and cones, constitute the first stage of visual images processing, hence the first neuron of the visual pathway. Thereby, the very light-sensitive rods account for vision in dim light and do not discern color, while cones contribute to color vision in the conditions of day-light (Masland, 2012). The respective axon-like extensions, terminating in distended synaptic bulbs, are situated within the outer plexiform layer (OPL) (Figure 3), where signal transmission to second-order neurons takes place (Young, 1967).

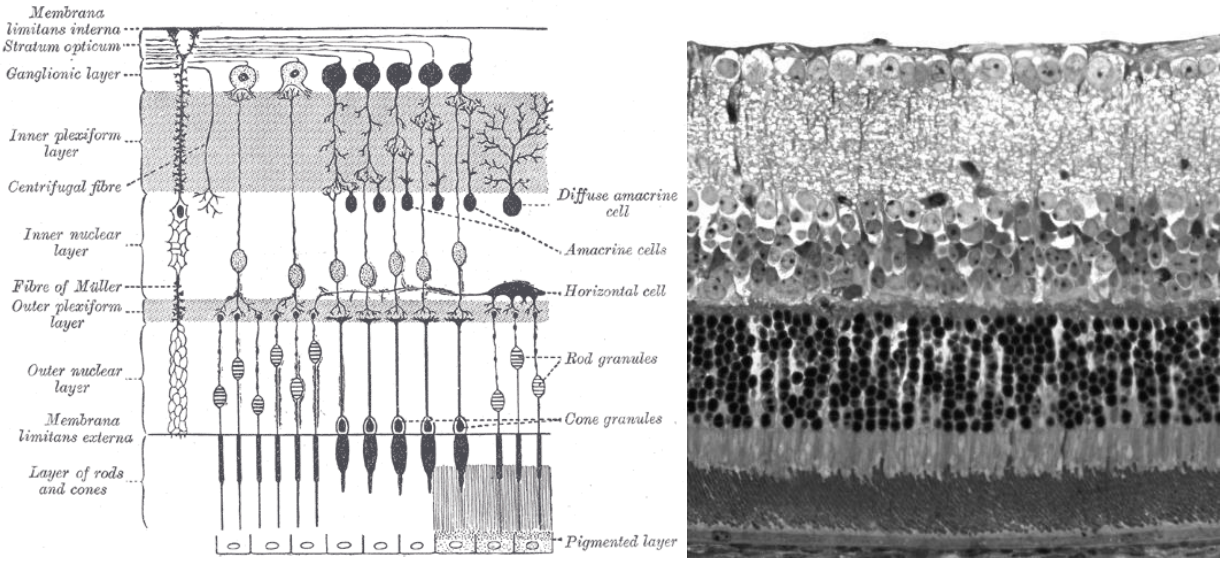


*Figure 3:* The retinal layers
A schematic and a corresponding semithin section, showing the configuration of the retinal layers. Left-hand side figure taken from: http://archive.org/stream/anatomyofhumanbo1918gray#page/1016/mode/2up; on the right-hand side: semithin section of the mouse retina (by Stefaniya Boneva).

Within almost all mammalian retinae rod photoreceptors, located primarily in the periphery, exceed numerically cone photoreceptors, which occupy the Fovea centralis, responsible for sharp central vision (Masland, 2012). The high acuity of human vision relies heavily upon this cone-rich region, located in the center of a yellowish spot within the human retina – the macula (Morrow et al., 1998). In the human retina rods outnumber cones by about 20-fold (120 million versus 6 million (Trepel, 2012)), while

estimates of the percentage of cones in the rod-dominated murine retina differ dramatically, ranging from an assumption of a pure rod retina (because of mice's nocturnal behavior) to numbers of approximately 10% (reviewed in (Carter-Dawson and LaVail, 1979)). Carter-Dawson and LaVail based their conclusion of 3% in both the central and peripheral retina on elegant nuclear counts and assumed subsequently the absence of a fovea-similar region by mice. Since the discrepant rate of rods' and cones' degeneration hallmarks inherited retinal dystrophies (e.g. retinitis pigmentosa), the knowledge of the cones' (approximate) share in photoreceptors' quantity is of great importance for studies, involving mice as animal models. To sum up, in contrast to humans, whose vision depends on three kinds of cones and only one variety of rods, rodents rely primarily on rod-mediated vision, since rods account for 97% of their photoreceptor cells (75% of all cells in the mouse retina) (reviewed in (Morrow et al., 1998)).

Photoreceptors are distinguishable especially by their either rod- or cone-shaped outward light-perceiving processes, each composed of both an outer and an inner segment. These extensions are adjacent to the retinal pigment epithelium (RPE) and represent the outermost layer of the Stratum nervosum (Figure 5B.). The highly specialized functional assignment of photoreceptors, which transmit the stimulus of light to corresponding brain centers, requires the mentioned segmental organization, featuring a great degree of intracellular compartmentalization (Young, 1967).

The outer segment of each photoreceptor cell is constituted of many hundreds of densely packed discs (Figure 4). Each of them represents a double-layered plasma membrane invagination: either in terms of membranous disc stacks (rods) (Figure 4A., 4C., 4D.), or as membrane enfoldings (cones) (Figure 4B., 4E.) (Welsch and Deller, 2010). The visual pigment is restricted, in the form of a transmembrane protein, to these cell membrane discs, which maximize the exposure surface area for photons, reacting with photopigments. In the adult vertebrate photoreceptor the process of packaging of the membrane into a stack of closely spaced discs accounts for the renewal of the outer segment (Steinberg et al., 1980). Radioautographic studies (Young, 1967) and ultrastructural analyses (Anderson et al., 1978) of retinal photoreceptor cells have demonstrated that the outer segments of both rods and cones, respectively, are regenerated within a balanced process: new lamellar material is continuously delivered at the basis of the segment (Figure 4B.), these newly-formed discs then proceed towards the apex of the respective segment, which is ultimately shed and phagocytized by the adjacent RPE. Protein constituents, including visual pigments, are synthesized within the

inner segment of each photoreceptor cell, more precisely in the ergatoplasm of its myoid region, then transferred to the corresponding Golgi complex and through the dense aggregations of mitochondria within the ellipsoid region, also part of the inner segment (Young, 1968). Upon passing through the extremely narrow modified cilium of the connecting stalk structure (Figure 4E.), which unites inner and outer segment, proteins are incorporated into the newly formed membranous discs at the basis of the outer segment (Young, 1968). Thus, the light-sensitive visual pigments are restricted to the outermost portion of the photoreceptor cells. The continuous assembly of new disc stacks involves the recycling of old material in a balanced manner (Young, 1971). Since the process of shedding detached discs is crucial for the renewal and the homeostasis of photoreceptor outer segments (Bonilha et al., 2006), their arrangement among the microvilli of the retinal pigment epithelial cells, appears to be not only contingent upon development, but also having functional issues.

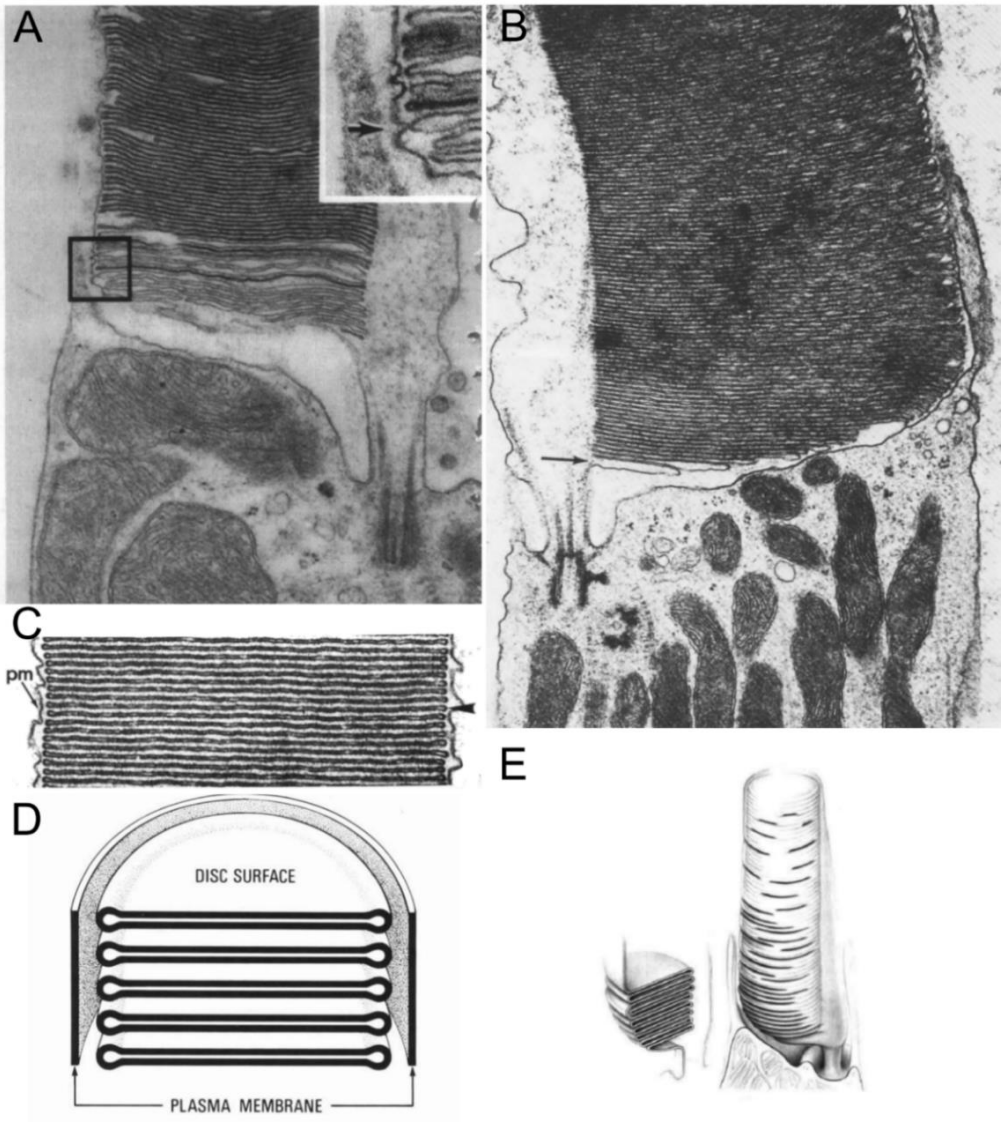


*Figure 4:* Ultrastructure of photoreceptors
A. An electron micrograph of a rod outer segment base in a 13-lined ground squirrel. The outlined area is shown in inset (on the top right). The small indentations of the cell membrane represent newly forming discs, while one disc is pinching off from the cell membrane (arrow). Slightly modified after (Anderson and Fisher, 1976). B. An electron micrograph of a cone outer segment base (rhesus monkey), the arrow pointing to the most basal membrane enfolding. The stacked membranes of the discs are very distinct due to the high electron-density of the proteins they contain. Picture taken from (Steinberg et al., 1980). C. and D. Parallel arrangement of disc lamellae within a rod outer segment. Electron micrograph of a longitudinal section through a part of a rod outer segment (rhesus monkey). Arrowhead pointing to the rim of a single disc) (C.). Diagram of a stack of mature discs, surrounded by the plasma membrane (pm) (D.). Both panels slightly modified after (Steinberg et al., 1980). E. Model for the structure of mammalian cone outer segments. Right panel: An entire outer segment and the distal portion of the cone inner segment. Left panel: Longitudinal section through a cone outer segment base. The membrane at the very base of the stack is continuous with the membrane that borders the connecting cilium, while the basal disc stack represents an interconnected network. Picture taken from (Anderson et al., 1978).

#### 1.1.1.2 The retinal pigment epithelium (RPE)

The highly specialized tasks, fulfilled by the retinal pigment epithelium (RPE), are of great importance for the unimpaired homeostasis of the neural retina. Phagocytosis of shed outer segments, aligned nutrients supply and recycling of waste products from photoreceptor cells, stable ion conductance, light absorption, growth and immunosuppressive factors secretion and visual pigment regeneration count among the essential functions of the RPE (Bonilha et al., 2006; Strauss, 2005). The detached tips of photoreceptor outer segments are fused with plenty of lysosomes, present in the cytoplasm of the RPE cells (Welsch and Deller, 2010; Young, 1969). Residual, i.e. not completely utilized, bodies within the lysosomal vesicles form lipofuscin particles, which accumulate within the retinal epithelium cells over a lifetime and which cannot be completely handled by means of the depicted autophagic process (de Jong, Paulus T. V. M., 2006). Consequently, the concentration of lipofuscin granula is the highest in the regions, where the metabolic functions of the retinal pigment epithelial cells are most distinct: in the parafoveal region (de Jong, Paulus T. V. M., 2006). Accumulation of excessive lipofuscin, beyond normal aging process proportions, is a commonly observed pathology in several retinal diseases, such as AMD and inherited dystrophies (Nandakumar et al., 2012). By means of *in vivo* laser scanning ophthalmoscopy (SLO) fundus imaging lipofuscin particles can be visualized, since RPE areas, containing the degradation material, emit fundus autofluorescence, when excited by blue light. The excitation efficiency of lipofuscin lies between 430 and 600 nm, with an emission spectrum, ranging from 480 to 800 nm (Nandakumar et al., 2012). By visualizing the topographical map of lipofuscin, SLO is able to assess the metabolic health and functionality of the RPE (Nandakumar et al., 2012).

The cuboidal epithelial cells project their delicate apical microvilli in the direction of photoreceptors and encompass the tips of their outer segments (Figure 5C.) (Young, 1971). This intimate morphological relationship between both layers is crucial for the maintenance of visual function, especially for regeneration and renewal of photopigments after absorption of light units. The process represents the recovery of photoreceptors' excitability, since rods and cones themselves are unable to re-isomerize all-*trans*-retinal back to 11-*cis*-retinal (Strauss, 2005).

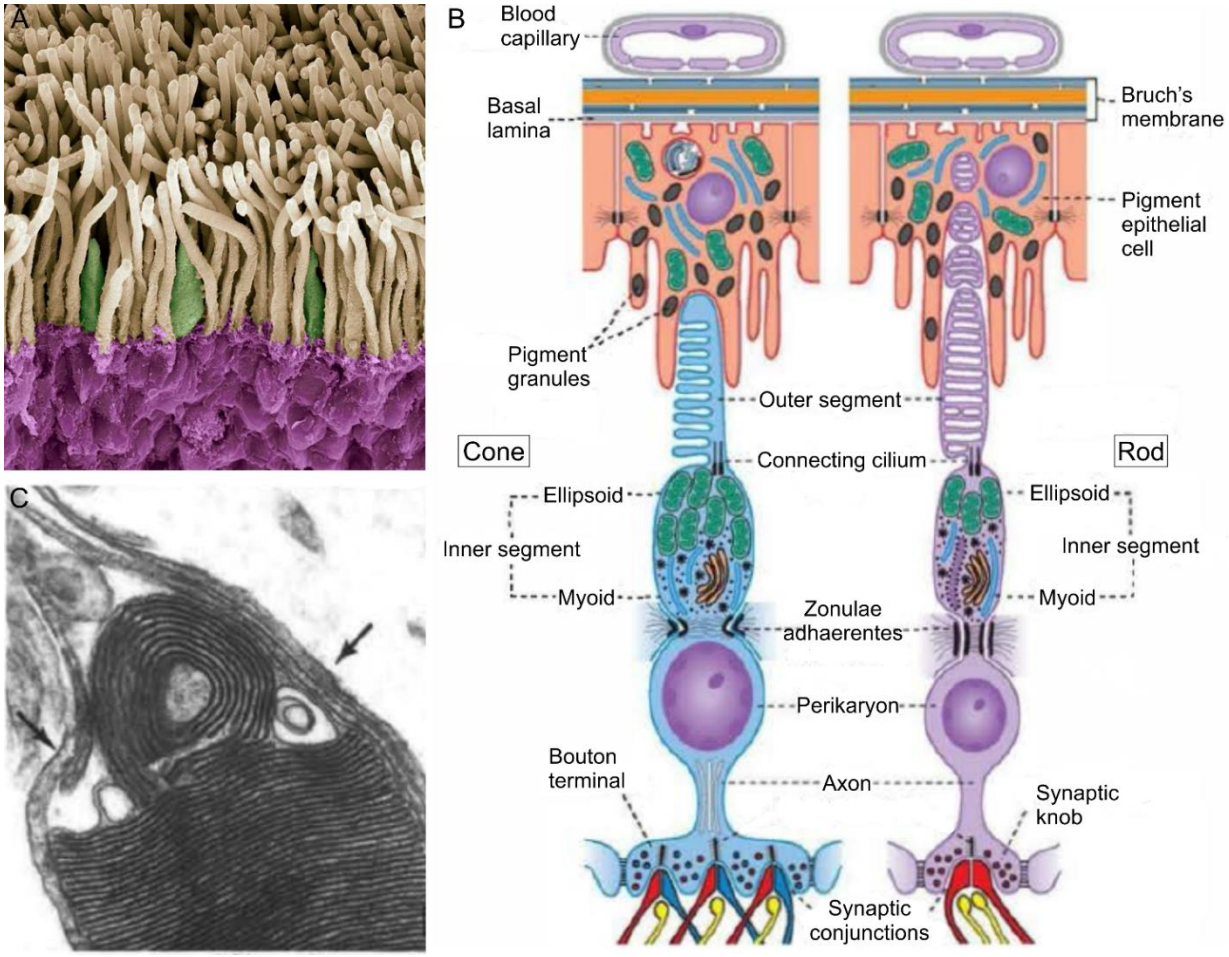


*Figure 5:* Photoreceptor cells and phagocytosis of shed discs by the RPE

A. A colored scanning electron micrograph of rods (yellow) and cones (green). Picture slightly modified after: http://fineartamerica.com/featured/sem-of-rods-and-cones--retina-spl.html

B. A schematic drawing of a cone (on the left) and a rod (on the right), as well as of the retinal pigment epithelium (RPE), responsible for phagocytosis of shed disc components. The outward processes of the receptor cells, adjacent to the RPE, are each comprised of an outer and an inner segment, containing the metabolic machinery for the cell's biosynthetic and energy-producing processes. The zonulae adhaerentes between the sensory cells and the Müller supporting cells form the outer limiting membrane (OLM). The RPE's basal surface faces the acellular Bruch's membrane, which is constituted of a basal lamina, collagen fibers and a dense network of elastic fibers and abuts the fenestrated endothelium of the choriocapillaris. Picture modified after (Welsch, 2005). C. Terminal disc shedding of a cone outer segment tip (extrafoveal human cone). The RPE apical processes (arrows) extend along both sides of the outer segment. Picture taken from (Steinberg et al., 1977).

## 1.2 Phototransduction cascade

### 1.2.1 Phototransduction

With the aid of the visual pigment, incorporated and very densely packed into the flattened membranous discs within the light-sensitive outer segment, photoreceptors detect the light stimulus and initiate the phototransduction cascade (Welsch and Deller, 2010). The respective rod photopigment is called rhodopsin, while cones contain three distinct variations of the visual pigment iodopsin, each of them with a specific maximal sensitivity in the red, blue, or green spectrum of the visible wavelength. Thus, the three functional types of cone cells, which are not distinguishable morphologically, are capable of detecting those colors in reflected light (Mescher, 2010). The diverging types of visual pigment, absorbing light most dynamically at limited wavelengths, are likely to illustrate the functional specificity of rods, which are extremely sensitive even to low light levels, responding to a single photon at dusk or nighttime, and cones, which are specialized for color vision in bright light. Each of these visual pigments is comprised of a transmembrane G-coupled receptor, the opsin, that is covalently bound to the light-sensitive chromophore retinal (Figure 6A.). When bleached by light, the visual pigment triggers the phototransduction cascade, which involves a similar process in both rods and cones, but is far better studied for the more abundant rod cells (Mescher, 2010).

In the dark the depolarized photoreceptor cell continuously releases the neurotransmitter glutamate at corresponding synapses to the neurons of the vertical pathways (Crooks and Kolb, 1992). The absorption of photons by the retinal of rhodopsin leads to a conformation change of the chromophore – from 11-*cis*-retinal to all-*trans*-retinal (Figure 6B.). Upon this stimulation, opsin activates transducin, a trimeric G-protein, which is coupled to the transmembrane receptor opsin. Subsequently, the activated transducin releases a single α-subunit, which stimulates another membrane protein, phosphodiesterase (PDE) (Figure 6A.). PDE is capable of hydrolyzing phosphoric diester bonds and thus catalyzing the chemical conversion of cGMP (guanosine 3',5'-cyclic monophosphate) to 5'-GMP (guanosine 5'-monophosphate). Since the high intracellular concentration of the second messenger cGMP keeps the abundant membrane cation channels open, equivalent to the depolarization of the photoreceptor cell, less cGMP stimulates the sodium channels to close. This results in a hyperpolarization of the cell – the amount of released neuromtransmitters at the synapse decreases. This change at the synapse depolarizes in its turn sets of bipolar neurons, which send action potentials to the ganglion cells of the optic nerve and initiate the visual stimulus to the brain (Mescher, 2010).

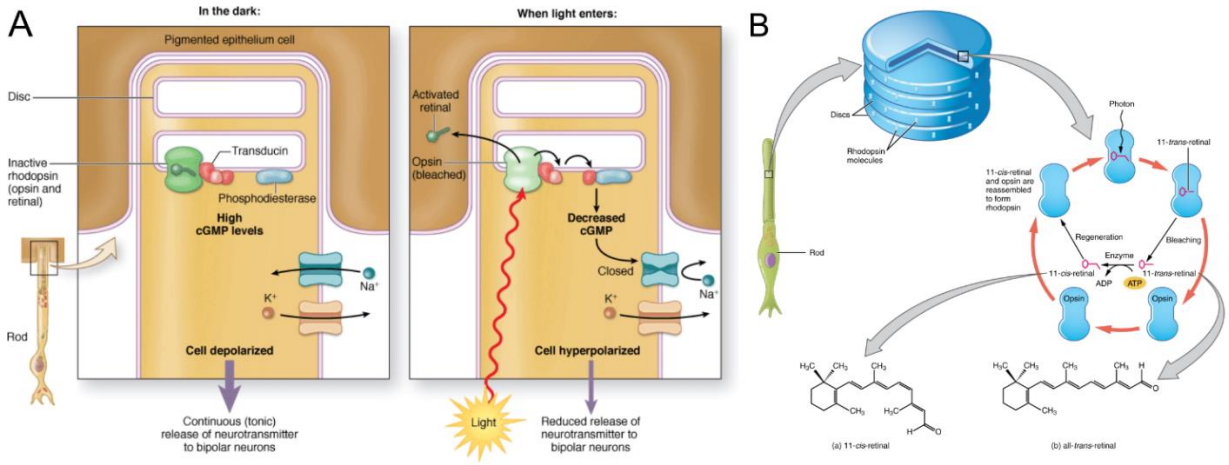


*Figure 6:* Rod cell phototransduction

A. The phototransduction signaling cascade is mediated via G-proteins: the visual pigment represents a transmembrane G-protein-coupled receptor, the opsin, covalently bound to the chromophore retinal. Upon light stimulation, retinal isomerizes from 11-*cis*-retinal to all-*trans*-retinal and the phototransduction cascade is initiated: the G-protein transducin is activated and releases a single α-subunit, which stimulates phosphodiesterase (PDE). PDE catalyzes the chemical conversion of cGMP (guanosine 3',5'-cyclic phosphate) to 5'-GMP (guanosine 5'-phosphate). High intracellular concentrations of cGMP keep the cation channels open, resulting in the depolarization of the photoreceptor cell, less cGMP stimulates the sodium channels to close and the cell hyperpolarizes (Further details are elaborated in the main text). Figure taken from (Mescher, 2010). B. The two isomers of the retinal molecule: before a photon interacts with it (a, 11-*cis*-retinal) and after light-induced photoisomerization (b, all-*trans*-retinal). Figure taken from:
http://cnx.org/contents/b375ea7d-22d5-4f47-b10a-41dd93637896@5/Sensory_Perception

### 1.2.2 The visual cycle

Upon light induction, the conformational change in retinal (Figure 6B.) also causes the chromophore to dissociate from the opsin, leaving a bleached opsin, which necessitates a reconstitution to the dark-adapted visual pigment form (de Jong, Paulus T. V. M., 2006). The free all-*trans*-retinal diffuses into the pigmented epithelium (Mescher, 2010). Since photoreceptors lack a *cis-trans* isomerase function for retinal regeneration after transduction of light energy into electrical stimuli (Baehr et al., 2003), the re-isomerization process, termed "visual cycle" (Redmond et al., 2005), occurs largely within the RPE through many complex intermediate steps. One of them includes the enzyme *Rpe65*, which is capable of converting all-*trans*-retinyl esters into 11-*cis*-retinol, a step, essential for the proper function of rods and cones (de Jong, Paulus T. V. M., 2006; Redmond et al., 1998). In order to ensure constant excitability of photoreceptors, the recycled retinal is transported back to rods or cones to allow further phototransduction

(Strauss, 2005). This cycle of retinal replenishment upon isomerization and rhodopsin recovery after bleaching by light may take about a minute and resembles the slow adaptation of the eyes from bright to dim light (Mescher, 2010).

Mutations of *Rpe65* or any other of the enzymes, involved in the regeneration of retinal, the chromophore of all visual pigments, result in blindness to a variable extent due to malfunction of the retinoid metabolism (reviewed in (Redmond et al., 2005)). The unimpaired flow of the visual cycle appears to be crucial for the execution of light damage experiments, since genetically altered mice, lacking either the visual pigment rhodopsin, or the gene *Rpe65*, proved to be completely resistant to light-induced apoptosis (Grimm et al., 2000). Allelic polymorphisms in the RPE-specific gene *Rpe65* account for a modified susceptibility to light, as it has been shown by Dancinger and coworkers (Danciger et al., 2000), who postulated that a single base change in codon 450 alters the sensitivity to damage, sustained after light exposure. This point mutation in the *Rpe65* gene is responsible for a Leu450Met amino acid substitution, which has been proven to increase retinal resistance against light-induced stress by slowing down the rate of rhodopsin regeneration (Grimm et al., 2000; Wenzel et al., 2001). Reduced levels of regenerated rhodopsin (re-synthesized opsin plus 11-*cis*-retinal) decrease the photon absorption rate, thus reducing retinal susceptibility to light damage. Since light exposure has been shown to exacerbate the course of retinal degenerative diseases, caused by inherited mutations (Sanyal and Hawkins, 1986; Wang et al., 1997), such inherent differences in light damage sensitivity appear to be very important for identifying modifying genes, affecting phenotypic severity.

In order to obtain a comparable situation between experimental individuals, we analyzed the animals for the mutation in the *Rpe65* gene and only homozygous leucine carriers were included in our light damage experiments.

## 1.3 The TGF-ß signaling pathway

Since the aim of this work comprises the characterization of the neuroprotective effects of TGF-ß signaling and the molecular mechanisms, mediating the prevention of apoptotic cell death, the following part is devoted to the detailed description of the signaling pathway.

### 1.3.1 TGF-ß ligands

The transforming growth factor beta (TGF-ß) protein was originally characterized in 1983 (Assoian et al., 1983; Frolik et al., 1983; Roberts et al., 1983), following its initial isolation from non-neoplastic tissues in 1981 (Roberts et al., 1981). Since then the knowledge, regarding the pivotal functions of TGF-ß in numerous physiological and pathological mechanisms, has grown exponentially, resulting in the identification of a broad spectrum of cellular targets and multifunctional actions (Roberts and Sporn, 1990). The distribution of TGF-ß family ligands in both invertebrate and vertebrate species, ranging from fruit flies (*Drosophila melanogaster*), over the African claw-toed frog (*Xenopus laevis*) to mammals, emphasizes the significance of these factors for developmental fate (reviewed in (Goumans and Mummery, 2000; Kingsley, 1994)). Up to date the encoding genes for five TGF-ß isoforms and their corresponding products have been isolated: three mammalian TGF-ß1, -ß2, and -ß3 (Cheifetz et al., 1987; Derynck et al., 1988; Seyedin et al., 1987), whereas TGF-ß4 (Jakowlew et al., 1988) and -ß5 (Kondaiah et al., 1990) probably represent the avian (chicken) (Burt and Paton, 1992) and amphibian (*Xenopus*) (Burt and Law, 1994) homologues, respectively, of the mammalian TGF-ß1 gene. The majority of them play essential roles during embryonic development and within maintenance of adult tissue homeostasis and morphogenesis (Feng and Derynck, 2005; Goumans and Mummery, 2000; Itoh et al., 2000; Wu and Hill, 2009).

### 1.3.2 Signaling receptors

In order to transduce signals to specific target genes, TGF-ßs act through cell surface receptors, assembled by two types of serine/threonine protein kinases (Massagué, 1998). Binding of the ligand induces the composition of a hetero-tetrameric receptor complex of two type I (acting as signal propagators) and two type II (fulfilling an activator task by phosphorylating the type I components) receptor components (Figure 7) (Massagué, 2012; Wrana et al., 1992). The signaling transmembrane receptors, are jointly designated as the TGF-ß receptor family (Massagué, 1998).

### 1.3.3 Signal flow within the receptor complex and downstream response mediation

The TβRII is a constitutively active kinase and auto-phosphorylated (in a ligand-independent manner), while TβRI is not phosphorylated in its basal state and unable to autonomously bind ligands from the extracellular microenvironment (Wrana et al., 1994). TβRII only requires a ligand, in order to interact with its substrate, the type I receptor, and thus generate the first step of the TGF-β pathway (Massagué, 1998). The receptor activates the TβRI by phosphorylation (Wrana et al., 1994), hereby inducing the assembly of a heteromeric complex of type I and type II receptors (Figure 7) (Wrana et al., 1992).

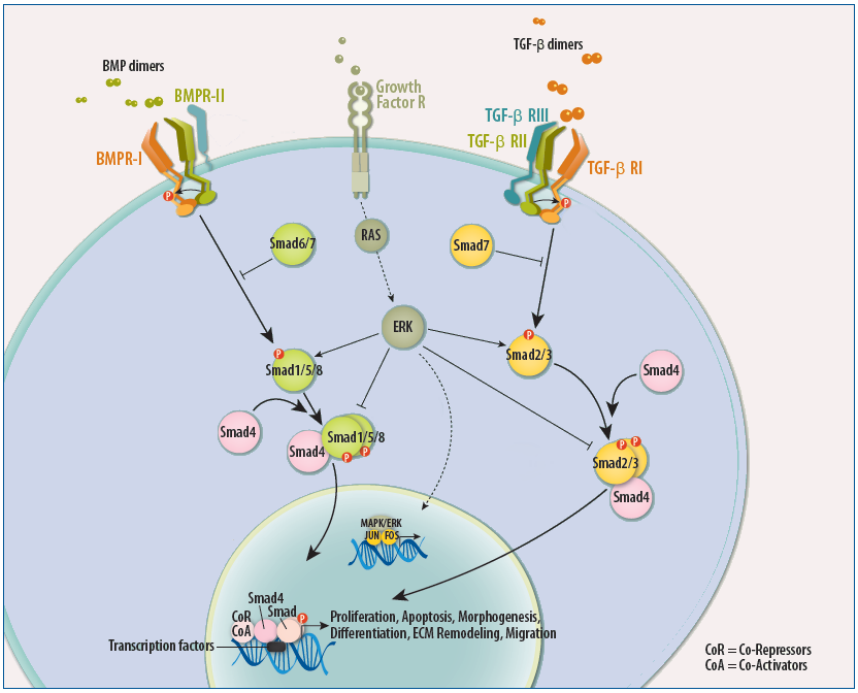


*Figure 7:* The TGF-β signaling pathway

Ligands from the TGF-β superfamily bind to heteromeric receptor complexes, exhibiting serine/threonine kinase domains. Subsequently, the type II receptor phosphorylates and thus activates the type I receptor, which in its turn phosphorylates a receptor-regulated SMAD (R-SMAD). Activated R-SMADs assemble with SMAD4 to form a trimeric complex, which is then translocated into the nucleus, where it can interact with certain co-activators and co-repressors. The particular type of cellular response to the altered gene transcription is fine-tuned at several levels through additional inputs, which eventually determine the ultimate output. This context-dependent nature of transduction is consistent with the diversity of versatile signal, elicited in response to TGF-β-like ligands. BMP, bone morphogenetic factors; BMPR-I and -II, bone morphogenetic factor receptors I and II; Growth Factor R, growth factor receptor; TGF-β, transforming growth factor beta; TGF-β RI, RII, RIII, transforming growth factor beta receptors I, II, III; MAPK/ERK = MEK (MAPK/ERK kinase, a mitogen-activated protein kinase kinase), MAPK, mitogen-activated protein kinase, ERK, extracellular signal-regulated kinase; Jun/Fos, transcription factors, forming together the AP-1 complex (Angel and Schorpp-Kistner, 2006). Figure modified after: http://www.rndsystems.com/Resources/Images/6906.pdf

The proteins, belonging to the SMAD family, are the first substrates for the catalytic kinase domain of the activated TβRI to be identified (Massagué, 1998). TGF-β receptor interactions with these transcription factors mediate gene expression and TGF-β signaling may be contextually altered according to the activated SMAD proteins (Massagué, 2012). SMADs can be classified in three separate groups: receptor-regulated SMAD proteins (R-SMAD proteins; SMAD1, -2, -3, -5 and -8), Co-SMADs (SMAD4), associating with the R-SMADs, and inhibitory SMADs (SMAD6 and -7), antagonizing the effects of both other groups (reviewed in (Attisano and Wrana, 2002)). R-SMADs act as direct substrates for the seven TGF-β receptor type I kinases (Macias-Silva et al., 1996). Three of the type I receptors (for TGF-β, activin and Nodal) phosphorylate SMAD2 and SMAD3, which thus act as transducers for TGF-β-like signals (Figure 7) (reviewed in (Attisano and Wrana, 2002; Massagué, 1998; Massagué, 2012)). Phosphorylated R-SMADs dissociate from the complex and subsequently consolidate with the collaborating SMAD4 (also known as DPC4, deleted in pancreatic carcinoma locus 4), which acts as a shared partner of all R-SMADs to mediate transcriptional responses (Massagué, 1998). As a signal transducer, the activated trimeric SMAD4-R-SMAD complex (two R-SMADs and one SMAD4) is then translocated into the nucleus, where it can access specific promoter elements, in order to generate a transcriptional complex and thus activate target genes to elicit a cellular response (Massagué, 2000; Shi and Massagué, 2003).

### 1.3.4 Negative regulation of SMAD-dependent transcription

Human SMAD6 and -7 belong to a subfamily of antagonistic SMADs, which structurally differ considerably from both other subfamilies (Massagué, 1998). These inhibitory SMADs are capable of adjusting the signal flow, as they interfere with the phosphorylation of R-SMADs (Massagué, 2000). This kind of antagonism counts among several crosstalk links and feedback loops, which alter the initial TGF-β input to determine the ultimate output (Yan et al., 2009). As the SMAD transduction pathway represents just a single thread in a complicated signaling network, its contribution may be altered in a process, called “signaling crosstalk”. Such kind of alteration generally consists in a negative regulation of the biochemical activity of TGF-β signal mediation processes, since the very powerful SMAD pathway most probably needs to be domesticated (Massagué, 2000). As primary transducers of TGF-β-like signals intracellularly, SMADs are subjected to the signaling potential of the Ras-MEK (MAPK/ERK kinase)-ERK (extracellular signal-regulated kinase) pathway, activated by agonists, such as EGF (epidermal growth factor) and other Ras-activating mitogens

(Figure 7) (Massagué, 1998). In response to growth factor receptor signals or oncogenic mutations of Ras ERK-mediated phosphorylations interfere with the accumulation of activated SMADs in the nucleus (Kretzschmar et al., 1999). While TGF-ß can overrule the effects of EGF and other Ras-mitogens in normal epithelial cells, oncogenic Ras mutations eliminate TGF-ß-antimitogenic and cytostatic effects (Kretzschmar et al., 1999). But more importantly, the idea that the MAPK (mitogen-activated protein kinase) pathway can alter the activity of SMAD complexes implies that some of the classical agonists of these pathways, such as cytokines (tumor necrosis factor-α (TNF-α)) or cellular stress, could also influence the activity of SMAD transcriptional complexes.

### 1.3.5 Disruption of the TGF-ß signaling pathway

Mutated genes, which ordinarily encode for components of the TGF-ß signaling pathway, can cause various types of human disorders, depending on the level, at which disruption occurs. Alterations in TGF-ß activity may have profound effects on embryological development and tissue homeostasis, including loss of growth inhibitory responses in cancer cells, excessive accumulation of fibrotic tissue due to immoderate gain of TGF-ß activity, inflammatory disorders and many others (Massagué, 1998). Thus, unravelling the extent and ambiguous consequences of pathway discrepancies would surely benefit not just our understanding of the context-dependent TGF-ß signaling in physiology and disease, but also the development of medicamentous options for the listed disorders.

## 1.4 The Cre/LoxP recombination system

The genetic process of enzymatic recombination is a widespread mechanism in both prokaryotes and eukaryotes, which enables not only DNA damage repair, but also rearrangements of DNA sequences within an individual genome. This kind of rearrangement leads to alterations in timing and level of gene expression that are crucial for facilitating the genetic diversity and the evolution of organisms in response to environmental changes (Alberts et al., 2008). Guided by a specialized set of proteins, site-specific recombination is capable of modifying gene order along a chromosome, as the enzymes break and rejoin two DNA double helices at specific recognition sequences, located on separate DNA molecules (donor and recipient DNA) (Alberts et al., 2008).

The Cre recombinase (cyclization recombination), a 38 kDa protein from the integrase family of site-specific recombinases, has its origin in the bacteriophage P1. This enzyme catalyzes the synapsis and recombination between two loxP (locus of X-over of P1) recognition sites (sequences of 34 bp each) (Hamilton and Abremski, 1984; Sternberg and Hamilton, 1981), in fact not needing any additional co-factors, or sequence elements (Figure 8). Each loxP nucleotide sequence consists of a 8 bp core spacer sequence (determining the orientation), flanked by two palindromic 13 bp sequences (recombinase binding elements). In the framework of a recombination event, a single enzyme is associated with each palindromic half of a loxP site. This dimer subsequently binds to another loxP site dimer, thus assembling a tetrameric recombination synapse and bringing the two loxP sites together in an antiparallel manner (Guo et al., 1997). The "floxed" double-stranded DNA segment is subsequently cleaved, leaving behind the two complementary halves of the pre-recombination sites (Nagy, 2000). The results of cell culture experiments, carried out by Sauer and Henderson in 1988 (Sauer and Henderson, 1988), demonstrated for the first time this type of controlled recombination with the aid of the prokaryotic enzyme in mammalian cells, implicating the great importance of this tool for creating any desired modification within the mammalian genome. Further investigations issued the development of a tissue- and site-specific chromosomal DNA recombination, as a function of particular recombinase expression for specifically modifying the mammalian genome *in vivo* (Orban et al., 1992).

In order to investigate the role of the TßRII inactivation in a complex multicellular organism, double transgenic mice were generated. Since a ubiquitous homozygous deficiency of the type II TGF-ß receptor results in embryonic lethality due to crucial defects in hematopoiesis and vasculogenesis (Oshima et al., 1996), the conditional deletion of the TßRII by using the Cre/LoxP system enables to restrict its deletion to

spatial or temporal boundaries. In the current thesis, *Tgfbr2*$^{fl/fl}$ mice, were used that carry the loxP sites as flanking sequences of the Exon2 of the TβRII gene (Chytil et al., 2002). These mice were mated with appropriate *cre* mice, heterozygous for either *α-Cre* or *LMOP-Cre*, in order to trigger a lineage-specific deletion. To inactivate the targeted sequence in neural retina cells, originating from the inner layer of the optic cup, the expression of the gene, encoding for the Cre recombinase of *α-Cre*-transgenic mice, was directed by a retina-specific promoter element (α) of murine *Pax6* (Marquardt et al., 2001). This alpha enhancer element is responsible for the restricted expression of *Pax6* within the developing neural retina (Kammandel et al., 1999). In transgenic *LMOP-Cre* mice, the expression of the Cre recombinase was confined to rod photoreceptors, as the gene is expressed under the control of the long (4.1 kb) mouse opsin-promoter (Le et al., 2006).

Genomic alteration was thus, according to the particular recombinase, restricted to either neural retina cells, originating from the inner layer of the optic cup, or rod photoreceptors, respectively.

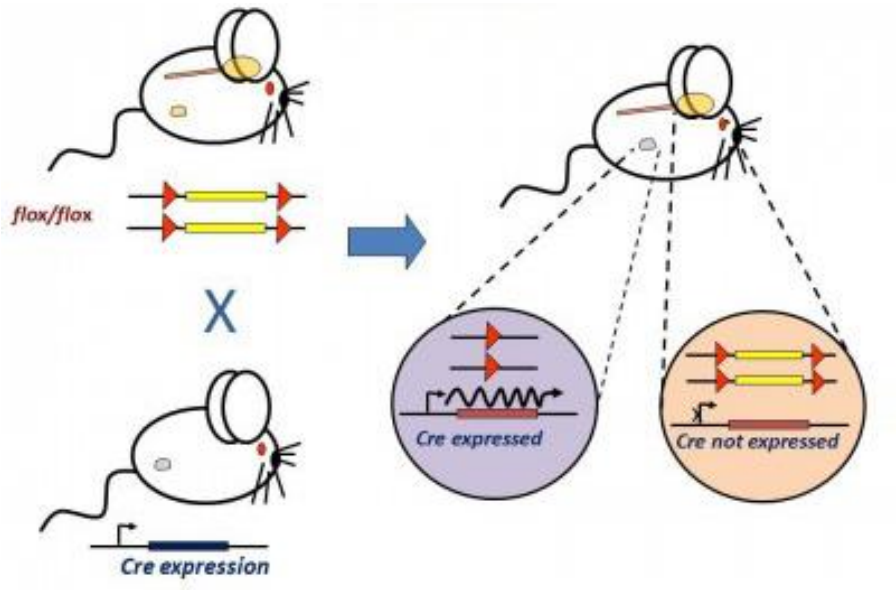


*Figure 8:* The Cre/LoxP principal

A "floxed mouse", created through homologous recombination, is crossed with a transgenic mouse, expressing the Cre enzyme under the control of a specific promoter. The loxP sites flank an allele of interest on each side, which is consequently being conditionally deleted. Thus, genome alteration in a particularly precise manner is enabled. Figure taken from: http://www.tcdm.fi/animal-models/gm-cre-expressing-mouse-lines/

## 1.5 The light damage model in the context of retinal degeneration

### 1.5.1 Retinitis pigmentosa (RP)

Retinitis pigmentosa (RP) comprises a heterogeneous subset of genetic pathologies, leading to the disease. It harbors multiple kinds of disorders, differing in their inheritance pattern (autosomal-dominant, autosomal-recessive or X-linked trait) and underlying gene mutations (more than 45 identified loci), but all of them featuring degeneration of rod and cone photoreceptors (Kellner, 2007). With a worldwide prevalence of about 1 in 4000 (for a total of more than 1 million affected individuals), RP accounts for the most common type of degeneration within the group of hereditary dystrophies of the human retina (Hartong et al., 2006).

The multiple phenotype forms of RP differ dramatically in two variables: the age of initial manifestation and the chronological progression of the disease. While some patients develop symptomatic visual loss in childhood or even suffer from congenital blindness, others remain asymptomatic until mid-adulthood (Kellner, 2007). In spite of this wide temporal range, many patients exhibit a classic sequence of night blindness as an early symptom in adolescence and slowly progressive loss of mid-peripheral visual field in young adulthood. Roughly speaking, the earlier the initial symptoms arise, the greater the progression and the severity of functional loss. Advanced stages of this pattern include complete side vision deprivation, progressive development of tunnel vision and eventual color vision disturbances and central vision loss, typically by the age of 60 years (Hartong et al., 2006). Given that the course of visual field constriction is extremely slow and familiar predisposition is not present, the disease may escape notice for a very long time (Kellner, 2007). Furthermore, a reduction in visual acuity can go undetected, until the density of cones in the fovea has decreased by nearly 90% (Geller et al., 1992). The set of visual symptoms resembles the gradual loss of the two photoreceptor types in the outer nuclear layer: rods, responsible for dark adaptation and achromatic vision in the dark, and cones, which mediate color and acuity vision in daylight (Hartong et al., 2006). In the majority of cases of this inherited retinal dystrophy, the rods' functional loss exceeds the deficits in cone sensitivity. Analyses of retinal functions within the framework of electroretinography provide evidence that diminishment of photoreceptor functionality occurs many years before initial subjective symptoms, such as impaired dark adaption, visual-field scotomas or visual acuity deficits, are reported (Berson, 1993). Universal ophthalmoscopy findings, for instance attenuation of retinal vessels, alterations of the retinal pigment epithelium and speckled intraretinal pigmentations in the periphery,

referred to as bone-spicule deposits and representing the migration of the RPE into the retina in response to photoreceptor-cell death (Li et al., 1995), hallmark RP, but might also be completely absent, especially early in the disease's course (Kellner, 2007).
Some of the mutations, causing RP, interfere with the rod photoreceptor transduction cascade, since the corresponding genes encode proteins, which are known to play essential roles in this biochemical pathway. The consequent death of rod cells is most probably attributable to the subsequently impaired physiology, while the death of cones is secondary and likely to imply the yet mysterious notion that certain rod factors promote cones' survival (reviewed in (Hartong et al., 2006)). For now, the only treatment options, RP patients benefit from, are restricted to a symptomatic deceleration of disease progression and include nutritional supplements, such as vitamin A palmitate and docosahexaenoic acid (DHA) (an omega-3 fatty acid), but other approaches (gene-therapy, transplantation of stem cells, RPE or photoreceptors and implantation of retinal stimulating devices) are greatly anticipated (reviewed in (Hartong et al., 2006)).

### 1.5.2 Age-related macular degeneration (AMD)

The age-related macular degeneration (AMD) is the main cause of irreversible visual impairment and blindness by people over 50 years in the developed countries (Jager et al., 2008; Pascolini and Mariotti, 2012). It is likely to become even more significant and to even double by the year 2020, due to the rapid growth of the elderly population (Friedman et al., 2004). In 1874 this condition was for the first time in the medical world referred to as "symmetrical central choroido-retinal disease, occurring in senile persons" (Hutchinson J, Tay W., 1874), while the label "age-related macular degeneration" was defined only about 30 years ago (de Jong, Paulus T. V. M., 2006).
The characteristic central visual loss, occurring in AMD, is the result of alterations within the physiological structure of the Ruysch's complex (de Jong, Paulus T. V. M., 2006). The complex is named after the Dutch anatomist Frederik Ruysch and comprises the retinal pigment epithelium (RPE), the Bruch's membrane and the choriocapillaris. The typical alterations within this complex occur as a reaction to the focal deposition of polymorphous debris between the RPE and the Bruch's membrane (Figure 9). This pathogenetic mechanism, is affiliated to the absent or incomplete phagocytosis of the abnormal material by the RPE cells, a process, essential to the renewal of photoreceptor visual pigment (Kanski, 2008).
The two major types of age-related macular degeneration are the non-exudative or "dry" and the exudative or "wet" AMD: the non-exudative form of AMD is characterized by the

existence of drusen and focal areas of RPE atrophy, while the "wet" form of AMD is marked by choroidal neovascularization (CNV) (Bhutto and Lutty, 2012). The clinical hallmark of age-related macular degeneration is the existence of drusen (Jager et al., 2008), representing a discrete accumulation of debris and observed as yellowish spots in the macular region during a funduscopic examination (Jager et al., 2008; Kanski, 2008). The accumulation of lipid residuals within RPE cells, as aforementioned (1.2.2), leads to enzymatic autolysis, cell death and thus to a progressive diminishment of the RPE (Schmidt-Erfurth, 2007). The blood and oxygen supply of the photoreceptor cells relies on the unimpaired function of the choriocapillaris and its fenestrated endothelium. However, the progressive destruction of the RPE leads to a secondary atrophy of the blood vessel layer, too (Korte et al., 1984; Schmidt-Erfurth, 2007). The resulting hypoxia impairs the proper oxygen consumption by photoreceptors and leads to the accumulation of free toxic radicals particularly in the macular region (Schmidt-Erfurth, 2007). The hypoxic state stimulates the release of angiogenic factors, such as vascular endothelial growth factor (VEGF) from the RPE cells, which accounts for the development of CNV (Figure 9) (Spilsbury et al., 2000). Other relevant alterations within the Ruysch's complex involve the deposition of extracellular membranous debris around the Bruch's membrane. These induce the recruitment of inflammatory cells to the retina, capable of secreting inflammatory cytokines and angiogenic factors (Figure 9) (de Jong, Paulus T. V. M., 2006; Hageman, 2001). Since the access to nutrients from the RPE is critical for the survival of photoreceptors, they undergo apoptotic cell death, once the RPE becomes dysfunctional, e.g. in the course of age-related macular degeneration (Bhutto and Lutty, 2012; Dunaief, 2002).

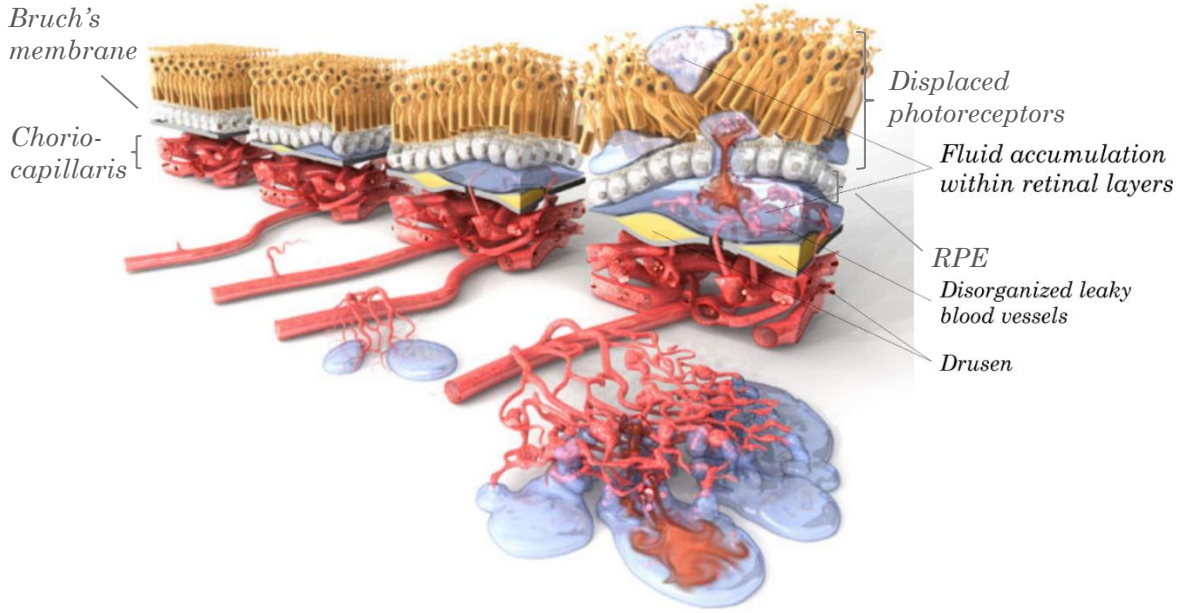


*Figure 9:* An illustrated explanation of AMD
The drusen and fluid accumulation between the Bruch's membrane and the photoreceptor layer, sitting atop the RPE, causes the recruitment of inflammatory cells to the retina. The release of inflammatory cytokines and growth factors stimulates the process of angiogenesis, resulting in the growth of new capillaries from preexisting vessels into and through the Bruch's membrane.
Figure slightly modified after http://www.scienceofamd.org/learn/, a website of The Angiogenesis Foundation, accessed on [October 31, 2016].

### 1.5.3 Light damage as a model for the study of retinal degeneration

In a healthy adult retina only a very small portion of photoreceptor cells are affected by cell death in humans (only 2 rods/mm$^2$ of retina per year in normal ageing eyes (Curcio, 2001)) and in the most animal models. Therefore, an experimental model of artificially induced apoptosis was developed to allow studies of the apoptotic mechanisms in photoreceptors (retinal dystrophies and age-related macular degeneration) (Wenzel et al., 2005). Hereby, the induction of cell death by a light stimulus is comparable to the supposed effect of excessive phototransduction signaling even in the absence of light – a scenario that results in retinal degenerative processes, according to the "equivalent light hypothesis", postulated by Fain and Lisman (Fain and Lisman, 1993). Since the decrease in rod density in the parafoveal visual field (by approximately 30% in ageing healthy eyes (Curcio et al., 1993) and much more severely in eyes, suffering from AMD (Curcio et al., 1996)) is the crucial variable in the initial phases of AMD, the model of light-induced retinal damage is supposed to resemble the loss of rods' function (Remé et al., 2003). The susceptibility of rodents' eyes to light of a visible wavelength at prevalent intensities

(Noell et al., 1966) is the essential condition, which allowed the observation of an accelerated and synchronized photoreceptor cell apoptosis. In this thesis, light damage experiments were performed to elucidate the role of the TGF-ß signaling pathway and its possible neuroprotective effect on photoreceptors.

### 1.5.4 Neuroprotective signaling upon light-induced stress and in the context of photoreceptor degeneration

The fact that photoreceptor degeneration of any kind almost indispensably induces Müller cell reactivity implies the existence of a relatively limited number of genes, responding to photoreceptor degeneration in the context of inherited diseases (Rattner and Nathans, 2005). Genes, coding for photoreceptor-derived *endothelin 2 (Edn2)*, count among the mostly upregulated transcripts in the case of retinal injury. The concomitant increase of the *endothelin receptor B (Ednrb)* in Müller cells indicates the signal function of *Edn2* through this receptor in the case of cell stress (Rattner and Nathans, 2005).

Another signal, identified as a neuronal survival factor, is represented by the *leukemia inhibitory factor (Lif)*, deriving from Müller cells (Joly et al., 2008). The expression of its gene is highly upregulated upon photoreceptor death within the INL and induces itself an intrinsic molecular defense mechanism, including *Edn2*, *Stat3 (signal transducer and activator of transcription 3), Fgf2 (fibroblast growth factor 2)* and *Gfap (glial fibrillary acid protein)* (Braunger et al., 2013a; Joly et al., 2008). *Bdnf (brain-derived neurotrophic factor)* is another factor, known to protect photoreceptors against retinal degenerative processes (Gauthier et al., 2005; LaVail et al., 1998).

TGF-ß signaling may increase the potency of certain neuroprotective factors, such as *Fgf2*, *ciliary neurotrophic factor (Cntf)*, and *glial cell line-derived neurotrophic factor (Gdnf)* (Krieglstein et al., 2002). In a model system of peripheral neurons, TGF-ß has been shown to regulate neuron survival by enhancing the functions of *Cntf* or *Fgf2*. However, it does not seem to act synergistically with neuropoietic cytokines, such as *Lif* (Krieglstein et al., 1998).

To sum up, in the context of the light damage experiments, performed in this study, an upregulation in the levels of *Bdnf*, *Lif* and other survival factors, which are most probably mediated through *Lif (Edn2 and Fgf2)*, was highly anticipated. Hence, the reaction of these transcripts to the retinal injury, sustained by light, was investigated by means of real-time polymerase chain reaction (RT-PCR).

## 1.6 Aim of the study

The major purpose of the current study consists in the definition of the protective role of TGF-ß signaling for photoreceptors' survival. Therefore, we will use two mouse strains with a recombined and inactivated TßRII either in the cells, which derive from the inner layer of the optic cup *(Tgfbr2$^{\Delta oc}$)*, or in rod photoreceptors only *(Tgfbr2$^{\Delta rod}$)*.

First of all, we aim to exclude possible side effects, which may arise from the expression of an exogenous protein, such as the Cre recombinase, in the retinal cells. To this end, we will perform ß-galactosidase staining, in order to visualize the expression pattern of the enzyme in both experimental mouse strains, and subsequently conduct morphology characterization and morphometric analyses of the inner (INL) and outer nuclear layer (ONL) thickness. The results will be depicted in form of Spider diagrams and the statistical evaluation of the measurements will expose any possible indications of interference of the recombinase enzyme with the tissue homeostasis. To further verify whether the expression of the protein would affect the neuronal vulnerability of photoreceptors, we will perform light damage experiments, followed by TUNEL-labeling of apoptotic cells.

We will further characterize the successful recombination events by performing the *Tgfbr2* deletion PCR, Western blot analyses and immunohistochemical staining for TßRII and pSMAD3, the cytosolic downstream transducer of TGF-ß signals. Following phenotype analysis of *Tgfbr2$^{\Delta oc}$* and *Tgfbr2$^{\Delta rod}$* will include the characterization of their morphology and the obtaining of statistical evaluations, concerning the thickness of the nuclear layers. For *Tgfbr2$^{\Delta oc}$* animals the retinal vasculature will by visualized by *in vivo* funduscopy and fluorescein angiography (FLA).

In order to assess the notion of the neuroprotective effect of the TGF-ß signaling pathway in the retina, we will subsequently perform light damage experiments. Morphometric analyses will show, whether the deficiency of the type II TGF-ß receptor would result in alterations, regarding the architecture of the retinal layers. TUNEL-labeling and quantification of apoptotic cells after light exposure will demonstrate, if the downregulation of TGF-ß signaling might diminish photoreceptor survival rates. *In vivo* laser scanning ophthalmoscopy (SLO), optical coherence tomography (OCT) imaging and ERG analyses will aim to confirm the gained results. The determination of the underlying molecular mechanisms, mediating the presumptive neuroprotective role of TGF-ß, will include real-time RT-PCR analyses for the mRNA levels of several specific factors before and after light exposure. Another potential downstream signaling pathway, including (p)AKT, will be explored on protein level through Western blot analyses.

# 2. Material and methods

## 2.1 Methods

### 2.1.1 Animal models

All procedures followed the tenets of the National Institutes of Health Guidelines on the Care and Use of Animals in Research and the EU Directive 2010/63/E. All mice were kept under standardized conditions for temperature (23ºC ± 2ºC), air humidity (55% ± 5%), light (an entraining light-dark cycle, comprising 12 h of light and 12 h of darkness, with lights on at 7 a.m. and off at 7 p.m.), light intensity (approximately 400 lux) and access to food and water ad libitum. All procedures were performed in mice of both sexes.

Following mouse strains were used in the *in vivo* experiments:

1. *Tgfbr2*$^{fl/fl}$ in a Blab-c background (originally in a 129SV background)
2. *α-Cre* mice in a FVB-N background
3. *LMOP-Cre* mice in a Balb-c background
4. Rosa-LacZ reporter mice in a 129SV background
5. Balb-c wildtype mice

Since it has been proven, that mouse strains vary in their susceptibility to light damage according to their genetic background (La Vail, M. M. et al., 1987; La Vail, Matthew M. et al., 1987; Noell et al., 1966), the first task before us was the conversion of the pigmented *Tgfbr2*$^{fl/fl}$ mice into an albino phenotype. For this purpose, mice carrying two unrecombined *Tgfbr2*$^{fl/fl}$ alleles were interbred with wild-type Balb-c mice. The backcrossing involved seven generations, whereby progeny, heterozygous for *Tgfbr2*$^{fl/-}$ were consistently mated with albino animals in a Balb-c background. After completion of this procedure F7 *Tgfbr2*$^{fl/-}$ mice were interbred with heterozygous mice, transgenic for *α-Cre* or *LMOP-Cre* (Figure 8). Progeny, heterozygous for both the floxed allele and the Cre recombinase, were crossed with *cre*-negative *Tgfbr2*$^{fl/-}$ animals from the F7 generation. Resulting offspring, carrying two *Tgfbr2*$^{fl/fl}$ alleles (Chytil et al., 2002) and differing in their genotype for *cre*, were used for further experiments.

Mice, carrying two *Tgfbr2*$^{fl/fl}$ alleles (Figure 10, upper panel) (Chytil et al., 2002) and heterozygous for *α-Cre* (*Tgfbr2*$^{fl/fl}$*;α-Cre*) (Figure 10, lower panel) (Marquardt et al., 2001),

had recombined and inactivated *Tgfbr2*$^{fl/fl}$ alleles in the neural retina cells that originate from the inner layer of the optic cup (Braunger et al., 2013b). For the sake of simplicity, *Tgfbr2*$^{fl/fl}$*;α-Cre* are referred to as *Tgfbr2*$^{\Delta oc}$ in this work, "oc" in resemblance to "optic cup". *α-Cre*-negative littermates with two unrecombined *Tgfbr2*$^{fl/fl}$ alleles were used as control mice.

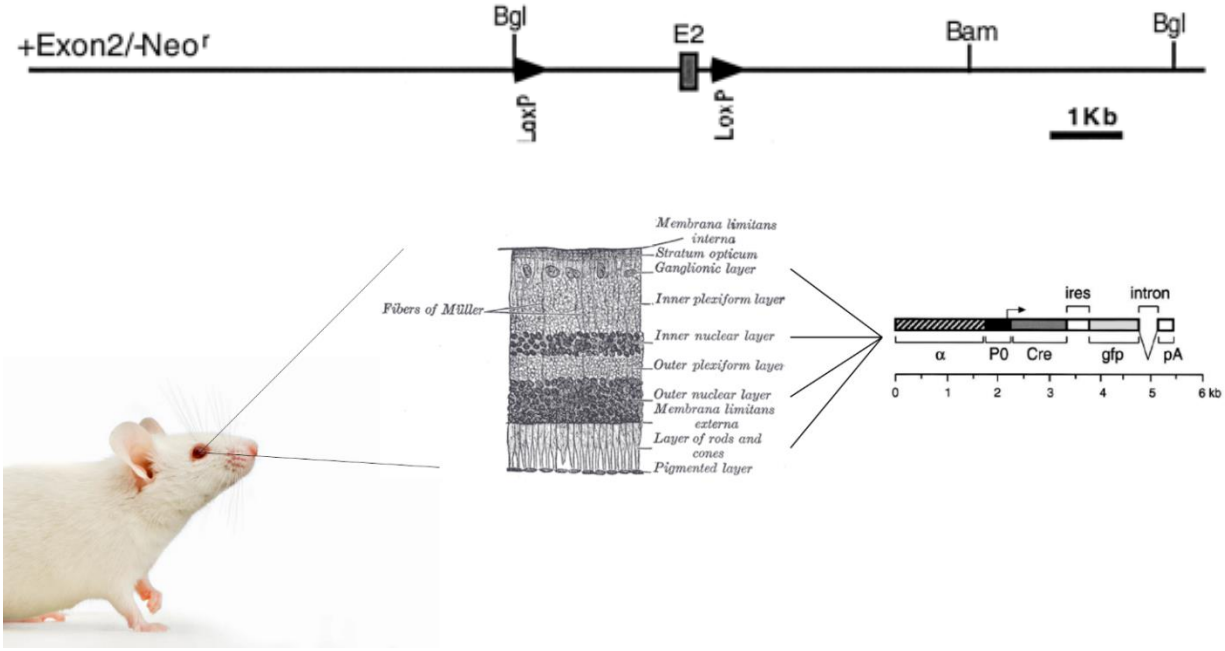


*Figure 10:* Schematic of the floxed TβRII gene and the *Pax6* α enhancer-directed *cre*-transgenic construct

Upper panel: A schematic of the targeted murine TβRII receptor gene. As a side note, mice showing deletion of Neo$^r$ cassette only were used as the founders for further conditional knockout studies of the TβRII receptor. Figure taken from (Chytil et al., 2002). Lower panel: In *α-Cre* mice, the sequence, encoding for the Cre recombinase, was placed under the control of an α enhancer element of the murine *Pax6* P0 promoter. A reporter gene-cassette *(IRES* (internal ribosomal entry site)-*gfp)* has been included in this construct, in order to encode common *cre*- and gfp-expression from a single mRNA. Figure of the construct taken from (Marquardt et al., 2001), the two other pictures taken from: http://www.emory.edu/EMORY_MAGAZINE/issues/2014/spring/features/animals.html and http://archive.org/stream/anatomyofhumanbo1918gray#page/1016/mode/2up

Mice, carrying two *Tgfbr2*$^{fl/fl}$ alleles (Figure 10, upper panel) (Chytil et al., 2002) and heterozygous for *LMOP-Cre* (a mouse rod opsin promoter-controlled *cre* transgene) (*Tgfbr2*$^{fl/fl}$*;LMOP-Cre*) (Figure 11) (Le et al., 2006), had recombined and inactivated *Tgfbr2*$^{fl/fl}$ alleles in rod photoreceptors and were used as experimental animals. For the sake of simplicity, *Tgfbr2*$^{fl/fl}$*;LMOP-Cre* are referred to as *Tgfbr2*$^{\Delta rod}$ in this work, "rod" in

resemblance to "rod photoreceptors". *LMOP*-negative littermates with two unrecombined *Tgfbr2*$^{fl/fl}$ alleles were used as control mice.

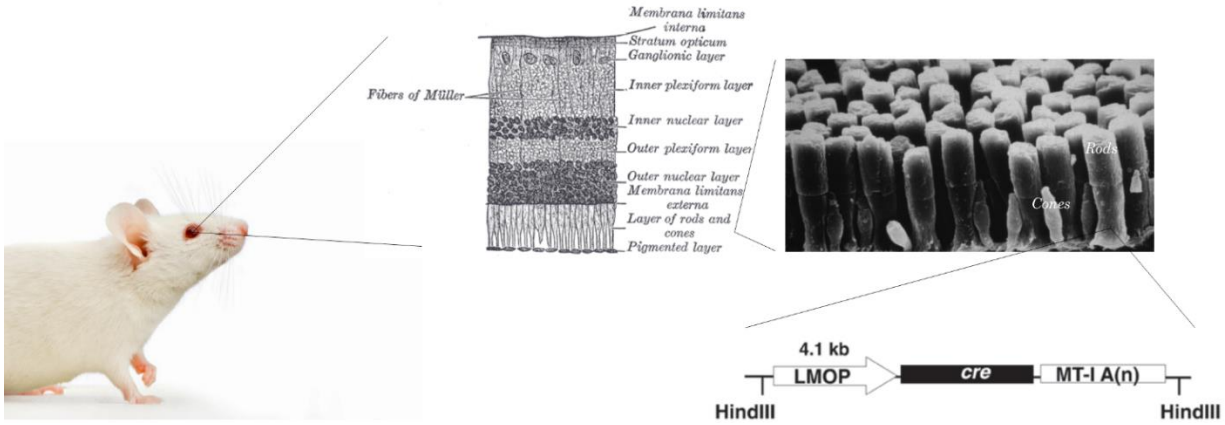


*Figure 11:* A schematic of the opsin promoter-directed *cre*-transgenic construct
LMOP represents the 4.1 kb-long mouse opsin promoter, followed by the coding region of the Cre recombinase gene, MT-I A(n), staying for an intron, containing a mouse metallothionein polyadenylation signal, and *Hind*III, representing restriction sites, flanking the transgene that carries the mouse opsin promoter.
Figure of the construct taken from (Le et al., 2006), the three other pictures taken from: http://www.emory.edu/EMORY_MAGAZINE/issues/2014/spring/features/animals.html, http://archive.org/stream/anatomyofhumanbo1918gray#page/1016/mode/2up
and
https://www.sas.upenn.edu/visual-studies/ (scanning electron micrograph (SEM) of rods' and cones' outer segments).

*Cre*-reporter mice (Rosa-LacZ) were purchased from the Jackson Laboratory (http://jaxmice.jax.org/, strain number: 3309, strain name: B6;129S4-Gt(ROSA)26Sor$^{tm1Sor}$/J). Mice, heterozygous for the Gtrosa26tm1Sor targeted mutation, were used to monitor the tissue/cellular expression pattern of the *cre* transgene in both *cre* mouse lines. Hence, homozygous Rosa-LacZ reporter mice (R26R) were interbred with either of both *cre*-transgenic strains (either *α-Cre*, or *LMOP*). Cre expression resulted in the removal of a loxP-flanked DNA segment that prevents the expression of the lacZ gene (Stop sequence), encoding the enzyme ß-Galactosidase. When crossed with a *cre*-transgenic strain, lacZ is expressed in cells/tissues where Cre is expressed (Figure 12) (Soriano, 1999). After performing ß-galactosidase staining, the blue color indicates tissue/cellular expression of the *cre* transgene in animals, heterozygous for both *cre* and the R26R allele. Animals, heterozygous for the R26R only, do not display any staining.

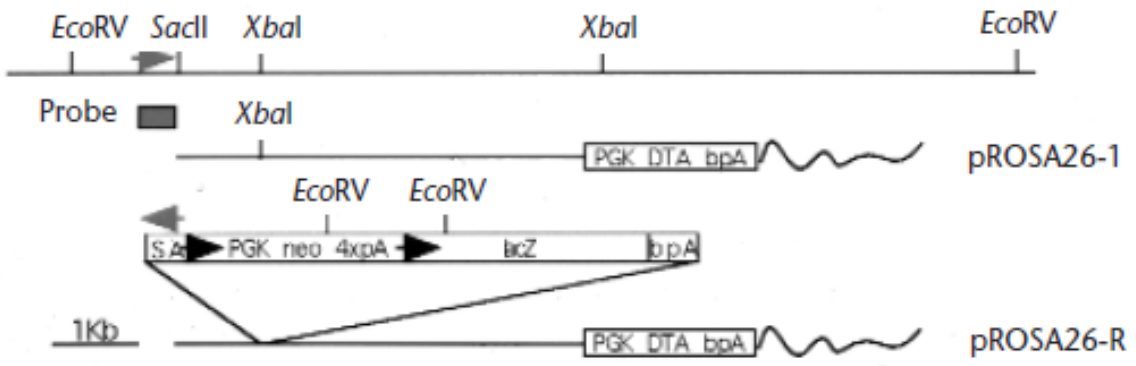


*Figure 12:* A schematic of the R26R construct
The ROSA26 locus of a gene-trap strain was targeted with a ROSA26 reporter (R26R) construct to generate a *cre*-reporter strain. The R26R construct was created by subcloning the pROSA26-1 vector and inserting a splice acceptor sequence (identical to the one, used in the original gene-trap allele), a neo expression cassette, flanked by loxP sites (indicated by black arrowheads), a lacZ gene and a polyadenylation sequence (bpA) at a unique *Xba*I site. Transcriptional read-through was prevented with the use of a triple polyadenylation sequence at the 3'-end of the neo expression cassette. Figure taken from (Soriano, 1999).

## 2.1.2 DNA analysis

### 2.1.2.1 DNA isolation from mouse tail biopsies

In order to obtain a tissue sample for the extraction of genomic DNA, the mice were sedated with isoflurane and the mouse tail tip, with a length of approximately 5 mm, was cut off and transferred to a 1.5 ml cup. Afterwards a mixture of 500 µl mouse tail lysis buffer (see Table 37) and 5 µl proteinase K (10 µg/µl stock solution, diluted hereby to a final concentration of 0.1 µg/µl) was pipetted thereto. The tissue samples were incubated at 50ºC overnight in a thermomixer at 13,000 rpm. DNA was precipitated (Table 1) prior to downstream applications.

*Table 1:* Procedure for DNA extraction

| Duration | Step | Result |
|---|---|---|
| 5 min | Add the same volume of isopropanol as lysis solution (500 µl), vortex thoroughly and incubate at -20ºC | DNA precipitation |
| 10 min | Centrifuge at 4ºC (13,000 rpm) and pipette the supernatant out (as few as possible – less than 50 µl, could be left over) | |
| 5 min | Add 500 µl of 70% ethanol and vortex to assure uniform dissemination throughout the sample<br>Incubate at room temperature | Alcohol washing the pellet and dissolving any remaining salt in the tube |
| 10 min<br>1 min | Centrifuge at 4ºC and 13,000 rpm, outpour the ethanol and centrifuge again | |
| 5 min | Pipette the rest of the ethanol out and air dry (not exceeding the indicated time limit, for drying out too long can interfere with following resuspension of the DNA) | |
| 5 min | Add 100 µl of 5mM Tris (pH 8.0) to each sample, vortex and incubate at room temperature | Resuspension of the DNA pellet |
| 1 min | Centrifuge at 4ºC and 13,000 rpm to get the hair at the bottom | |

5 µl of the supernatant of each tissue sample (through purification obtained concentration of 100-200 ng/µl) were diluted to a final concentration of 50 ng/µl. 1 µl of the dilution was taken as a DNA template for application in polymerase chain reaction (PCR) analysis.

### 2.1.2.2 Determination of the concentration of nucleic acids and assessment of their purity

The concentration of DNA samples was determined by measuring the intensity of absorbance at wavelengths 260 nm and 280 nm with the help of an UV-Vis Spectrophotometer NanoDrop 2000c (Thermo Fisher Scientific GmbH, Schwerte, Germany).

Based on the NanoDrop measurements each DNA tissue sample, which had a 260/280-ratio of absorbance ($A_{260/280}$) of at least 1.8, was diluted to a concentration of 50 ng/µl for application in polymerase chain reaction (PCR) analysis.

### 2.1.2.3 Genotyping: Polymerase chain reaction (PCR)

The polymerase chain reaction (PCR) was developed in 1983 by Kary Mullis (Mullis et al., 1986) and is a technique for the selective amplification of specific nucleotide sequences by a factor of $10^6$. Two oligonucleotide primers, flanking sequences of interest to be

amplified, are used in repeated cycles of enzymatic extension by a DNA polymerase. The essential steps in each cycle are heat denaturation of double-stranded target molecules, primer annealing to their complementary sequences within both strands and enzymatic synthesis of DNA. Each successive cycle essentially doubles the amount of DNA, synthesized in the previous cycle, hence the oligonucleotide primers can also bind to the complementary products. As a result, the flanked sequence accumulates exponentially to about $2^n$, n staying for the number of cycles. The use of the thermostable DNA polymerase, purified from the thermophilic bacterium Thermus aquaticus (Taq polymerase) makes the reaction simple and very specific (Saiki et al., 1988; Vosberg, 1989).

PCR analysis in this project was used in order to screen genotypes and distinguish wild-type from transgenic *α-Cre*, *LMOP*, *Tgfbr2*$^{fl/fl}$ and R26R animals. The detailed protocols are presented in Table 2-6, the PCR programs – in Table 7-11. Primer sequences are shown in Table 12. Mouse tail DNA was used as a template in all of the given protocols. After successful extraction of the genomic DNA from tail biopsies and purification of the nucleic acid samples prior to concentration measurement (Table 1), 50 ng DNA was used in each reaction to test for transgenic sequences.

A verification of transgenic *cre* animals *(α-Cre* or *LMOP)* was accomplished with the aid of Cre recombinase PCR.

*Table 2:* PCR protocol for Cre recombinase PCR

| Master mix | Volume |
|---|---|
| 5x DNA buffer | 3 µl |
| dNTPs (10 mM) | 0.3 µl |
| $MgCl_2$ (50 mM) | 0.5 µl |
| Cre primer fwd (10 µM) | 0.3 µl |
| Cre primer rev (10 µM) | 0.3 µl |
| *Taq* DNA polymerase | 0.15 µl |
| $H_2O$ | 9.45 µl |
| DNA template | 1 µl |
| Total reaction volume | 15 µl |

The TßRII PCR was used to determine, whether the transgenic sequence of TßRII was flanked by *flox* sites on both sides.

*Table 3:* PCR protocol for genotyping of *Tgfbr2*$^{fl/fl}$ animals

| Master mix | Volume |
|---|---|
| 5x DNA buffer | 5 µl |
| dNTPs (10 mM) | 0.5 µl |
| $MgCl_2$ (50 mM) | 0.75 µl |
| TGF-ß-R2 fwd (10 µM) | 0.5 µl |
| TGF-ß-R2 rev (10 µM) | 0.5 µl |
| *Taq* DNA polymerase | 0.5 µl |
| $H_2O$ | 16.25 µl |
| DNA template | 1 µl |
| Total reaction volume | 25 µl |

A *LacZ* PCR was performed to screen genotypes for *lacZ* expression in *cr*e-reporter mice.

*Table 4:* PCR protocol for genotyping of *LacZ* animals

| Master mix | Volume |
|---|---|
| 5x DNA buffer | 5 µl |
| dNTPs (10 mM) | 0.5 µl |
| $MgCl_2$ (50 mM) | 0.75 µl |
| Rosa26-LacZ fwd (10 µM) | 1 µl |
| Rosa26-LacZ rev (10 µM) | 1 µl |
| Mango *Taq* | 0.2 µl |
| $H_2O$ | 15.5 µl |
| DNA template | 1.05 µl |
| Total reaction volume | 25 µl |

To screen for the deletion of TßRII in the conditional knockout animals, a PCR analysis from Chytil and coworkers was used (Chytil et al., 2002) and the genotypes of the offspring from Cre-expressing transgenic *Tgfbr2*$^{fl/fl}$ animals were tested. To this end, whole retinae were isolated from adult *Tgfbr2*$^{\Delta oc/\Delta rod}$ and their control littermates.

*Table 5:* PCR protocol for *Tgfbr2* deletion

| Master mix | Volume |
|---|---|
| 10x DNA buffer | 2.5 µl |
| dNTPs (10 mM) | 0.5 µl |
| $MgCl_2$ (50 mM) | 0.75 µl |
| Chytil fwd (10 µM) | 0.5 µl |
| Chytil rev (10 µM) | 0.5 µl |
| *Taq* DNA polymerase | 0.5 µl |
| $H_2O$ | 18.75 µl |
| DNA template | 1 µl |
| Total reaction volume | 25 µl |

A point mutation in the *Rpe65* gene is responsible for a Leu450Met amino acid substitution, which is proven to increase retinal resistance against light-induced damage by slowing rhodopsin regeneration (see 1.2.2) (Grimm et al., 2000; Wenzel et al., 2001). Therefore, all of the animals, exposed to light in our experiments, were tested by a PCR analysis for the transgenic sequence of the leucine encoding allele. Since albino animals have a disposition to carrying the light-sensitive leucine variant (Danciger et al., 2000; Wenzel et al., 2003), most of our animals were identified as homozygous for the leucine type of the point mutation and only homozygous animals were included in this study.

*Table 6:* PCR protocol for genotyping for the leucine variant of *Rpe65* genotype at codon 450

| Master mix | Volume |
|---|---|
| 5x DNA buffer | 10 µl |
| dNTPs (10 mM) | 2 µl |
| $MgCl_2$ (50 mM) | 3 µl |
| MwoI fwd (10 µM) | 2 µl |
| MwoI rev (10 µM) | 2 µl |
| Mango *Taq* | 1 µl |
| $H_2O$ | 26 µl |
| DNA template | 4 µl |
| Total reaction volume | 50 µl |

To exclude false positive results, a negative control (the DNA template was substituted by water in such a solution) was run simultaneously together with the DNA-containing samples for every PCR analysis. The PCR products were separated on the agarose gel and the size of the signals was compared to a standard and a positive control that contained DNA of an already verified genotype.

Each PCR reaction tube was vortexed and centrifuged to get all of the solution to the bottom of the cup. PCR was run in a Thermocycler (T100™ Thermal cycler, Bio-Rad Laboratories GmbH, Munich, Germany) according to following protocols:

*Table 7:* Thermal cycle profile for Cre recombinase PCR

| Step | Temperature | Duration | |
|---|---|---|---|
| 1. Initialization | 95°C | 3 min | |
| 2. Denaturation | 95°C | 30 sec | 35x |
| 3. Annealing | 61°C | 30 sec | |
| 4. Extension/elongation | 72°C | 35 sec | |
| 5. Final elongation | 72°C | 5 min | |
| 6. Final hold | 12°C | ∞ | |

The distinguishing product of transgenic animals had the length of 270 bp. Controls did not show bands of a corresponding size.

*Table 8:* Thermal cycle profile for genotyping of *Tgfbr2*$^{fl/fl}$ animal

| Step | Temperature | Duration | |
|---|---|---|---|
| 1. Initialization | 95°C | 3 min | |
| 2. Denaturation | 95°C | 30 sec | 30x |
| 3. Annealing | 61°C | 1 min | |
| 4. Extension/elongation | 72°C | 1 min | |
| 5. Final elongation | 72°C | 5 min | |
| 6. Final hold | 8°C | ∞ | |

Depending on the presence of *flox* sites in *Tgbr2*$^{fl/fl}$ animals, two distinct bands were expected on an agarose gel: one band with a size of 556 bp for a wild-type allele, a product of 711 bp appears for a "floxed" allele. Heterozygous animals would show both signals.

*Table 9:* Thermal cycle profile for genotyping of *LacZ* animals

| Step | Temperature | Duration | |
|---|---|---|---|
| 1. Initialization | 94°C | 3 min | |
| 2. Denaturation | 94°C | 30 sec | 34x |
| 3. Annealing | 60°C | 30 sec | |
| 4. Extension/elongation | 72°C | 35 sec | |
| 5. Final elongation | 72°C | 5 min | |
| 6. Final hold | 10°C | ∞ | |

Every *LacZ* transgenic sample generated an amplified product with the molecular size of 315 bp.

*Table 10:* Thermal cycle profile for *Tgfbr2* deletion

| Step | Temperature | Duration | |
|---|---|---|---|
| 1. Initialization | 96°C | 3 min | |
| 2. Denaturation | 96°C | 30 sec | 34x |
| 3. Annealing | 62°C | 1 min | |
| 4. Extension/elongation | 72°C | 1 min | |
| 5. Final elongation | 72°C | 10 min | |
| 6. Final hold | 10°C | ∞ | |

The *Tgfbr2* deletion product was only amplified in samples, when the Cre recombinase had been active. This circumstance is caused through the fact that the product size for

control littermates accounts for 3974 bp, while the product size for transgenic animals is equal to 636bp. Due to the elongation time of the PCR program of 1 min, only a signal after Cre-mediated TßRII deletion (636 bp) is amplified (Braunger et al., 2013b). Actin was used as a loading control.

*Table 11:* Thermal cycle profile for genotyping for the leucine/methionine variant of the *Rpe65* gene

| Step | Temperature | Duration | |
|---|---|---|---|
| 1. Initialization | 94°C | 2 min | |
| 2. Denaturation | 94°C | 30 sec | 34x |
| 3. Annealing | 55°C | 45 sec | |
| 4. Extension/elongation | 72°C | 1 min | |
| 5. Final elongation | 72°C | 10 min | |
| 6. Final hold | 10°C | ∞ | |

4.5 µl of the PCR product (concentration: 100-150 ng/µl) were digested with 3 µl $H_2O$ and 0.3 µl *MwoI* for 3.5 h at 37°C. A manufacturer-recommended buffer could also be used instead of water. The digested samples were visualized on a 1% agarose gel, supplemented with ethidium bromide. The leucine variant of the *Rpe65* gene resulted in 2 bands (437 bp and 236 bp) after digestion (refer to 2.1.6.2), the methionine codon would generate just one band (673 bp). Heterozygous animals would have all three of the bands.

*Table 12:* Genotyping primer pairs

| Name | Mouse strain | Oligonucleotide sequence |
|---|---|---|
| Cre primer fwd<br>Cre primer rev | *α-Cre, LMOP* | 5'-ATGCTTCTGTCCGTTTGCCG-3' (sense)<br>5'-CCTGTTTTGCACGTTCACG-3' (antisense) |
| TGF-ß-R2 fwd<br>TGF-ß-R2 rev | *Tgfbr2$^{fl/fl}$* | 5'-GCAGGCATCAGGACCTCAGTTTGATCC-3' (sense)<br>5'-AGAGTGAAGCCGTGGTAGGTGAGCTTG-3' (antisense) |
| Rosa26-LacZ fwd<br>Rosa26-LacZ rev | R26R | 5'-ATCCTCTGCATGGTCAGGTC-3' (sense)<br>5'-CGTGGCCTGATTCATTCC-3' (antisense) |
| MwoI fwd<br>MwoI rev | Leu/met variant of Rpe65 | 5'-CACTGTGGTCTCTGCTATCTTC-3' (sense)<br>5'-GGTGCAGTTCCACTTCAGTT-3' (antisense) |
| Chytil fwd<br>Chytil rev | *Tgfbr2* deletion | 5'-TAAACAAGGTCCGGAGCCCA-3' (sense)<br>5'-AGAGTGAAGCCGTGGTAGGTGAGCTTG-3' (antisense) |

#### 2.1.2.4 Agarose gel electrophoresis

To visualize and check whether the PCR amplified the anticipated DNA sequence, agarose gel electrophoresis was used to separate the PCR products. For preparation of the gel, 1g of agarose was dissolved in 100 ml of TBE buffer. The mixtute was heated up in a microwave oven for 5 min, gently shaken halfway through this procedure and afterwards let to cool down for a couple of minutes. 3 µl of ethidium bromide was added to the then lukewarm solution, prior to pouring it in a slide and letting it cure for at least 30 min. Ethidium bromide is an intercalating agent, used as a nucleic acid stain because of its fluorescing with an intensive orange color, when exposed to ultraviolet light. 3.5 µl of DNA loading Dye (a dense compound, containing glycerol) was added to each one of the PCR products before vortexing, centrifuging and loading them on the agarose gel. TBE buffer was used as running buffer in the flatbed electrophoresis chamber. All agarose gels were run under following conditions for 45 min: 120 V, 500 mA. According to their molecular length, PCR products were separated by applying an electric field to the agarose gel matrix. The size of the DNA product was determined by comparing it to a DNA ladder (GeneRuler 100 bp DNA ladder, Fermentas, St. Leon-Rot), loaded in the very left well of the agarose gel and run alongside the PCR products. Furthermore, the amplicon was compared to DNA fragments of known size (positive control), allowing a correct determination of the product length. Subsequently, photos of the gels were taken using the IDA Gel Documentation Systems (raytest GmbH, Straubenhardt).

### 2.1.3 RNA analysis

The used RNA samples were isolated from retinae. Prior to this step, the animals were sacrificed (6 h after light damage) through cervical dislocation, the eye balls were harvested and the top the cornea then cut with a razor blade. The lens and the anterior part of the eye were carefully removed before separating the retina from the RPE, starting off at the optic nerve head.

#### 2.1.3.1 RNA isolation

The isolated samples were put in 2 ml Eppendorf tubes, arranged on ice, and immediately upon collection, total RNA was extracted from the retinae using 250 µl TRIzol (Invitrogen) for each one of the samples. TRIzol is a ready-to-use solution of phenol and guanidine isothiocyanate, facilitating an effective inhibition of RNase activity and integrity of the RNA during sample homogenization (Life Technologies, 2012). Following step consists in adding of chloroform to each one of the samples and centrifugation,

leading to the dissolution of the homogenate into three layers: a clear upper liquid layer (containing RNA), a semi-solid middle layer (containing DNA), and a red-colored bottom organic layer (containing DNA and proteins). Further details, regarding the RNA isolation protocol, are listed in Table 13 below, referring to (Life Technologies, 2012).

*Table 13:* RNA isolation procedure

| Duration | Step | Result |
|---|---|---|
| 5 min | Incubate the homogenate at room temperature | Dissolution of cell components |
| 15 sec | Add 0.2 mL of chloroform per 1 mL of TRIzol, then vortex | Separation in three phases |
| 2-3 min | Incubate at room temperature | |
| 15 min | Centrifuge the sample at 12,000 x g at 4°C | |
| | Pipette the upper colorless aqueous phase out to a new 1.5 ml tube | |
| | Add 0.5 mL of 100% isopropanol to the aqueous phase, per 1 ml of TRIzol, used for homogenization | RNA precipitation |
| 10 min | Incubate at room temperature | |
| 10 min | Centrifuge at 12,000 x g at 4°C | |
| | Remove the supernatant, leaving the RNA pellet only | |
| | Wash the pellet, with 1 mL of 75% ethanol per 1 ml of TRIzol (initial homogenization) | RNA wash |
| 5 min | Vortex briefly, then centrifuge at 7,500 x g at 4°C | |
| 5-10 min | Dry the RNA pellet | |
| | Re-suspend in RNase-free water or proceed to downstream application, or store at –80°C | RNA-resuspension |

### 2.1.3.2 Complementary DNA (cDNA) synthesis

A complementary copy is most often generated from a fully spliced mRNA template in a reaction, catalyzed by the enzyme reverse transcriptase (RT). This RNA-dependent DNA polymerase, which naturally occurs in retroviruses, operates on a single strand of the mRNA, synthesizing its complementary DNA. The reaction is based on the hybridizing of RNA base pairs (A, U, G and C) to the desoxyribonucleotide triphosphates (T, A, C and G, respectively). First-strand cDNA synthesis was performed using the iScript cDNA Synthesis Kit (BioRad) according to manufacturer's instructions - 1 µg of RNA in nuclease-free $H_2O$ was reverse transcribed according to the protocol below (Table 14) and the obtained cDNA was used as a template to amplify targeted genes (Table 15).

*Table 14:* cDNA synthesis: reagents and amplification program

| Reagents | In presence of RT | In absence of RT |
|---|---|---|
| iScript reverse transcriptase | 1 µl | - |
| 5x iScript reaction mix | 4 µl | 4 µl |
| 1 µg RNA template in $H_2O$ | 15 µl | 16 µl |
| Total reaction volume | 20 µl | 20 µl |

*Table 15:* Applied amplification program

| Temperature | Duration |
|---|---|
| 25°C | 5 min |
| 42°C | 30 min |
| 85°C | 5 min |
| 4°C | ∞ |

### 2.1.3.3 Quantitative real-time RT-PCR

A real-time polymerase chain reaction (RT-PCR) is a method, applied to quantitatively measure the amplification of DNA/mRNA with the aid of a fluorescent stain (SYBR-Green I). The use of a thermal cycler, which is capable of exposing the samples to light of a specific wavelength and sensing the emitted fluorescence, enables the detection of a target gene simultaneously to the observation of the reaction in *real time*. An increase in a certain DNA product during the PCR leads to an enhancement in fluorescence intensity, thus allowing DNA concentrations to be quantified. Quantitative RT-PCR analyses were performed using the Bio-Rad iQ5 Real-Time PCR Detection System. RNA that was not previously reverse transcribed (see Table 14) and $H_2O$ were run as negative controls simultaneously to minimize error probability. Further details, regarding the reaction mix and the thermal cycle profile, are displayed in Table 16, respectively Table 17.

*Table 16:* PCR protocol for quantitative real-time RT-PCR analysis

| Reagents | Volume |
|---|---|
| Sample (with/without addition of RT or with $H_2O$) | 0.15 µl |
| 10x PCR buffer | 1.5 µl |
| $MgCl_2$ (25 mM) | 0.6 µl |
| dNTPs (25 mM) | 0.12 µl |
| *Taq* DNA polymerase (5 U/µl) | 0.06 µl |
| SYBR-Green I (7.4% (v/v) in DMSO) | 0.19 µl |
| Fluorescein | 0.015 µl |
| Primer fwd | 0.17 µl |
| Primer rev | 0.17 µl |
| Nuclease-free $H_2O$ | 12.03 µl |
| Total reaction volume | 15.005 µl |

*Table 17:* Thermal cycling conditions for quantitative real-time RT-PCR analysis

| Temperature | Duration | |
|---|---|---|
| 95°C | 15 min | |
| 95°C | 10 sec | 40x |
| 60°C | 40 sec | |
| 72°C | 10 sec | |
| 95°C | 1 min | |
| 55°C | 1 min | |
| 55°C + 0.5°C per cycle (melting curve) | 6 sec | 81x |

As a last point in the depicted analysis, it was essential to run a dissociation (melting) curve. SYBR-Green I as a DNA-intercalating fluorophore would detect any double-stranded DNA, for example primer dimers or samples, contaminating actual DNA. The molecule slots by definition into the grooves of the double-stranded helix, an action, which has a stabilizing effect on DNA's structure, leading to a higher melting temperature. So by running a melting curve, we certified that the desired amplicon only was detected.

#### 2.1.3.4 Primer pairs for quantitative real-time RT-PCR

All primer pairs were purchased from Invitrogen and designed to extend over exon-exon splice junctions with one of the amplification primers potentially spanning the actual exon-intron boundary (except for *Gapdh*). Since intron-containing DNA would not be amplified, the risk of contamination due to non-coding gene fragments was reduced this way. For sequences of primer pairs, melting temperatures and real-time RT-PCR product sizes refer to Table 18.

*Table 18:* Primer sequences, used for quantitative real-time RT-PCR, melting temperatures and product sizes

| Gene | Sequence | Position | TM [°C] | Product size |
|---|---|---|---|---|
| *Gapdh* | 5'-tgtccgtcgtggatctgac-3' | 763–781 | 60 | 75 bp |
| | 5'-cctgcttcaccaccttcttg-3' | 818–837 | 60 | |
| *Gnb2l1* | 5'-tctgcaagtacacggtccag-3' | 514–533 | 59 | 88 bp |
| | 5'-acgatgatagggttgctgct-3' | 582–601 | 59 | |
| *Rpl32* | 5'-gctgccatctgttttacgg-3' | 29–47 | 59 | 98 bp |
| | 5'-gactggtgcctgatgaact-3' | 107–126 | 59 | |
| *Lif* | 5'-aaacggcctgcatctaagg-3' | 172–190 | 60 | 93 bp |
| | 5'-agcagcagtaagggcacaat-3' | 245–264 | 59 | |
| *Bdnf* | 5'-agtctccaggacagcaaagc-3' | 614–633 | 59 | 94 bp |
| | 5'-tgcaaccgaagtatgaaataacc-3' | 685–707 | 60 | |
| *Edn2* | 5'-acctcctccgaaagctgag-3' | 502–520 | 59 | 76 bp |
| | 5'-tttcttgtcacctctggctgta-3' | 556–577 | 59 | |
| *Fgf2* | 5'-cggctctactgcaagaacg-3' | 285–303 | 59 | 108 bp |
| | 5'-tgcttggagttgtagtttgacg-3' | 371–392 | 60 | |

The precision of the performed quantification was certified through a normalization of the expression level of the target gene to that of a stably expressed gene – a housekeeper gene. Hence, the relative quantification in this type of analyses was based on internal reference genes to determine and correct non-specific variations in the change of the expression level of the target gene. This way, possible differences in RNA quantity or quality across experimental samples were detected. In order to determine the most suitable internal control gene, three different potential housekeeping genes were tested: *Gapdh*, *guanine nucleotide binding protein, beta polypeptide 2-like 1 (Gnb2l1)* and *ribosomal protein L32 (Rpl32)*. After an initial statistical algorithm was carried out for the different housekeepers, the geo mean of the genes was used for the relative quantification of retinae samples. Relative quantification was performed applying Bio-Rad iQ5 Standard-Edition (Version 2.0.148.60623) software (BioRad Laboratories GmbH, Munich) and the ΔΔCt method in Excel (Microsoft Corp., Redmond, WA, USA).

### 2.1.4 Protein analysis

#### 2.1.4.1 Protein isolation

Neural retinae were treated with TRIzol (Invitrogen) following the manufacturer's instructions, similarly as described for RNA samples previously. The proteins were isolated from the phenol-ethanol supernatant layer, left over after an optional DNA

precipitation (DNA can be obtained from the interphase and phenol-chloroform layer, saved from the phase separation step – refer to 2.1.3.1 and Table 13 for a brief recollection). Further details, regarding this procedure, are itemized in Table 19 and based on (Life Technologies, 2012).

*Table 19:* Protein isolation procedure

| Duration | Step | Result |
|---|---|---|
| | Add 0.3 ml of 100% ethanol per 1 ml of TRIzol (used for the initial homogenization) to the interphase and phenol-chloroform layer, saved from the phase separation step | |
| 2-3 min | Incubate samples at room temperature | (Optional) |
| 5 min | Centrifuge at 2,000 x g at 4°C to pellet the DNA | DNA isolation |
| | Transfer the phenol-ethanol supernatant to a new tube | |
| | (Proceed with the DNA wash step and the DNA resuspension, using the DNA pellet, if desired) | |
| | Add 1.5 ml of isopropanol to the phenol-ethanol supernatant per 1 ml of initially used TRIzol | |
| 10 min | Incubate samples at room temperature | Protein precipitation |
| 10 min | Centrifuge at 12,000 x g at 4°C to pellet the protein, remove and discharge the supernatant | |
| 3x 20 min | Incubate the protein pellet in 2 ml of a prepared wash solution (consisting of 0.3 M guanidine hydrochloride in 95% ethanol) per 1 ml of TRIzol (used for the initial homogenization) (to remove rests of dye and phenol) | |
| 3x 5 min | Centrifuge at 7,500 x g at 4°C to re-acquire the pellet, remove and discharge the wash solution | Precipitated protein wash |
| | Add 2 ml of 100% ethanol to the protein pellet and vortex | |
| 5 min | Centrifuge at 7,500 x g at 4°C, remove and discharge the | |
| 5-10 min | ethanol wash. Dry the protein pellet | |
| | Add a) 1% SDS (200 µl) to the protein pellet and protease inhibitors (1:1000) – to recover phosphorylated proteins – | |
| Overnight | and incubate at 50°C in a heat block to completely solubilize the protein pellet | |
| | **OR** b) urea buffer as an alternative approach (if the protein pellet is insoluble in SDS – poor solubility may be traced | |
| 15 min | back to inappropriate solvents) and incubate at 65°C | Protein resuspension |
| 10 min | Sediment by centrifugation at 10,000 x g at 4°C to get any insoluble material to the bottom of the tube | |
| | Transfer the supernatant, containing the solution with the extracted protein, to a clean tube | |
| | Proceed to downstream applications immediately, or store the sample at –80°C | |

#### 2.1.4.2 Western blot analysis

The Western blot analysis is a molecular biology technique, used to detect target proteins. This method makes use of an electrophoretic transmission of proteins from polyacrylamide/agarose composite gels, where they are fractioned initially by molecular weight, and then transferred in a second step to nitrocellulose membranes. These membranes are then stained with antibodies, specific to the target protein (Renart et al., 1979; Towbin et al., 1979). The method originates from the laboratory of Harry Towbin (Towbin et al., 1979). W. Neal Burnette referred to the technique first-time as Western blot (Burnette, 1981), which is an allusion to the name Southern blot – a method for DNA detection by probe hybridization, called after its developer Edwin Southern.

In detail, the protein samples, used in Western blot analyses, were first separated by SDS-PAGE (10% acrylamide gel electrophoresis) and then transferred by semidry blotting (blot device, run for 1.5 h at 25 V and to a maximum of 2000 mA) onto activated (by Methanol) polyvinyl difluoride membranes (PVDF; Millipore). Subsequently, the membranes were incubated at room temperature with a blocking reagent (refer to Table 20), solved in Tris-buffered saline (TBS), containing 0.1% Tween 20 (TBS-T; pH 7.2). The following incubation step was performed at 4ºC overnight. To this end, the membranes were transferred to a falcon and incubated with a primary antibody (TβRII-L21, pSMAD3, pAKT or AKT), solved in BSA or non-fat dry milk in TBS-T. The antibodies and the appropriate blocking reagents thereto are listed in Table 20. The membranes were washed thoroughly (3x 5 min) with TBS-T, prior to an incubation step of the respective secondary antibody in a 1:5000 or 1:2000 proportion for an hour at room temperature. After washing the membranes again with TBS-T (3x 5 min), a horseradish peroxidase (HRP) detection reagent was applied and chemiluminescence was analyzed on a BAS 3000 imager workstation (Fujifilm). For normalization, protein samples were also stained with antibodies for the housekeeping gene glyceraldehyde 3-phosphate dehydrogenase (GAPDH, in a 1:5000-ratio, horseradish peroxidase-conjugated, Abcam). Western blot signals were compared by relative densitometry with the Aida Image Analyzer v.4.06 software (Raytest) (method presented in (Braunger et al., 2013b)).

*Table 20:* Antibodies and respective blocking reagents, used for Western blot analyses

| Primary antibody | Blocking reagent | Secondary antibody |
|---|---|---|
| TβRII-L21 (Santa Cruz Biotechnology); 1:200 in 0.5% BSA in TBS-T | 5% non-fat dry milk in TBS-T for 10 min + 5% BSA in TBS-T for 30 min | Chicken anti-rabbit, coupled to horseradish peroxidase (Santa Cruz Biotechnology); 1:5000 |
| pSMAD3 (Abcam); 1:300 in 0.5% BSA in TBS-T | 5% BSA in TBS-T for an hour | Chicken anti-rabbit, coupled to horseradish peroxidase (Santa Cruz Biotechnology); 1:5000 |
| pAKT (Cell Signaling); 1:500 in 0.3% BSA in TBS-T | 3% BSA in TBS-T for an hour | Chicken anti-mouse, coupled to alkaline phosphatase (Santa Cruz Biotechnology); 1:2000 |
| AKT (Cell Signaling); 1:1000 in 0.5% non-fat dry milk in TBS-T | 5% non-fat dry milk in TBS-T for an hour | Goat anti-rabbit, coupled to horseradish peroxidase (Rockland); 1:2000 |
| Glyceraldehyde 3-phosphate dehydrogenase (Abcam); 1:5000 in 0.5% BSA in TBS-T | 5% BSA in TBS-T for 30 min | **no** secondary antibody required |

### 2.1.5 Histology

#### 2.1.5.1 Epon embedding, semithin sections and phenotype analysis

In order to accomplish morphologic and morphometric analyses, untreated (no light) and light-exposed animals were sacrificed. To this end, the enucleated eyes of experimental light-exposed mice were analyzed 14 days after light damage and the eyes of their untreated control littermates were taken at age between 6 and 8 weeks. Prior to enucleation, the eyes were marked on the superior limbus (12 o'clock) using a 27-gauge needle, heated with the Bunsen burner, and then fixed for at least 24 h in Ito's fixative (Ito, S. and Karnovsky, M.J, 1968) – consisting of 2.5% paraformaldehyde (PFA) plus 2.5% glutaraldehyde (Serva, Heidelberg) in sodium cacodylate buffer (0.2 M; pH 7.6; Serva, Heidelberg). This here slightly modified fixative is colloquially known as "Karnovsky's fix", referring to (Karnovsky, 1965), according to the Science Citation Index the publication with the most cited abstract in the history of science. Two hours after starting the fixation, the branding identification tag was assigned by a metal minutiens, since it is easier to handle during and after the embedding process. Then, the cornea was sliced, allowing the fixative to enter the eye ball, as fundus appearance was most important for our experiments (detailed method elaborated in a manuscript in

preparation (Braunger et al.)). Following the 24 h fixation step, the eyes were repeatedly rinsed (at least 4x 30 min) with Caco buffer (sodium cacodylate buffer, diluted in distilled water in a 1:1 proportion) and post-fixed for another 3.5 h in osmium ferrocyanide (2% $OsO_4$ (Science Service, München), 1.6% potassium ferrocyanide (Merck, Darmstadt), diluted in 0.2 M cacodylate buffer) (after (Forbes and Sperelakis, 1977; Moses and Claycomb, 1982)) at 4ºC. The use of a potassium ferrocyanide-reduced osmium post-fixation was suggested by Elbers and coworkers and Karnovsky (Elbers, P. F. et al., 1965; Karnovsky, 1971) to promote the integrity of cell membranes, thus contributing to stable fixation. Osmium was thereafter washed out through distilled $H_2O$ in at least 4 steps at 10ºC, in order to prevent any precipitating deposits. Subsequently, the eyes underwent a serial dehydration treatment, consisting of an alcohol sequence of a gradually increasing concentration. Further details, considering the wash steps, are listed in Table 21.

*Table 21:* Dehydration prior to Epon embedding

| Step | Reagent | Temperature | | Duration |
|---|---|---|---|---|
| 1., 2. | 25% ethanol | 4ºC | 2x | 15 min |
| 3., 4. | 35% ethanol | 4ºC | 2x | 15 min |
| 5., 6. | 50% ethanol | 4ºC | 2x | 15 min |
| 7., 8. | 60% ethanol | 4ºC | 2x | 15 min |
| 9., 10. | 70% ethanol | 4ºC | 2x | 15 min |
| 11. | 70% ethanol | 4ºC | | Intermediate storage (at least 2 d) |
| 12., 13. | 80% ethanol | 4ºC | 2x | 40 min |
| 14., 15., 16. | 90% ethanol | Room temp. | 3x | 40 min |
| 17., 18., 19. | 100% ethanol | Room temp. | 3x | 45 min |

Eventually, the specimens were embedded in Epon (Serva, Hidelberg, Germany) according to standard methods, as previously described in (Kritzenberger et al., 2011) (Table 22). Automated dehydration and embedding steps were both performed in the tissue processing automat Leica EM TP (Leica microsystems GmbH, Wetzlar, Germany), which is capable of maintaining a constant resin processing temperature.

*Table 22:* Standard methods for Epon embedding

| Step | Reagent | Proportion | | Duration |
|---|---|---|---|---|
| 1., 2. | Propylene oxide | | | 20 min |
| 3. | Propylene oxide/Epon | | 2x | 120 min |
| 4. | Propylene oxide/Epon | 3:1 | | 120 min |
| 5. | Propylene oxide/Epon | 1:1 | | 120 min |
| 6. | Epon | 1:3 | | Overnight |
| 7. | Fresh Epon (in a sealable dessicator) | | | 1-2 days |

A polymerization step was performed in an incubator: first for 2 h at 30ºC and then at 60ºC for 48 h. The samples were eventually left to cool down for 30 min at 4ºC.
The next step in processing the specimens for light microscopy and assessing the impact of light damage was the slicing of semithin sections with a thickness of 1.0 µm using an Ultracut E Reichert-Jung Microtome (Cambridge Instruments GmbH, Nussloch, Germany) and beginning at the inferior side. It was especially paid attention to the slices being cut along the mid-horizontal plane (in a nasal-temporal orientation through the middle of both quadrants) and to displaying the middle of the optic nerve head (ONH) and the pupil, in order to guarantee a similar position in each sample this way. Comparable quadrants were essential for further analyses, since it is established knowledge that the extent of photoreceptor light damage to rodents' eyes differs among retinal regions (La Vail, M. M. et al., 1987; La Vail, Matthew M. et al., 1987; Tanito et al., 2008). Subsequently, the obtained sections were stained according to the Richardson's protocol (Richardson, K. C. et al., 1960) for 15-30 sec at 60ºC. Images of the retina were acquired with the help of a light microscope with a panorama function – Axio Imager Z1 (Zeiss, Göttingen, Germany) – and at a high enough resolution (63x lens).

#### 2.1.5.2 Morphometric analysis

Before measuring the thickness of the inner (INL) or outer nuclear layer (ONL), the respective measurement points were defined. Therefore, the distance between the ora serrata (OS) and the optic nerve head (ONH) was quantified following the circumference of the retinal pigment epithelium (RPE) in each hemisphere. As this step requires the measurement of a curved line, it was accomplished via the morphometric software ImageJ (module: Segmented line). The traced distance was then divided into tenths, using an ImageJ plug-in, purpose-written by Sebastian Koschade, and the final nine measure points were assigned between each tenth of total length (Figure 13A.) (referring to similar methods (Hao et al., 2002; La Vail, M. M. et al., 1987) and to a manuscript in preparation (Braunger et al.)).
The thickness of the INL and ONL was subsequently measured at the nine marked positions, starting off at the periphery of the temporal side and proceeding across the ONH to the OS on the opposite nasal side. The narrow angle between the ONH and the sclera was labeled to be on the nasal half of the mid-horizontal plane through the eyeball. The measurement step was performed via the image acquisition and analysis software AxioVision SE64 (release 4.9.1, Carl Zeiss, Göttingen, Germany; module: measure length). The means and corresponding standard deviations and standard errors of the

mean were calculated for each one of the equidistant loci (in each of the experimental and control groups of animals) in Excel (Microsoft Corporation, Redmond, WA, USA) and the results were depicted in form of spider diagrams (Figure 13B.) (method described in a manuscript in preparation (Braunger et al.)).

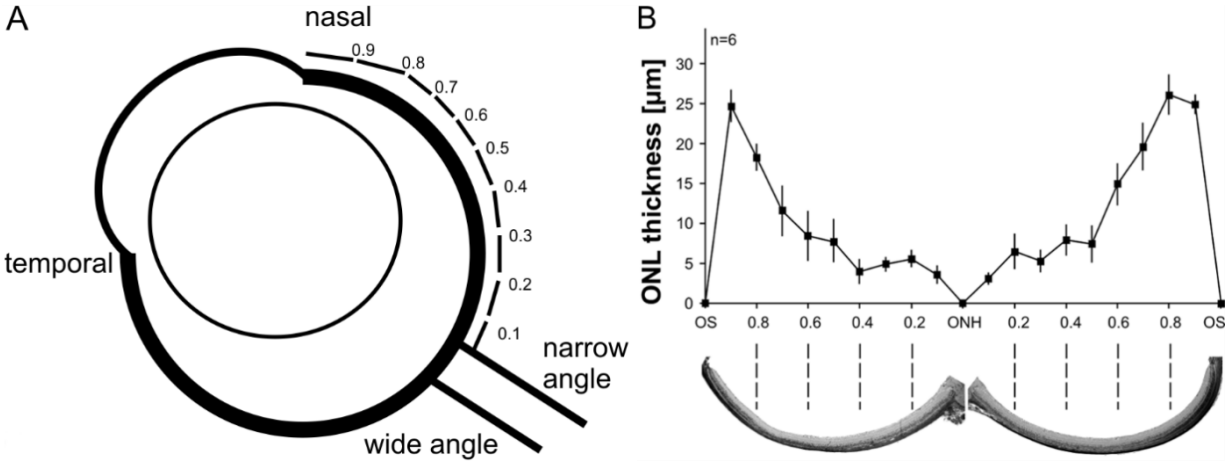


*Figure 13:* Morphometric analysis following light exposure
A. A schematic of the exemplary positioning of nine measure points (between each 10th of total length) on the nasal hemisphere for inner (INL) and outer nuclear layer (ONL) thickness quantification. The following measurements were performed at the assigned marks. The narrow angle between the optic nerve and the sclera was assigned to be on the side of the nasal hemisphere. B. The exemplary spider diagram of a light-exposed retina displays the ONL thickness at 21 adjacent measure points and corresponds to the panorama light microscopy image below. OS, Ora serrata; ONH, optic nerve head. Figure taken from a manuscript in preparation (Braunger et al.).

### 2.1.5.3 Paraffin embedding and slices

Prior to paraffin embedding, the enucleated eyes were brand marked on the superior limbus (12 o'clock), fixed for 4 to 6 h in 4% paraformaldehyde in 0.1 M phosphate buffer (pH 7.4) and subsequently rinsed thoroughly according to standard protocols (refer to Table 23 for further details).

*Table 23:* Washing steps, prior to paraffin embedding of enucleated eyeballs

| Step | Reagent | | Duration |
|---|---|---|---|
| 1., 2., 3., 4. | 0.1 M phosphate buffer (pH 7.4) | 4x | 20 min |
| 5. | 50% isopropanol | | 1 h |
| 6. | 70% isopropanol | | 1 h |
| 7. | 70% isopropanol | | Storage |

As elaborated in 2.1.5.1, the branding identification tag was subsequently assigned by a metal minutiens to facilitate the embedding procedure. Following dehydration (a procedure, consisting of an alcohol sequence with gradually ascending concentration), clearing and infiltration steps (Table 24) were performed in a paraffin tissue processor HMP 110 (Microm International, Walldorf, Germany).

*Table 24:* Paraffin dehydration and embedding program

| Step | Reagent | Duration |
|---|---|---|
| 1. | 70% isopropanol | 1 h |
| 2. | 80% isopropanol | 1 h |
| 3. | 96% isopropanol | 1 h |
| 4. | 96% isopropanol | 2 h |
| 5. | 100% isopropanol | 1 h |
| 6. | 100% isopropanol | 1 h |
| 7. | 100% isopropanol | 2 h |
| 8. | Xylene | 1 h |
| 9. | Xylene | 1.5 h |
| 10. | Paraffin | 2 h |
| 11. | Paraffin | 8 h |

Following this processing sequence, the tissue specimens were overlaid in a paraffin wax embedding centre type MPS/P2 (SLEE Medical, Mainz, Germany). The paraffin sections (6.0 µm) were cut along the mid-horizontal plane, as described in 2.1.5.1, with the aid of a Reichert-Jung Supercut 2050 Microtome (Cambridge Instruments GmbH, Nussloch), transferred to a water heat bath and then mounted onto microscope slides (SuperFrost/Plus; Menzel).

Prior to downstream procedures, the prepared formalin-fixed, paraffin-embedded tissue sections needed to be deparaffinized and rehydrated, undergoing an alcohol array of decreasing concentration (Table 25).

*Table 25:* Deparaffinization and rehydration of paraffin-embedded sections

| Step | Reagent | | Duration |
|---|---|---|---|
| 1., 2. | Xylene | 2x | 10 min |
| 3., 4. | 100% isopropanol | 2x | 10 min |
| 5., 6. | 96% isopropanol | 2x | 5 min |
| 7., 8. | 80% isopropanol | 2x | 5 min |
| 9. | 70% isopropanol | | 5 min |
| 10. | 50% isopropanol | | 5 min |

Thereupon, the deparaffinized sections were rinsed in deionized water with stirring for 5 min, washed with phosphate buffered saline (PBS) for 5 min, immersed in a 0.89% NaCl for 5 min and then washed again with PBS twice, each time for 5 min.

#### 2.1.5.4 Immunohistochemistry for detection of TßRII and pSMAD3

The technique of immunohistochemistry visualizes the distribution of specific tissue components by assessing the chemical linkage between target epitopes and suitable antibodies, tagged to a fluorophore (e.g. fluorescein). Although it had been known since the 1930s, following method was first described by (Coons et al., 1942), who used FITC-labeled antibodies to investigate Pneumococcal antigens in infected tissue.

Following the deparaffinization step (see Table 25), which enables the antibody-mediated antigen detection, the sections were treated according to Table 26**,** in order to investigate the localization of TßRII and pSMAD3 proteins in the retina. Formalin-fixed sections underwent a retrieval with boiling citrate buffer (pH 6) to unmask antibody epitopes, crosslinked by methylene bridges, which were induced by formaldehyde fixation. To diminish the effect of background staining and emphasize the preferential avidity of the antibody, the specimens were incubated with a blocking buffer at room temperature (in this case 2% BSA, diluted either in PBS (for TßRII), or in TBS-T (for pSMAD3)). Primary antibodies (listed in Table 27), solved in a 1:20 proportion (in 0.2% BSA in PBS or TBS-T, respectively) to help stabilize the antibody and facilitate coherent dissemination, were applied at 4ºC overnight. The washing steps before every antibody application were essential for the removal of unbound antibodies. Subsequently, the specimens were treated for an hour with biotinylated secondary antibodies, solved in a 1:500 proportion (in 0.2% BSA in PBS or TBS-T), and then (for another hour) with Streptavidin Alexa 488 in a 1:1000 proportion (in 0.2% BSA in PBS or TBS-T). Streptavidin constitutes a fluorescently labeled biotin-binding protein that enables the most common indirect method of detecting and amplifying the target signal. The conjugated fluorescent reporter was later detected by fluorescent microscopy (Axio Imager Z1 (Zeiss, Göttingen, Germany)). Counterstaining was performed with DAPI (4',6-Diamidion-2-phenylindole, Vectashield; Vector Laboratories, Burlingame, CA), diluted in a 1:10 proportion in a fluorescent mounting medium (DakoCytomation, Hamburg, Germany), in order to intensify and give contrast to the initial stain. Eventually, the specimens were sealed by mounting a coverslip to stabilize the stain and discourage bleaching of the fluorescent marker.

*Table 26:* Immunohistochemistry for TßRII and pSMAD3

| Step | Reagent | | Duration |
|---|---|---|---|
| 1. | Boiling citrate buffer (pH 6) | | 10 min |
| 2. | Deionized water | | 5 min |
| 3. | 0.1 M phosphate buffer | | 5 min |
| 4., 5., 6. | 0.1 M phosphate buffer (*TßRII*)/TBS-T (*pSMAD3*) | 3x | 5 min |
| 7. | 2% bovine serum albumin in 0.1 M PBS/ TBS-T respectively | | 45 min |
| 8. | TßRII-L21/pSMAD3 (1:20 in 0.2% BSA in 0.1 M PBS/TBS-T) | | overnight |
| 9., 10., 11. | 0.1 M phosphate buffer or TBS-T | 3x | 5 min |
| 12. | Anti-rabbit, biotinylated (1:500 in 0.2% BSA) | | 1 h |
| 13., 14., 15. | 0.1 M phosphate buffer or TBS-T | 3x | 5 min |
| 16. | Streptavidin Alexa 488 (1:1000 in 0.2% BSA) | | 1 h |
| 17., 18., 19. | 0.1 M phosphate buffer or TBS-T | 3x | 5 min |
| 20. | Counterstaining with DAPI (1:10 in Dako) | | |

*Table 27:* Antibodies, used for immunohistochemistry

| Primary antibody | Fixation | Secondary antibody |
|---|---|---|
| *TßRII-L21* (Santa Cruz Biotechnology); 1:20 in 0.2% BSA in 0.1 M PP | 4% PFA | Anti-rabbit, biotinylated (Vector); 1:500 and Streptavidin Alexa 488 (Invitrogen); 1:1000 |
| *pSMAD3* (Cell Signaling Technology); 1:20 in 0.2% BSA in TBS-T | 4% PFA | Anti-rabbit, biotinylated (Vector); 1:500 and Streptavidin Alexa 488 (Invitrogen); 1:1000 |

### 2.1.5.5 ß-Galactosidase histochemistry

ß-Galactosidase staining (Byrne et al., 1994) was performed, in order to assay for ß-Galactosidase activity and verify the recombinase efficiency and pattern, generated by the expression of the *cre* transgene. Hence, homozygous Rosa-LacZ reporter mice (R26R) (Soriano, 1999) were interbred with either of both *cre*-transgenic strains (either *α-Cre*, or *LMOP*), as described in 2.1.1). Enucleation of the eyes of their offspring was performed at age between 7 days and 4 weeks, followed by a fixation step in 0.2% glutaraldehyde in 0.1 M PBS (pH 7.3) for approximately 30 min (according to previously published protocols (Baulmann et al., 2002; DasGupta and Fuchs, 1999)). Subsequently, the eyes were washed extensively (3x 10 min) with a detergent rinse, consisting of 0.01% sodium deoxycholate (NaDC), 0.02% Tergitol NP-40 (to reduce surface tension of the solution), 2 mM MgCl2 and 0.1 M phosphate buffer, pH 7.3, and incubated in X-Gal staining solution (Byrne et al., 1994) (0.01% sodium deoxycholate (NaDC), 0.02% Tergitol NP-40, 2 mM $MgCl_2$ and 0.1 M phosphate buffer, pH 7.3, 5 mM potassium ferricyanide ($K3[Fe(CN)_6]$), 5 mM potassium ferrocyanide ($K_4[Fe(CN)_6] \cdot 3\ H_2O$) and 1 mg/ml X-Gal) at 37°C in the dark. The target protein ß-Galactosidase was detected by employing its enzymatic activity of

converting the colorless substrate 5-bromo-4-chloro-3-indolyl-ß-D-galactopyranoside (X-Gal) to an insoluble blue product 5,5'-dibromo-4,4'-dichloro-indigo (Byrne et al., 1994). After the staining procedure the samples were rinsed thoroughly again (3x 10 min) with the mentioned wash buffer and with 0.1 phosphate buffered saline (PBS) for 10 min. The specimens were then processed for paraffin embedding (2.1.5.3), after undergoing the washing steps 5.-7., listed in Table 23. The ß-Gal activity was later visualized by light microscopy (Axio Imager Z1 (Zeiss, Göttingen, Germany)). After performing lacZ staining, the blue color indicated tissue/cellular expression and activity of the *cre* transgene in animals, heterozygous for both *cre* and the R26R allele, whereas heterozygous R26R animals (not transgene for *cre*) did not generate any chromogenic response (Soriano, 1999).

### 2.1.5.6 Apoptotic cell death: TUNEL analysis

Apoptosis is a programmed cell death, associated with endogenous endonuclease activity (Wyllie, 1980) and hallmarked by chromatin cleavage into low molecular weight fragments (Kerr et al., 1972). It is defined by some morphological features, including nuclear chromatin condensation, shrinkage of cytoplasmatic organelles, protrusion of the cell membrane and chromosomal DNA fragmentation (Kerr et al., 1972; Wyllie et al., 1984), followed by phagocytosis and digestion by resident cells (Wyllie et al., 1980).

The TUNEL (terminal deoxynucleotidyl transferase-mediated dUTP nick end labeling) assay was originally described by Gavrieli et al. in 1992 as a method for in situ labeling of DNA breaks at single-cell level and for application in the study of tissue dynamics (Gavrieli et al., 1992) and significantly improved in its sensitivity in the following years (Negoescu et al., 1996; Negoescu et al., 1998). The method utilizes the specific interaction of 3'-OH nick ends of DNA with terminal deoxynucleotidyl transferase (TdT). This enzyme catalyzes the incorporation of fluorescently modified 2'-deoxyuridine-5'-triphosphate (fluorescein-12-dUTP) at sites of DNA breaks, materializing a polydeoxynucleotide polymeric tail (Gavrieli et al., 1992).

Following a 30 min exposure to light, the eyes of experimental light-exposed animals and their untreated control littermates were enucleated 30 h thereafter. Nuclear DNA fragmentation, resulting from the apoptotic signaling cascade, was analyzed and quantified by the TUNEL imaging assay, using the Apoptosis Detection System (DeadEnd Fluorometric TUNEL system; Promega) and according to the slightly modified manufacturer's instructions (Promega, 2009). Prior to TUNEL analysis, which was performed on formalin-fixed, paraffin-embedded tissue sections (6.0 µm), the samples

were processed, as described previously (2.1.5.3), and deparaffinized and rehydrated, undergoing an alcohol array of decreasing concentration according to the protocol, described in Table 25. Thereupon, the deparaffinized sections were rinsed in deionized water with stirring for 5 min, washed with phosphate buffered saline (PBS) for 5 min, immersed in a 0.89% NaCl for 5 min and then washed again with PBS twice, each time for 5 min.

Subsequently, TUNEL-labeling was performed on the pretreated deparaffinized sections according to Table 28 (Promega, 2009). In order to permeabilize tissues to the staining reagents in the following steps, 10 mg/ml Proteinase K was diluted in a 1:500 proportion with PBS and applied thereto. A standard 50 µl volume of rTdT (recombinant terminal deoxynucleotidyl transferase) reaction mix, designated for an area not larger than 5 $cm^2$, was prepared by compounding 45 µl Equilibration buffer, 5 µl nucleotide mix and 1 µl rTDT enzyme. It was added to each one of the tissue samples, prior to incubation at 37°C and avoiding exposure to light from this step forward. Counterstaining was performed with DAPI (4',6-Diamidion-2-phenylindole, Vectashield; Vector Laboratories, Burlingame, CA), diluted in a 1:10 proportion in fluorescent mounting medium (DakoCytomation, Hamburg, Germany), in order to intensify and give contrast to the primary stain. Eventually, the specimens were sealed by mounting a coverslip.

*Table 28:* TUNEL reaction (after modified manufacturer's instructions (Promega, 2009))

| Step | Reagent | | Duration | Intention |
|---|---|---|---|---|
| 1. | 4% PFA in PBS | | 15 min | Fixate |
| 2., 3. | PBS | 2x | 5 min | Wash |
| 4. | 100 µl of 20 µg/ml Proteinase K | | 8-10 min | Permeabilize |
| 5., 6. | PBS | 2x | 5 min | Wash |
| 7. | 4% PFA in PBS | | 5 min | Fixate |
| 9., 10. | PBS | 2x | 5 min | Wash |
| 11. | 100 µl Equilibration buffer | | 10 min | Equilibrate |
| 12. | 50 µl rTDT incubation buffer | | 60 min | Label |
| 13. | 2x SSC | | 15 min | Stop reaction |
| 14. | PBS | | 5 min | Wash (unincorporated fluorescein-12-dUTP) |
| 15. | Distilled $H_2O$ | | 5 min | Wash |

Fluorescein-12-dUTP incorporation in the nuclei of apoptotic cells was visualized by fluorescence microscopy. The direct detection of the fluorescent reporter was performed through a standard fluorescein filter, set to view the green fluorescence at 520 ± 20 nm (GFP channel). DAPI-stained nuclei were visualized at 460 nm (DAPI channel). Images of

the entire retina were taken, using a fluorescence light microscope Axio Imager Z1 (Zeiss, Göttingen, Germany). To quantify the rate of apoptotic cells following light exposure, the number of TUNEL-positive nuclei per ONL (in $mm^2$) was counted via the morphometric software ImageJ (plug-in: Analyze, Cell counter) and normalized to the total area of the ONL, reckoned via the image acquisition and analysis software AxioVision SE64 (release 4.9.1, Carl Zeiss, Göttingen, Germany; module: Measure outline).

### 2.1.6 Animal experiments

#### 2.1.6.1 Light damage

Following method was elaborated extensively in a manuscript in preparation (Braunger et al.). 6-8 week-old animals were initially adapted to cyclic dim light (< 100 lux) for 5 days and then transferred to complete darkness for at least 18 h (a lightproof box with guaranteed ventilation). Experimental mice were moved to a light damage box (Figure 14), containing transparent cages with stainless steel bar lids on the illumination shelf to house the mice for the duration of the light exposure. Light damage was subsequently performed either for 30 min (RNA analysis, morphometric analysis, detection of apoptosis via TUNEL-assay and ERG), or for an hour (morphometric analysis) – according to the intended read-out, and with an intensity of 5000 lux.

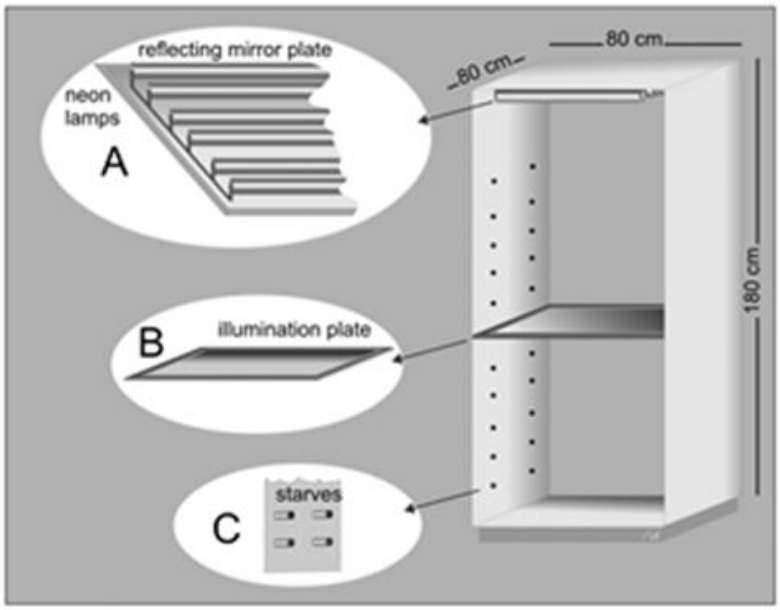


*Figure 14:* A schematic drawing of a light damage box
A. Three double 18 W gas neon lamps, attached to the mirror ceiling and emitting diffuse cool white light. B. Illumination plate with a reflecting surface, the height of which can be adjusted according to the desired intensity (C.). Figure taken from (Braunger et al.).

Following light exposure, mice were transferred back to the dark adaption room, in order to convalesce in the conditions of dim light (< 100 lux) for not less than 6 h. According to the downstream application, the animals were sacrificed at following points of time after performed light damage: 6 h (for RNA analysis), 30 h (for TUNEL-mediated apoptosis detection) or 14 days (for morphometric analysis). Mice, involved in functional analysis, were processed for electroretinograms, which were recorded 14 days after light damage.
The depicted experiment was always performed at the same time of the day, in the early morning, since there are established hypotheses (by (Duncan and O'Steen, 1985; Organisciak et al., 2000; White and Fisher, 1987)) that the susceptibility to light-induced damage in a rat model (and probably also by mice) depends on the circadian rhythm.

### 2.1.6.2 Point mutation at codon 450 in the *Rpe65* gene: altered susceptibility to light damage

The retinal susceptibility to light stress could be altered by certain allelic polymorphisms, including a single point mutation at position 450 in the RPE-specific gene *Rpe65* (Danciger et al., 2000). The resulting Leu450Met amino acid substitution increases the retinal resistance against light-induced damage (see 1.2.2). Therefore, only homozygous leucine carriers (Figure 15) were included in our light damage experiments, after performing a PCR analysis for the known mutation in the *Rpe65* gene (see 2.1.2.3).

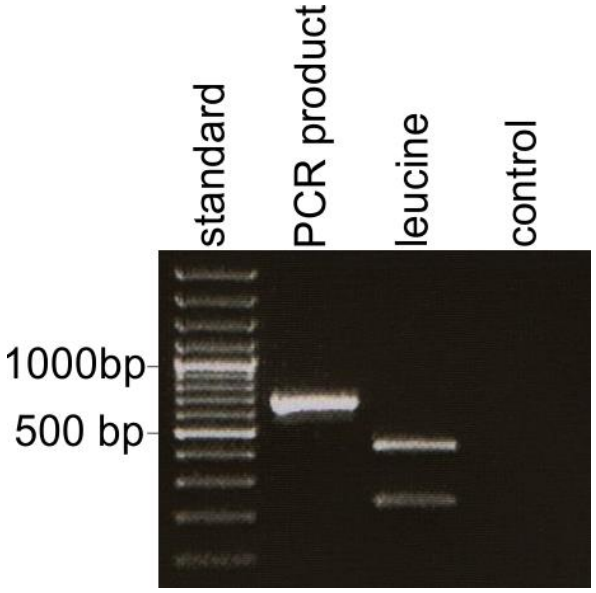


*Figure 15:* PCR for the leucine/methionine variant of the *Rpe65* gene at position 450
The PCR product (left well) was digested with MwoI. Since the leucine variant of the gene generates a restriction site for the enzyme, digestion results in 2 bands (437 bp and 236 bp, middle well). The methionine codon would generate just one band (673 bp, not shown). Heterozygous animals would have all three of the bands (not shown).

### 2.1.6.3 Light damage and morphometric read-out in terms of a spider diagram

Morphometric analysis was applied, in order to investigate the extent of light-induced damage. Experimental mice were exposed to light with an intensity of 5000 lux for either 30 min, or 1 h and sacrificed 14 days thereafter. The enucleated eyes were treated according to the previously extensively described protocols (2.1.5.1) and INL and ONL measurements were performed on semithin sections (with a thickness of 1.0 µm and along the mid-horizontal plane) (Figure 16). The means, standard deviations and standard errors of the mean were calculated for each one of the equidistant loci (in each of the experimental and control groups of animals) using Excel (Microsoft Corporation, Redmond, WA, USA). The results were depicted in form of spider diagrams (method described in a manuscript in preparation (Braunger et al.)). Control animals' diagrams were compared to those of transgenic animals at each one of the obtained 21 measure points.

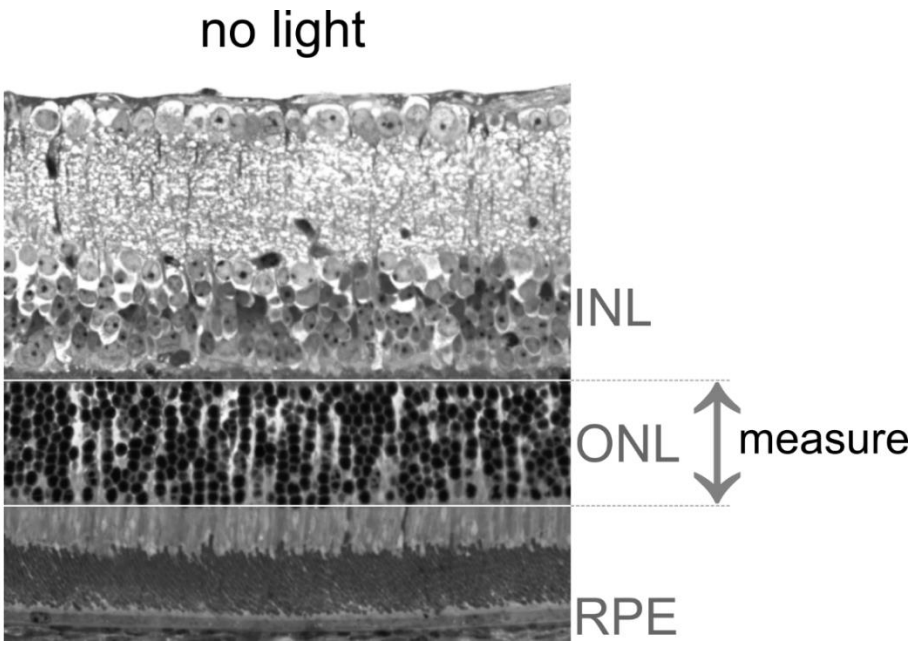


*Figure 16:* A semithin section, exemplary showing the outer nuclear layer (ONL) measure technique

The depicted ONL measure technique is shown here exemplary on a semithin section (for an untreated animal ("no light")). INL, inner nuclear layer; RPE, retinal pigment epithelium.

### 2.1.6.4 *In vivo* funduscopy and fluorescein angiography (FLA)

Fundus imaging and angiography were both performed in cooperation with Prof. Jägle, Regensburg, and following a method, already elaborated in (Braunger et al., 2013a). The purpose of these investigations was to analyze and compare the retinal and choroidal

vascular phenotype and circulation flow of *Tgfbr2*$^{\Delta oc}$ mice with that of their control littermates. Retinal imaging was executed, using a commercially available imaging system (Micron III; Phoenix Research Laboratories, Inc.). The mice were anaesthetized by injecting ketamine (65 mg/kg b.w.) and xylazine (13 mg/kg b.w.) subcutaneously and their pupils were dilated with tropicamide eye drops (Mydriaticum Stulln; Pharma Stulln) prior to image acquisition. Light source path and imaging path filters (low band-pass and high band-pass) were used for fluorescein angiography (FLA), performed after administering 75 mg/kg body weight sodium fluorescein (Alcon) subcutaneously. Sodium fluorescein possesses a relatively low molecular weight and thereby it can diffuse through the Bruch's membrane and the pores of the choriocapillaris. In the course of the experiment, the animal eyes were illuminated with blue light with a wavelength of 465-490 nm (white light after passing a blue excitation filter), which was absorbed by fluorescein particles within the blood vessels. Only the emitted fluorescence (yellow-green light with a wavelength in a spectrum of 520-530 nm) passed a barrier filter, due to the relapse of the excited particles to a lower energy level, and was captured by a fundus camera to obtain angiograms (Jurklies and Puls S., 2007).

#### 2.1.6.5 *In vivo* laser scanning ophthalmoscopy (SLO) and optical coherence tomography (OCT)

Scanning laser ophthalmoscopy (SLO) is a confocal imaging technology that uses a laser beam to sense ("scan") the retina point by point and then capture the reflected light, passing through a small aperture. By means of this principle, scattered light, which otherwise would blur the image, is suppressed and the obtained real-time raster images are sharp and high-contrast. These can be assigned unambiguously to a certain point (lesion) in the corresponding retinal area, which is being laser scanned at this exact point of time (Grus and Kottler, 2007).

Optical coherence tomography (OCT) is a non-invasive diagnostic imaging procedure, employing low-coherence (near-infrared light with a wavelength of 830 nm) interferometry to assess the propagation delay of a reflected laser diode beam, normalized to a reference beam. The elapsed time is then converted to information of the depth of the reflecting layer, which renders an *in vivo* two-dimensional cross sectional view of the retina, accurate to within at least 10-15 microns in its resolution (Grus and Kottler, 2007).

SLO and OCT were also performed in cooperation with Prof. Jägle, Regensburg, with the objective to visualize *in vivo* the retinae of *Tgfbr2*$^{\Delta oc}$ mice and of their control littermates

before and after light damage. Prior to each procedure the mice were anaesthetized and their pupils were dilated, as just described for fundus imaging and FLA (2.1.6.4).

### 2.1.6.6 Functional analysis: Electroretinography (ERG)

Functional analyses in the form of electroretinograms (ERGs) were performed in cooperation with Prof. Jägle, Regensburg, in order to investigate potential differences in the extent of photoreceptor light damage between control and *Tgfbr2*$^{\Delta oc}$ mice, exposed to light 2 weeks beforehand. The purpose of the examinations was also the validation of results, acquired through morphometric analysis and *in vivo* imaging (SLO and OCT), with regard to functional alterations (method extensively described in (Braunger et al., 2013b)).

By employing electroretinographic techniques, light-evoked electrical responses of photoreceptors and downstream retinal neurons can be quantitatively analyzed. These responses ensue as a result of electrical potential alterations, contributed by ion concentration shifts, particularly sodium and potassium currents (Jurklies, 2007). The regular waveform of the ERG reflects the activity of retinal cells, evoked by standardized light stimuli and displayed as time course of the signal's amplitude (in Volt). The initial negative deflection, known as the a-wave, is a result of the phototransduction cascade processes at the level of cones and rods (Wolpert and Tsang, 2011). The subsequent rise towards the positive peak, known as the b-wave, is due to a depolarization, caused by the on-bipolar cells, according to an already postulated theory (Stockton and Slaughter, 1989). The ascending slope from the a-wave to the peak of the b-wave typically shows several small oscillatory potentials, or OPs, and reveals the function of the amacrine cells and the feedback loops between amacrine cells and bipolars, as well as between amacrine cells and retinal ganglion cells (Jurklies, 2007). Under scotopic conditions the evoked responses originate primarily from the rod system, while examinations on a light-adapted eye (in presence of background illumination) reflect the activity of the cone system. Stimulus characteristics (a single flash or flickering) can also alter the generated responses. Scotopic threshold responses (STRs) are evoked on a maximally dark-adapted eye by very weak light flash intensities (approximately one log unit below the b-wave threshold) to yield minor negative components, primarily elicited by the inner retina, proximal to bipolar cells (Saszik et al., 2002). They thus represent the most sensitive response on a dark-adapted eye.

Prior to execution of the experiments, mice were dark-adapted for at least 12 h and anesthetized by injecting ketamine (65 mg/kg b.w.) and xylazine (13 mg/kg b.w.)

subcutaneously, their pupils were dilated with tropicamide eye drops (Mydriaticum Stulln, Pharma Stulln). Silver needle electrodes, attached to the forehead and the tail of each mouse, served as reference and ground, respectively, while gold wire ring electrodes represented active electrodes. Corneregel (Bausch&Lomb) was essential to keeping the eyes moisturized and preserving good electrical contact. ERGs were recorded with the aim of a Ganzfeld bowl (Ganzfeld QC450 SCX; Roland Consult), an amplifier and recording unit (RETI-Port; Roland Consult). Both eyes were examined simultaneously, results band-pass filtered (1–300 Hz), and averaged. Single-flash scotopic (dark-adapted) responses to a series of 10 LED-flash intensities (ranging from -3.5 to 1.0 log cd.s/$m^2$ with an interstimulus interval of 2 to 20 s (for the maximal intensity)) were recorded. For the evaluation of temporal characteristics responses to flickering stimuli with an intensity of 0.5 log cd.s/$m^2$ and frequencies, ranging from 4 to 25 Hz, were registered. After 10 min of adaptation to white background illumination (25 cd/$m^2$), single-flash photopic (light-adapted) responses to three Xenon-flash intensities (1, 2, and 3 log cd.s/$m^2$), as well as responses to flickering stimuli (intensity 1.0 log cd.s/$m^2$) with frequencies, ranging from 4 to 25 Hz, were plotted. The STRs, evoked by very weak white flashes (flash intensities: -4.05, -3.70, and -3.53 log cd.s/$m^2$), were recorded after dark adaptation, starting 16 h before examinations. Oscillatory potentials were extracted from higher intensity waveforms, recorded under dark-adapted conditions by band-pass filtering (100–300 Hz). For flicker response waveforms, a fast Fourier transform was used to calculate the response magnitude and phase and estimate signal significance. All analyses and plotting was performed with R 2.15.2 (The R Foundation for Statistical Computing) and ggplot2 0.9.3 (Wickham, 2009).

### 2.1.7 Statistical analysis

All of the presented results are expressed as mean ± SEM. Statistical comparative analyses between the mean variables of individual test populations were performed using the heteroscedatic, two-tailed Student's *t* test and utilizing the Excel software (Microsoft Corporation, Redmond, WA, USA) or ANOVA analyses in SPSS (IBM Corporation, Armonk, New York, USA). *P* values $\leq 0.05$ were considered to be statistically significant.

## 2.2 Material

### 2.2.1 Chemicals and reagents

#### 2.2.1.1 Laboratory chemicals

*Table 29:* Laboratory chemicals

| Reagent | Company |
|---|---|
| 5x Mango *Taq* Colored Reaction Buffer | Bioline, Luckenwalde |
| 10x $NH_4^+$ Reaction Buffer | Bioline, Luckenwalde |
| 2-Dodecenylsuccinic acid anhydride (DDSA) | Serva, Heidelberg |
| 2-Mercaptoethanol | Roth, Karlsruhe |
| 2,4,6-Tris(dimethylaminomethyl)phenol (DMP-30) | Serva, Heidelberg |
| Agarose | Roth, Karlsruhe |
| Ammoniumperoxodisulfate (APS), 10% (w/v) | Roth, Karlsruhe |
| Azur II | Merck, Darmstadt |
| Bovine Serum Albumin Fraction V (BSA) | Roth, Karlsruhe |
| Bromphenol blue | Sigma-Aldrich, Taufkirchen |
| Chloroform | Roth, Karlsruhe |
| Dimethyl sulfoxide (DMSO) | Roth, Karlsruhe |
| Deoxyribonucleoside triphosphate (dNTP) | Bioline, Luckenwalde |
| Disodium hydrogen phosphate dihydrate ($Na_2HPO_4 \cdot 2\ H_2O$) | Roth, Karlsruhe |
| Dry milk (skimmed milk powder) | Roth, Karlsruhe |
| Ethanol, absolute | Roth, Karlsruhe |
| Ethidium bromide | Serva, Heidelberg |
| Fluorescein | Quiagen, Hilden |
| Fluorescent Mounting Medium | DakoCytomation, Hamburg |
| Formaldehyde | Roth, Karlsruhe |
| Glutaraldehyde | Serva, Heidelberg |
| Guanidine hydrochloride (HCl) | Roth, Karlsruhe |
| Glycerin | Roth, Karlsruhe |
| Glycid ether | Serva, Heidelberg |
| Glycine | Merck, Darmstadt |
| Hydrochloric acid 37% (HCl) | Merck, Darmstadt |
| Immobilon Western HRP-substrate | Millipore, Billerica, USA |
| Isoflurane | Baxter, Unterschleißheim |
| Isopropanol | Roth, Karlsruhe |
| Ketamine | Wirtschaftsgenossenschaft deutscher Tierärzte (WDT), Garbsen |
| Magnesium chloride ($MgCl_2$) (50 mM) | Bioline, Luckenwalde |
| Methanol | Merck, Darmstadt |
| Methylene blue | Merck, Darmstadt |
| Methylnadic anhydride (MNA) | Serva, Heidelberg |

| | |
|---|---|
| Mydriaticum Stulln (tropicamide) eye drops | Pharma Stulln GmbH |
| Osmium tetroxide | Science Service, München |
| Paraformaldehyde (PFA) | Sigma-Aldrich, Taufkirchen |
| Paraffin | Engelbrecht, München |
| Phosphate buffered saline (PBS) | Invitrogen, Karlsruhe |
| Potassium chloride | Roth, Karlsruhe |
| Potassium dihydrogen phosphate ($KH_2PO_4$) | Roth, Karlsruhe |
| Potassium ferricyanide ($K_3[Fe(CN)_6]$) | Merck, Darmstadt |
| Potassium ferrocyanide ($K_4[Fe(CN)_6] \cdot 3\ H_2O$) | Merck, Darmstadt |
| Propylene oxide | Serva, Heidelberg |
| Protease-Inhibitor Mix M | Serva, Heidelberg |
| Proteinase K | Roth, Karlsruhe |
| Rotiphorese® Gel 30 (30% acrylamide/bisacrylamide stock solution, mixing ratio 37.5:1) | Roth, Karlsruhe |
| Sodium cacodylate buffer | Serva, Heidelberg |
| Sodium chloride | Roth, Karlsruhe |
| Sodium dihydrogen phosphate monohydrate ($NaH_2PO_4 \cdot H_2O$) | Merck, Darmstadt |
| Sodium dodecyl sulfate (SDS) | Serva, Heidelberg |
| SYBR-Green I | Quiagen, Hilden |
| TEMED (N,N,N',N'-tetramethylethylenediamine) | Roth, Karlsruhe |
| Tergitol | Sigma-Aldrich, Taufkirchen |
| Tris(hydroxymethyl)aminomethan (Tris) ultrapure, MB Grade | Usb Corporation, Cleveland, USA |
| Tris/HCl | Roth, Karlsruhe |
| TRIzol Reagent | Invitrogen, Karlsruhe |
| Tween 20 | Roth, Karlsruhe |
| Urea | Sigma-Aldrich, Taufkirchen |
| Vectashield Mounting Medium for fluorescence with 4',6-diamidino-2-phenylindole (DAPI) | Vector Laboratories, Burlingame, USA |
| Water Rotislov (RNase-free) | Roth, Karlsruhe |
| Xylazine | Serumwerk Bernburg, Bernburg |
| Xylene | Merck KgaA, Darmstadt |

#### 2.2.1.2 Enzymes and Taq polymerase

*Table 30:* Enzymes and Taq Polymerase

| Enzyme | Company |
|---|---|
| Mango *Taq* DNA Polymerase | Bioline, Luckenwalde |
| MwoI restriction endonuclease | New England Biolabs |
| Proteinase K | Roth, Karlsruhe |
| *Taq* DNA Polymerase | New England Biolabs |

#### 2.2.1.3 Reaction kits

*Table 31:* Reaction kits

| Kit | Company |
|---|---|
| DeadEnd™ Fluorometric TUNEL System | Promega, Madison, Wisconsin, USA |
| iScript™ cDNA Synthesis Kit | BioRad Laboratories, München |

#### 2.2.1.4 DNA and protein ladders

*Table 32:* DNA and protein ladders

| Ladder | Company |
|---|---|
| GeneRuler 100 bp DNA ladder | Fermentas, St. Leon-Rot |
| PageRuler™ Prestained Protein Ladder | Fermentas, St. Leon-Rot |

### 2.2.2 Laboratory consumable supplies and equipment

#### 2.2.2.1 Consumables

*Table 33:* Consumable supplies

| Item | Company |
|---|---|
| 3 MM Whatman blotting paper | Neolab, Heidelberg |
| Adhesive PCR film | Peqlab Biotechnologie, Erlangen |
| Biosphere filter tips | Sarstedt, Nümbrecht |
| Conical tubes – 15 ml, 50 ml | Sarstedt, Nümbrecht |
| Cover slips, 24x 60 mm | Menzel-Gläser, Braunschweig |
| Disposal bags for autoclavation | Sarstedt, Nümbrecht |
| Ear clips | Hauptner & Herebrholz, Solingen |
| Epon | Serva, Heidelberg |
| Glass pipettes | Brand, Wertheim |
| iQ™ 96-well PCR plates | Bio-Rad, München |
| Laboratory glass ware | Schott, Roth, VWR |
| Microseal® 'B' adhesive seals | Bio-Rad, München |
| Multi-reaction tubes – 0.5 ml, 1.5 ml, 2.0 ml | Roth, Karlsruhe |
| Multidishes Nunclon | Nunc, Roskilde, DK |
| Nitrile gloves | VWR, Darmstadt |
| Nylone membrane | Roche, Mannheim |
| Omnifix sterile single-use syringes | B. Braun, Wertheim |
| Parafilm | Pechiney Plastic Packaging, Chicago, USA |
| Pasteur pipettes | Brand, Wertheim |
| Personna razor blades | American Safety Razor Company, Verona |
| Pipette tips | Sarstedt, Nümbrecht |
| PVDF western blotting membrane | Roche, Mannheim |
| Serological pipettes | Sarstedt, Nümbrecht |
| Sterican® single-use injection needle | B. Braun, Wertheim |

| | |
|---|---|
| Super PAP pen Liquid blocker | SCI Science Services, München |
| SuperFrost Ultra Plus® glass slide | Menzel-Gläser, Braunschweig |

#### 2.2.2.2 Equipment

*Table 34:* Laboratory equipment

| Item | Company |
|---|---|
| Aida Advanced Image Data Analyzer v.4.06 | Raytest, Straubenhardt |
| Axio Imager Z1 microscope | Zeiss, Göttingen |
| Axiovert 40 CFL | Zeiss, Göttingen |
| Centrifuges 5415D, 5415R, 5804R, 5810R | Eppendorf, Hamburg |
| Electrophoresis power supply E835 | Biorad, Hercules, USA |
| Excel | Microsoft, Redmond, WA, USA |
| Gel chamber for electrophoresis | Peqlab Biotechnologie, Erlangen |
| ImageJ | LOCI, Madison, Wisonsin |
| Innova 4200 shaker | New Brunswick, New Jersey, USA |
| IQ5 Multicolor Real-time PCR Detection System + iCycler | BioRad Laboratories GmbH, Munich, Germany |
| Inolab pH-meter | WTW GmbH, Weilheim |
| Julabo SW20 water bath | Julabo, Seelbach |
| Kern PJL 2100-2M balance | Kern & Sohn, Balingen-Frommern |
| LAS 3000 Intelligent dark box | Fujifilm, Düsseldorf |
| Mastercycler gradient | Eppendorf, Hamburg |
| Microm HM 500 OM cryostat | Microm International, Walldorf |
| Milli-Q Plus PF water purification system | Millipore Corporation, Billerica, USA |
| Model 45-101-i class II electrophoresis system | Peqlab Biotechnologie, Erlangen |
| NanoDrop 2000c UV-Vis Spectrophotometer | Thermo Fisher Scientific, Schwerte |
| Paraffin tissue processor HMP 110 | Microm International, Walldorf |
| Paraffin wax embedding centre type MPS/P2 | SLEE Medical, Mainz, Germany |
| PerfectBlue Gelsystem Mini L | Peqlab Biotechnologie, Erlangen |
| Pipetman pipette | Gilson, Middleton, USA |
| Polymax 1040 shaker | Heidolph, Kelheim |
| Electrophoresis power supply E835 | Consort, Turnhout, BE |
| Research pipettes | Eppendorf, Hamburg |
| Semi-dry electrophoretic transfer cell | Peqlab Biotechnologie, Erlangen |
| SPSS | IBM Corporation, Armonk, New York, USA |
| Supercut 2050 Reichert-Jung Microtome | Cambridge Instruments GmbH, Nussloch |
| Systec V75 autoclave | Systec GmbH, Wettenburg |
| Thermomixer compact | Eppendorf, Hamburg |
| Tissue processing automat Leica EM TP | Leica microsystems GmbH, Wetzlar |
| T100TM Thermal cycler | BioRad, Munich |
| Ultracut E Reichert-Jung Microtome | Reichert-Jung, Kirchseeon |
| Vortex Genie 2 | Scientific Industries, New York, USA |

## 2.2.3 Buffers, dilutions and gels compounding

### 2.2.3.1 Buffers and dilutions

*Table 35:* Histology – buffers and dilutions

| | Preparation |
|---|---|
| 0.1 M $Na_2HPO_4 \cdot 2\ H_2O$ (Buffer I) | 35.6g in 2 l $H_2O$ dest. |
| 0.1 M $NaH_2PO_4 \cdot H_2O$ (Buffer II) | 13.8g in 1 l $H_2O$ dest. |
| 0.1 M phosphate buffer, pH 7.4 | Buffer I:buffer II in a proportion 5:1, pH 7.4 |
| 0.2 M Sodium cacodylate buffer, pH 7.4 | 0.2 M sodium cacodylate buffer (42.8 g/1000 ml)<br>Adjust pH (to 7.4) with 0.2 M HCl |
| 25% PFA | 12.5 g paraformaldehyde (PFA) in 40 ml $H_2O$ dest. (heated up to 70ºC), ad $H_2O$ dest. to 50 ml |
| 4% Paraformaldehyde (PFA) fixation solution | 4 g formaldehyde (4%) in 100 ml 0.1 M phosphate buffer, pH 7.4 |
| EM fixation medium, pH 7.4 | 10 ml 25% paraformaldehyde<br>50 ml 0.2 M cacodylate buffer, pH 7.4<br>30 ml $H_2O$ dest. + 10 ml 25% glutaraldehyde |
| Epon stock solution | 43.2 g glycid ether<br>16.8 g DDSA Epon hardener (2-Dodecenylsuccinic acid anhydride)<br>30.0 g MNA Epon hardener (Methylnadic anhydride)<br>1.5 ml DMP-30 Epon accelerator (2,4,6-Tris(dimethyl-aminomethyl)phenol) |
| LacZ fixation buffer | 48.4 ml 0,1 M phosphate buffer, pH 7.3<br>100 µl 1 M $MgCl_2$<br>1.0 ml 0.250 M EGTA, pH 7.3<br>0.4 ml 25% glutaraldehyde |
| LacZ stain | 72.0 ml LacZ wash buffer<br>3.0 ml X-Gal (25 mg/ml in DMSO)<br>0.159 g $K_4Fe(CN)_6 \cdot 3\ H_2O$<br>0.123 g $K_3Fe(CN)_6$ |
| LacZ wash buffer | 1 ml 1 M $MgCl_2$<br>5.0 ml 1% sodium desoxycholate (NaDC)<br>5.0 ml 2% Tergitol<br>489 ml 0.1 M phosphate buffer, pH 7.3 |
| Osmium ferrocyanide | 2% $OsO_4$<br>1.6% potassium ferrocyanide (96 mg/6 ml), diluted in 0.2 M cacodylate buffer |
| Richardson's stain | Stock solution I: 5 g 1% Azur II in 500 ml $H_2O$ dest.<br>Stock solution II: 5 g methylene blue in 500 ml 1% sodium tetraborate (Borax)<br>Stock solution I:Stock solution II:$H_2O$ dest. in a proportion 1:1:2 |

*Table 36:* Protein analysis – buffers and dilutions

| | Preparation |
|---|---|
| 0.9% NaCl | 0.9% (w/v) in $H_2O$ dest., autoclave |
| 10x Phosphate buffered saline (PBS), pH 7.4 | 80 g sodium chloride<br>2 g potassium chloride<br>4.4 g disodium hydrogen phosphate ($Na_2HPO_4$)<br>2.4 g potassium dihydrogen phosphate ($KH_2PO_4$)<br>ad $H_2O$ dest. to 1 l, autoclave |
| 10x SDS electrophoresis buffer | 250 mM Tris/HCl<br>400 mM glycine<br>1% (w/v) SDS<br>Solve in $H_2O$; ad 1 l |
| SDS solution, 10% (w/v) | 10 g SDS, solved in $H_2O$ dest.; ad 100 ml |
| 10x SDS PAGE buffer | 250 mM Tris/HCl<br>400 mM glycine<br>1% (w/v) sodium dodecyl sulfate (SDS)<br>Solve in $H_2O$; ad 1 l |
| 4x SDS sample buffer (Laemmli buffer) | 0.25 M Tris/HCl, pH 6.8<br>30% glycerin<br>8% (w/v) sodium dodecyl sulfate (SDS)<br>0.02% (w/v) bromphenolblue<br>10% ß-mercaptoethanol |
| 10x TBS, pH 7.4 | 30 g Tris(hydroxymethyl)aminomethan (Tris)<br>80 g sodium chloride<br>2 g potassium chloride<br>Solve in $H_2O$; ad 1 l, autoclave |
| 1x TBST | 100 ml 10x TBS<br>0.05% (v/v) Tween 20<br>Solve in $H_2O$; ad 1 l |
| 10x Transfer buffer | 5.8 g Tris(hydroxymethyl)aminomethan (Tris)<br>2.9 g glycine<br>200 ml methanol<br>3.7 ml 10% (w/v) sodium dodecyl sulfate (SDS)<br>Solve in $H_2O$; ad 1 l |
| 1 M Tris/HCl, pH 6.8 | 121.14 g Tris(hydroxymethyl)aminomethan (Tris)<br>Solve in $H_2O$; ad 1 l; adjust pH |
| 1.5 M Tris/HCl, pH 8.8 | 181.71 g Tris(hydroxymethyl)aminomethan (Tris)<br>Solve in $H_2O$; ad 1 l; adjust pH |
| Urea buffer | 25 ml 10% sodium dodecyl sulfate (SDS)<br>10 ml 1 M Tris(hydroxymethyl)aminomethan (Tris), pH 6.8<br>100 µl 0.5 M ethylenediaminetetraacetic acid (EDTA), pH 8<br>750 µl ß-mercaptoethanol<br>24 g urea |
| Wash buffer for protein isolation | 0.3 M Guanidin HCl<br>Solve in 95% Ethanol |

| | |
|---|---|
| Detection buffer, pH 9 | 0.1 M Tris/HCl<br>0.1 M sodium chloride (NaCl) |

*Table 37:* DNA analysis – buffers and dilutions

| | Preparation |
|---|---|
| Mouse tail lysis buffer | 40 ml 1 M Tris/HCl, pH 8.0 (100 mM Tris/HCl, pH 8.0)<br>80 ml 25 mM ethylenediaminetetraacetic acid (EDTA) (5 mM EDTA)<br>8ml 10% sodium dodecyl sulfate (SDS) (0.2 % SDS)<br>26.6 ml 3 M sodium chloride (200 mM NaCl)<br>ad $H_2O$ dest. to 400 ml |
| DNA loading dye | Bromphenol blue 0.25% (w/v)<br>Xylene cyanol FF 0.25% (w/v)<br>Ficoll 15% (w/v) |
| 10x TBE buffer | 108g Tris(hydroxymethyl)aminomethan (Tris)<br>55 g borate<br>40 ml 0.5 M ethylenediaminetetraacetic acid (EDTA), pH 8<br>ad H2O dest. 1 l |

### 2.2.3.2 Sodium dodecyl sulfate polyacrylamide gel electrophoresis (SDS-PAGE)

*Table 38:* SDS-PAGE gels composition

| Gels for SDS-PAGE | Stacking gel (1 ml) | Resolving gel, 10% | Resolving gel, 15% |
|---|---|---|---|
| $H_2O$ dest. | 0.68 ml | 1.9 ml | 1.3 ml |
| Rotiphorese® Gel 30 | 0.17 ml | 1.7 ml | 2.3 ml |
| 1 M Tris/HCl, pH 6.8 | 0.13 ml | - | - |
| 1.5 MTris/HCl, pH 8.8 | - | 1.3 ml | 1.3 ml |
| 10% SDS | 0.01 ml | 0.05 ml | 0.05 ml |
| 10% APS | 0.01 ml | 0.05 ml | 0.05 ml |
| TEMED | 0.001 ml | 0.002 ml | 0.002 ml |

# 3. Results

## 3.1 Conditional deletion of TβRII in cells of the neural retina

In order to investigate the presumably protective role of TβRII for mature photoreceptors under light-induced stress, we generated *Tgfbr2*$^{fl/fl}$*;α-Cre* and *Tgfbr2*$^{fl/fl}$*;LMOP* mice, which were supposed to have the type II TGF-β receptor conditionally inactivated either in the cells, originating from the inner layer of the optic cup, or in the rod photoreceptors only, respectively. For the sake of simplicity, *Tgfbr2*$^{fl/fl}$*;α-Cre* mice are referred to as *Tgfbr2*$^{\Delta oc}$ and *Tgfbr2*$^{fl/fl}$*;LMOP* mice as *Tgfbr2*$^{\Delta rod}$, in resemblance to the corresponding cells, affected by the conditional downregulation of TGF-β signaling. Mice, carrying two unrecombined *Tgfbr2*$^{fl/fl}$ alleles, are referred to as controls.

### 3.1.1 Conditional deletion of TβRII in optic cup-derived cells of the neural retina

#### 3.1.1.1 Cellular expression of the Cre recombinase in the *α-Cre* strain

In order to monitor the tissue expression pattern of the *cre* transgene in the *α-Cre* strain, Rosa-LacZ reporter mice (R26R) were interbred with the *α-Cre* strain and β-galactosidase staining was performed for the progeny. Since lacZ is only expressed in cells/tissues where Cre is expressed and active (Soriano, 1999), double transgenic *α-Cre*/R26R mice reacted with an intense signal throughout the neural retina and the non-pigmented epithelium of the ciliary body (Figure 17), i.e. all the cells, deriving from the inner layer of the optic cup. In contrast, the eyes of control animals showed no detailed signal, but a faint bluish background reaction within the inner retinal layers (Figure 18).

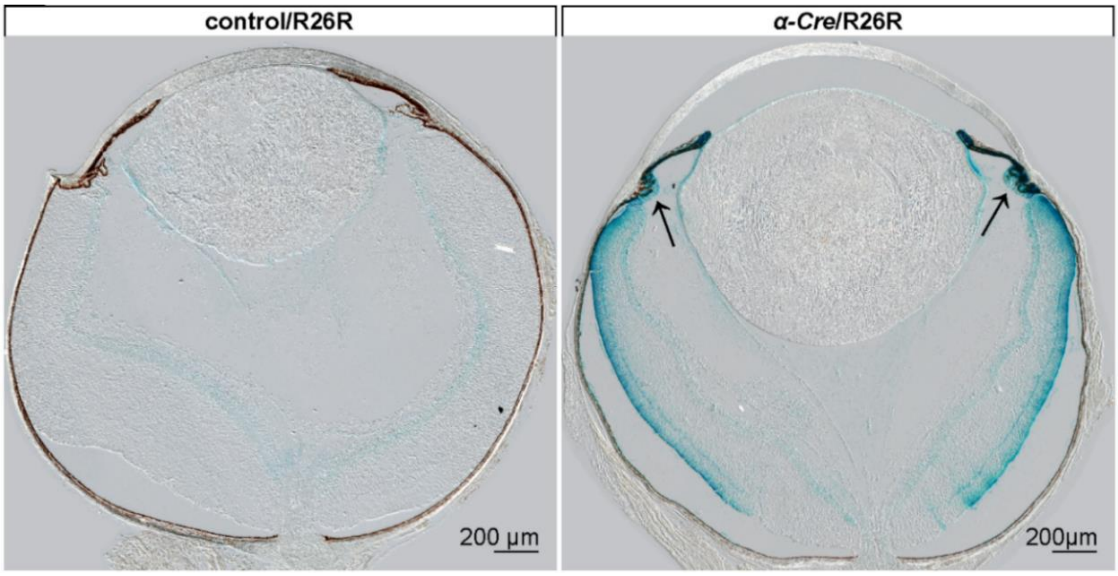


*Figure 17:* Rosa-LacZ reporter mice (R26R): panorama view of ß-galactosidase-stained eyes

The panorama picture of the eye of a 7-day-old *α-Cre*/R26R mouse shows a much more enhanced reaction in its neural retina and non-pigmented epithelium of the ciliary body (arrows) in comparison to the control/R26R. Figure modified after (Boneva et al., 2016).

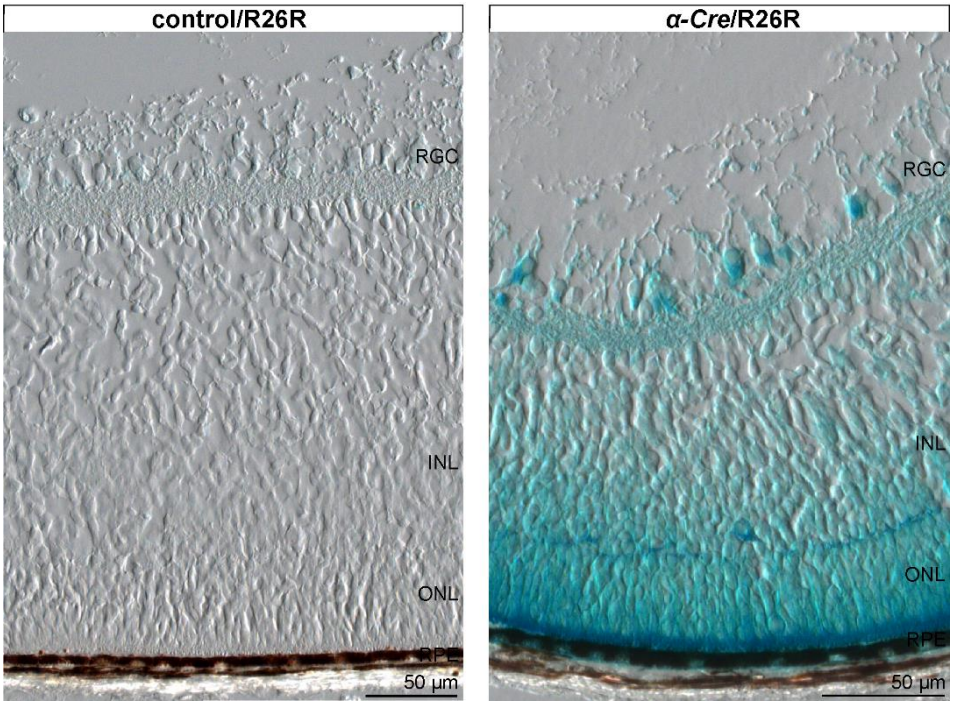


*Figure 18:* Rosa-LacZ reporter mice (R26R): detailed view of ß-galactosidase-stained eyes of 7-d-old animals

The higher magnification of the ß-galactosidase-stained *α-Cre*/R26R eye from Figure 17 shows an intense reaction throughout the neural layers of the retina, implying the homogenous distribution and activity of the Cre enzyme within all of the cells, deriving from the inner layer of the optic cup. RGC, retinal ganglion cells; INL, inner nuclear layer; ONL, outer nuclear layer; RPE, retinal pigment epithelium. Figure modified after (Boneva et al., 2016).

### 3.1.1.2 The Cre recombinase in the *α-Cre* strain: influence upon retinal morphology and reaction to light-induced stress

Since the expression of the Cre enzyme itself disguises the remote possibility of morphological and functional alterations of the retina, the initial approach of this work included a phenotype comparison between *α-Cre* animals and their wild-type littermates. First of all, the eyes of 6-8-week-old mice were enucleated and processed for light microscopy, in order to study the morphology and to perform morphometric analyses of the retinal layers. The thickness of the INL and ONL was measured on mid-horizontal sections, stretching from the temporal to the nasal side through the optic nerve head (ONH), and the results were visualized in form of Spider diagrams (refer to Figure 19 for INL and to Figure 20 for ONL). The statistical evaluation did not reveal any significant differences between the thickness of the INL or ONL in *α-Cre* animals, when compared to wild-type littermates. Consequently, the expression of the Cre recombinase on its own did not affect the structural characteristics of the retina.

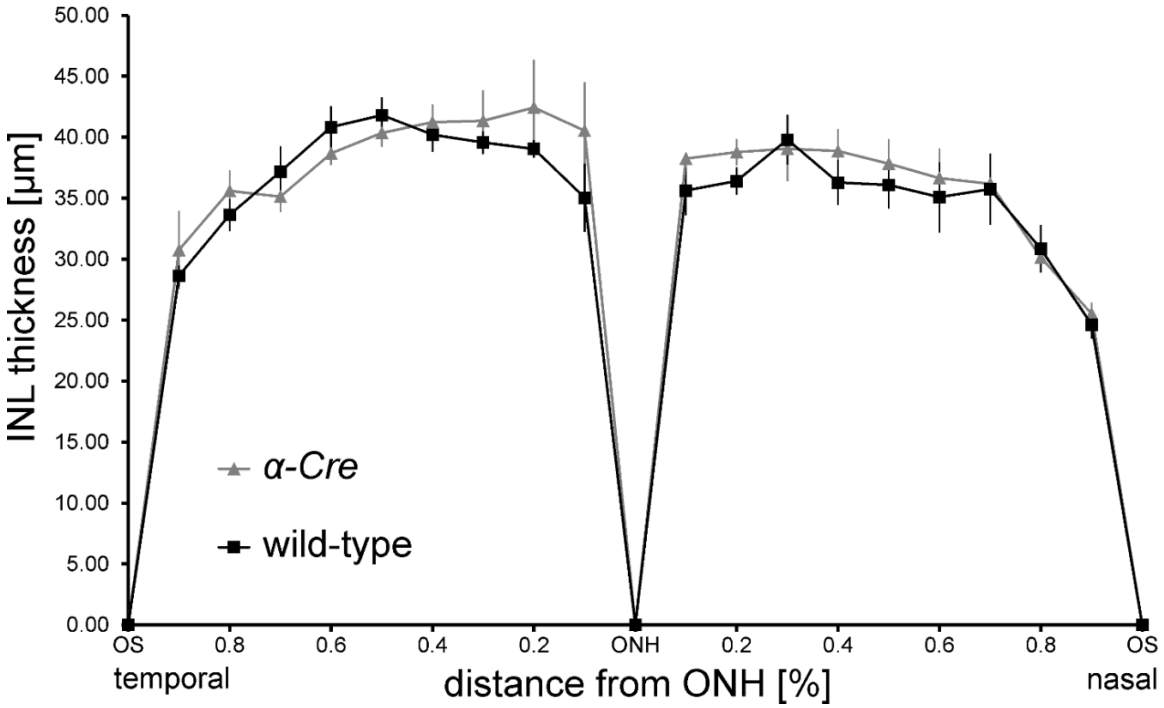


*Figure 19:* Morphometric analysis of the thickness of the inner nuclear layer (INL), measured on mid-horizontal Richardson-stained semithin sections through the eyes of 7-8-week-old untreated wild-type animals and their *α-Cre* littermates

The thickness of the INL was quantified by morphometric analyses and visualized in form of a Spider diagram. The statistical evaluation of the results did not reveal any significant differences between both experimental groups. Mean ± SEM, n = 7/5 (wild-type to transgenic animals). Morphometric analysis performed in cooperation with Tatjana Groß. OS, ora serrata; ONH, optic nerve head. Experiment published in (Boneva et al., 2016).

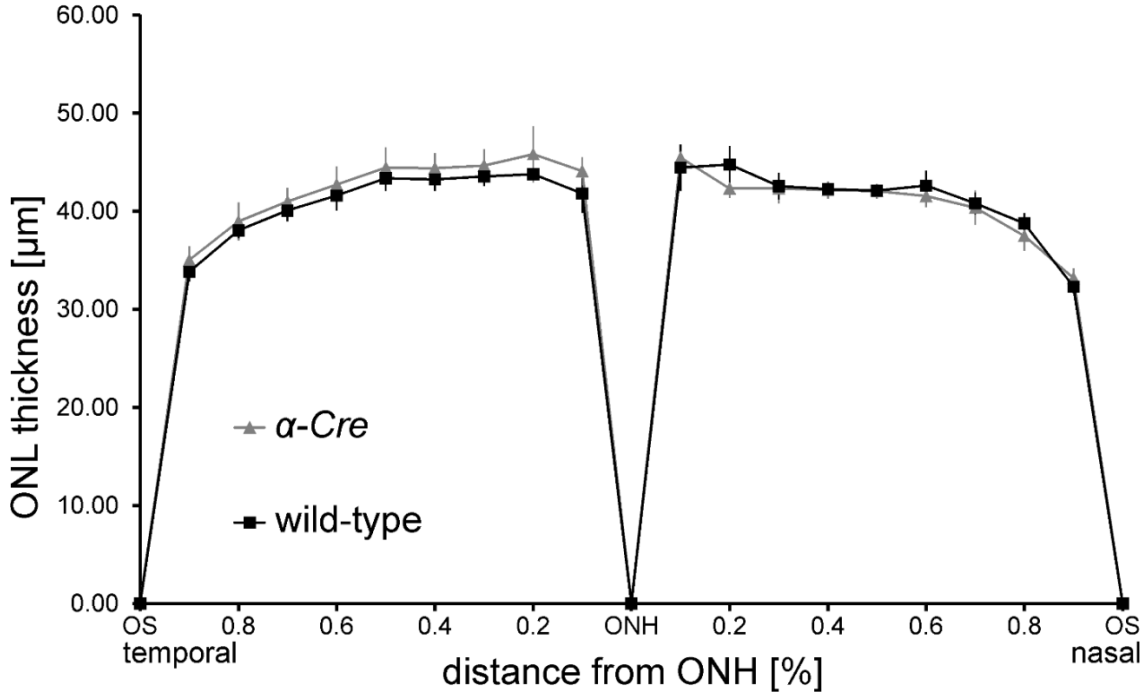


*Figure 20:* Morphometric analysis of the thickness of the outer nuclear layer (ONL), measured on mid-horizontal Richardson-stained semithin sections through the eyes of 7-8-week-old untreated wild-type animals and their *α-Cre* littermates

Throughout the circumference of the retina the thickness of the ONL did not differ between the eyes of wild-type animals and transgenic littermates (n = 7/5). Data are shown as mean ± SEM. Morphometric analysis performed in cooperation with Tatjana Groß. OS, ora serrata; ONH, optic nerve head; ONL, outer nuclear layer. Experiment published in (Boneva et al., 2016).

To further verify, whether the expression of the Cre recombinase itself would affect the neuronal vulnerability and therefore interfere with the planned experiments, light damage was performed with wild-type animals and *α-Cre* littermates, followed by TUNEL labeling for apoptotic cells. Since the TUNEL assay specifically tags them, the number of fluorescing nuclei was counted and normalized to the ONL area (Figure 21B.). The typical pattern of light damage, hallmarked by major concentration of apoptosis in the central retina of the ONL, could be observed in the mid-horizontal sections, stretching from the temporal OS through the ONH to the nasal side (Figure 21A., right-hand side panel). The acquired results were statistically evaluated and no significant differences between the apoptotic rates for wild-type and *α-Cre* animals could be discerned (Figure 21A., left-hand side panel). Consequently, the *α-Cre* strain suited the expectations for a recombinase enzyme, which would only delete a certain "floxed" sequence, namely under direction of the *Pax6* α enhancer element. Further events, regarding parallel activities of the Cre, did not need to be anticipated in the following (light damage) experiments.

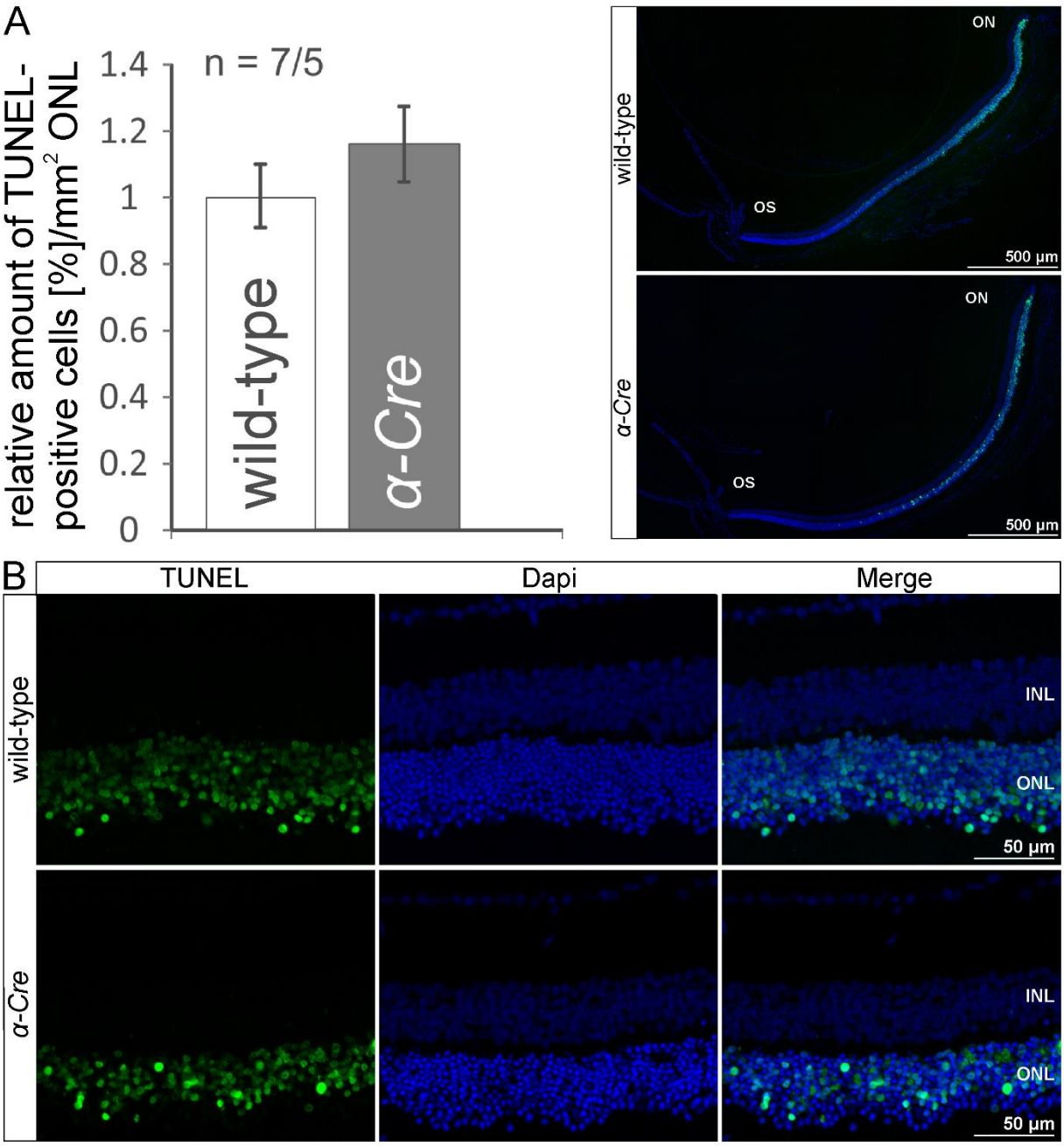


*Figure 21:* Neuronal vulnerability of *α-Cre* and wild-type mice: TUNEL labeling in the retinae of 6-7-week-old animals 30 h after light-induced damage

A. Right-hand side panel: The horizontal TUNEL-labeled (green channel) sections through the retinal hemispheres of light-exposed animals demonstrate the characteristic pattern of retinal damage, sustained by light, i.e. the concentration of apoptotic signals in the central retina. Nuclei were stained with DAPI (blue). Left-hand side panel: the statistical quantification of TUNEL-labeled cells per 1 mm² ONL area did not indicate any significant differences between wild-type and *α-Cre* apoptotic rates upon light damage. Data is mean ± SEM, n = 7/5 (wild-type to transgenic mice).

B. The higher magnification of the central retinae shows the localization of the fluorescing nuclei within the ONL. Apoptotic cells fluoresced with green signal. OS, ora serrata; ONH, optic nerve head; INL, inner nuclear layer; ONL, outer nuclear layer. Figure modified after (Boneva et al., 2016).

### 3.1.1.3 *Tgfbr2* deletion PCR: characterization of a successfully occurred recombination event (*Tgfbr2*$^{\Delta oc}$-mice)

As mentioned previously, in *Tgfbr2*$^{\Delta oc}$ mice Exon2 of TßRII was removed by Cre recombinase within the cells, originating from the inner layer of the optic cup. To prove that recombination has occurred throughout the concerned layers, primer pairs, shown to amplify a corresponding PCR product for transgenic mice, were used in the performed PCR analysis (Chytil et al., 2002). A positive signal was detected for the retinal layer (Figure 22). Due to the differing product sizes (no deletion: 3974 bp; after deletion: 636 bp) and the given elongation time of 1 min, the deletion product only was amplified in samples, following a Cre-mediated recombination. Actin was used as a loading control.

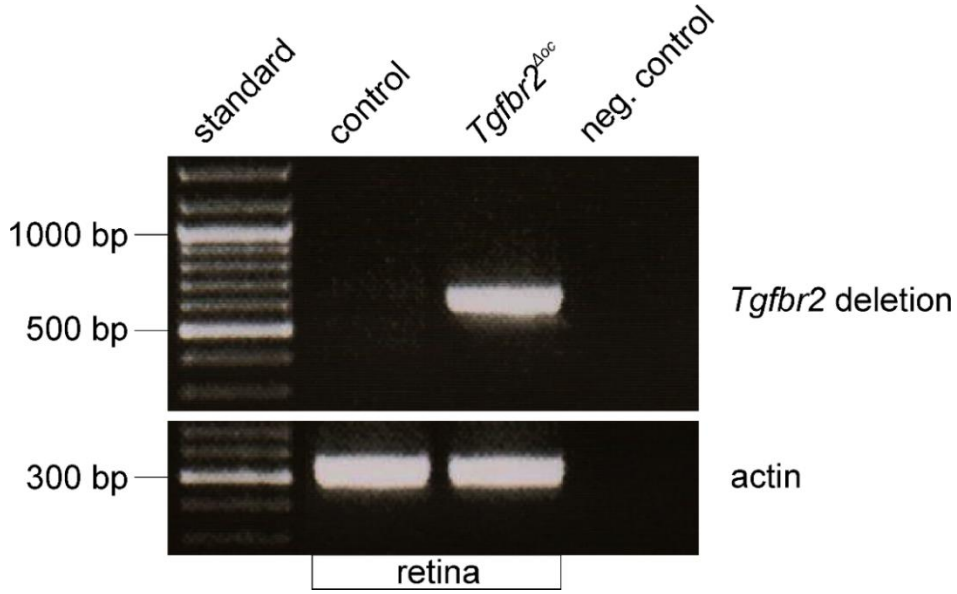


*Figure 22: Tgfbr2* deletion PCR with retinal genomic DNA of a 6-week-old *Tgfbr2*$^{\Delta oc}$ mouse and its control littermate

In *Tgfbr2*$^{\Delta oc}$ mice recombination was proven to occur in the retinal cells.

### 3.1.1.4 Western blot analysis: protein translation, analyzed in retinae extracts

To further demonstrate the conditional downregulation of TGF-ß signaling (by deleting TßRII) on a protein level, Western blot analyses were performed. Protein extracts from the retinae of control and *Tgfbr2*$^{\Delta oc}$-animals were tested for the translation of the TßRII protein. A distinct band migrated at the expected molecular weight of 70 kDa for the retinal lysates of the control animals, while the signal was attenuated in the protein extracts from TßRII-deficient littermates (Figure 23A.). GAPDH was run as a loading control. The densitometric analysis showed a significantly less intense signal in *Tgfbr2*$^{\Delta oc}$ animals, when compared to controls (Figure 23B.).

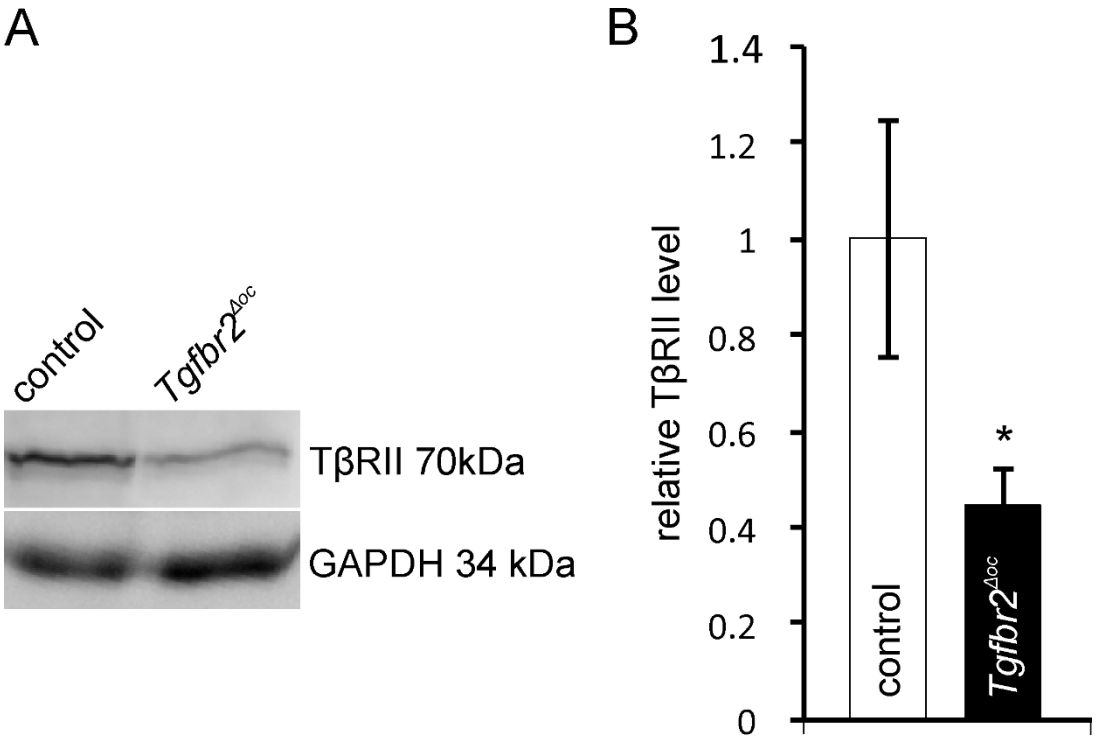


*Figure 23:* Western blot analysis for TßRII in retinae, extracted from 6-8-week-old *Tgfbr2*$^{\Delta oc}$ animals and their control littermates

A. The TßRII Western blot analysis shows a signal at the expected molecular weight of 70 kDa for the retinal lysates of control animals, whereas the signal is markedly reduced in the protein extracts of *Tgfbr2*$^{\Delta oc}$ animals. GAPDH was run as a loading control. B. Statistical evaluation of the densitometric analysis. Data is mean ± SEM, n = 7/8 (controls to *Tgfbr2*$^{\Delta oc}$-mice), $*p = 0.0388$.

### 3.1.1.5 Immunohistochemistry: localization of TßRII within the transgenic retina

To further specify the localization of the TßRII protein and ultimately attribute it to certain retinal layers, immunohistochemical staining reactions were performed. For the retinae of adult control mice distinct immunoreactivity for TßRII was observed within the layers of the inner retina, especially the ganglion cell layer (GCL), the INL and some extension-like structures within the ONL (Figure 24). TßRII immunoreactivity was considerably weaker, even barely detectable (Figure 24), in the retinal layers of *Tgfbr2*$^{\Delta oc}$ animals.

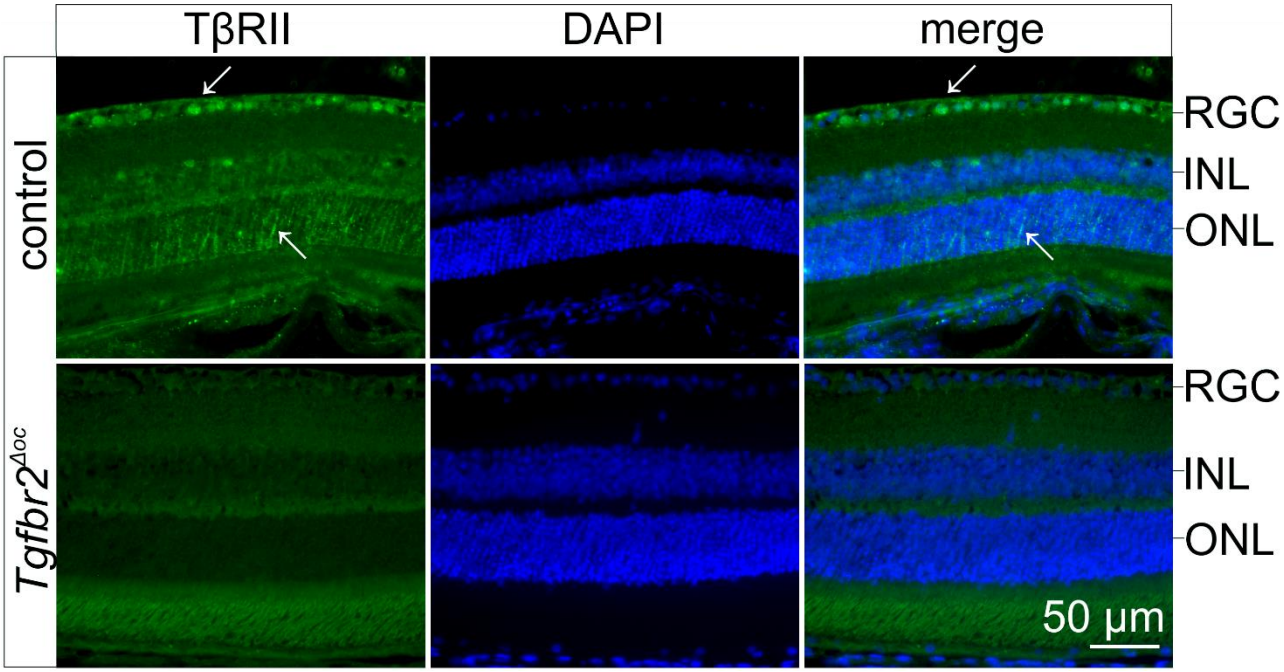


*Figure 24:* Immunohistochemical staining for TßRII in the retinae of a 6.5-week-old *Tgfbr2*$^{\Delta oc}$ animal and its control littermate

Specific immunohistochemical reactivity for TßRII (green) was detectable (arrows) within the GCL, the inner nuclear layer (INL) and some extension-like structures within the outer nuclear layer (ONL) of a control animal (exemplary shown for the central retina). The transgenic animal did not show a similar reaction in the retina. Nulcei were stained with DAPI (blue channel). RGC, retinal ganglion cells; INL, inner nuclear layer; ONL, outer nuclear layer.

### 3.1.1.6 TGF-ß signaling pathway activation in the retinae of control and *Tgfbr2*$^{\Delta oc}$ animals

Upon receptor-mediated phosphorylation of SMAD3, the molecule acts as a transducer for TGF-ß-like signals (Attisano and Wrana, 2002). To prove whether the intracellular TGF-ß signaling cascade is affected in the retinae of *Tgfbr2*$^{\Delta oc}$ mice, an immunohistochemical staining reaction for pSMAD3 was performed. In the eyes of control mice, the specific immunohistochemical responses were restricted to the perikarya within the INL and the GCL (Figure 25). On the contrary, no such pattern could be observed for the retinae of *Tgfbr2*$^{\Delta oc}$ animals (Figure 25). An antibody control section confirmed the specificity of the secondary antibody (Figure 26) and the successful diminishment of eGFP activity, originating from the *α-Cre* background (Marquardt et al., 2001), most likely due to the fixation and paraffin embedding processes.

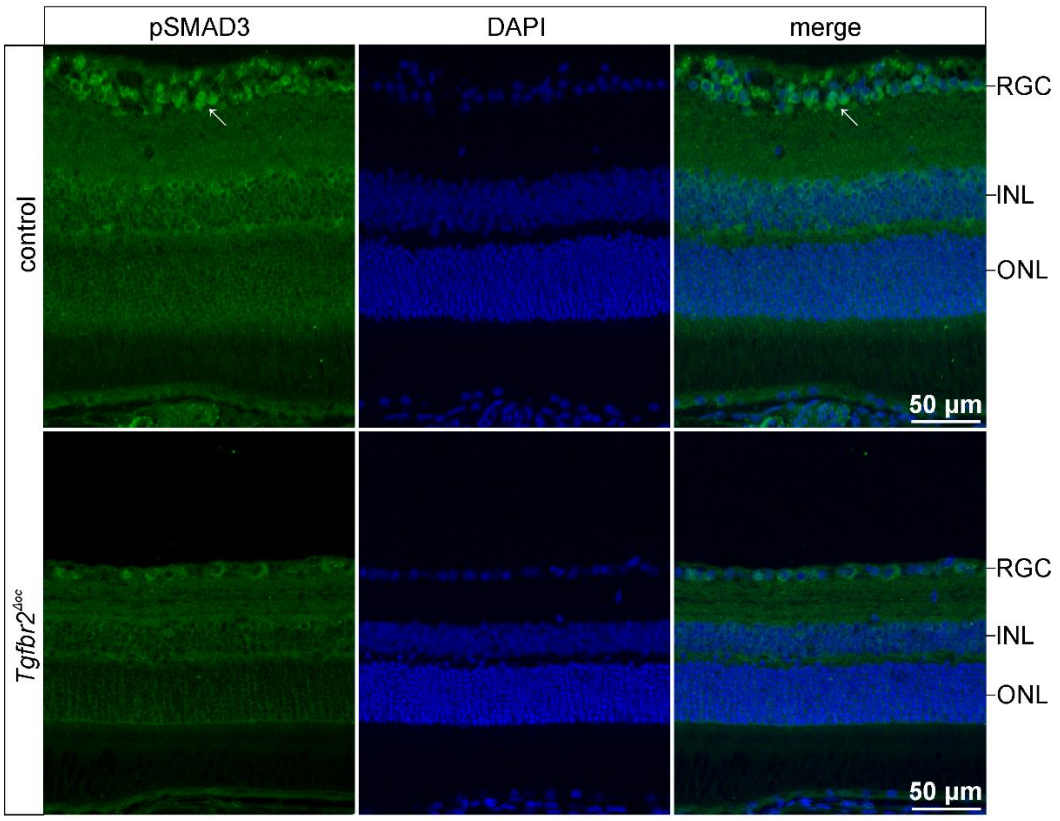


*Figure 25:* SMAD3 activity in the neural retinae of a control animal and its *Tgfbr2*$^{\Delta oc}$ littermate

The 6.5-week-old control animal shows a specific immunohistochemical reaction (green) in the central retinal regions, within the cells of the GCL and the INL. Comparable signals are considerably weaker, even absent in the retina of the *Tgfbr2*$^{\Delta oc}$ littermate. Nuclei are stained with DAPI (blue). RGC, retinal ganglion cells; INL, inner nuclear layer; ONL, outer nuclear layer.

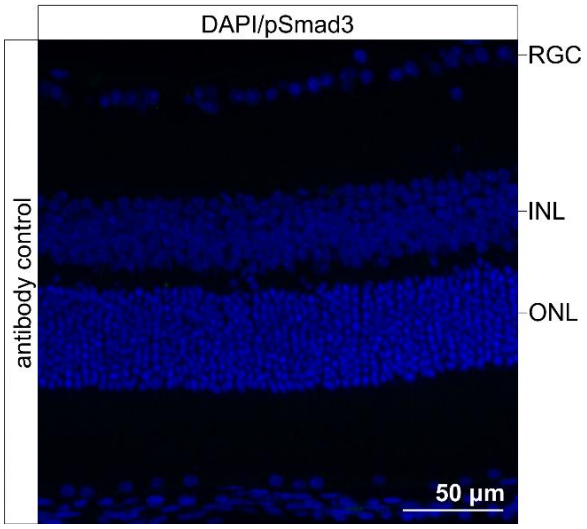


*Figure 26:* Antibody control

The section indicates the specificity of the antibody and the successful diminishment of eGFP activity, originating from the *α-Cre* background. RGC, retinal ganglion cells; INL, inner nuclear layer; ONL, outer nuclear layer.

To further confirm the downregulation of the TGF-ß signaling pathway in TßRII-deficient animals, Western blot analyses for pSMAD3 were performed. Here, a specific signal was detected at the expected molecular weight of 54 kDa in lysates of the neural retinae of adult control mice (Figure 27). The signal was considerably weaker in *Tgfbr2*$^{\Delta oc}$ animals. Relative densitometry showed a significantly higher amount of phosphorylated SMAD3 in retinal lysates of control animals, compared to transgenic mice.

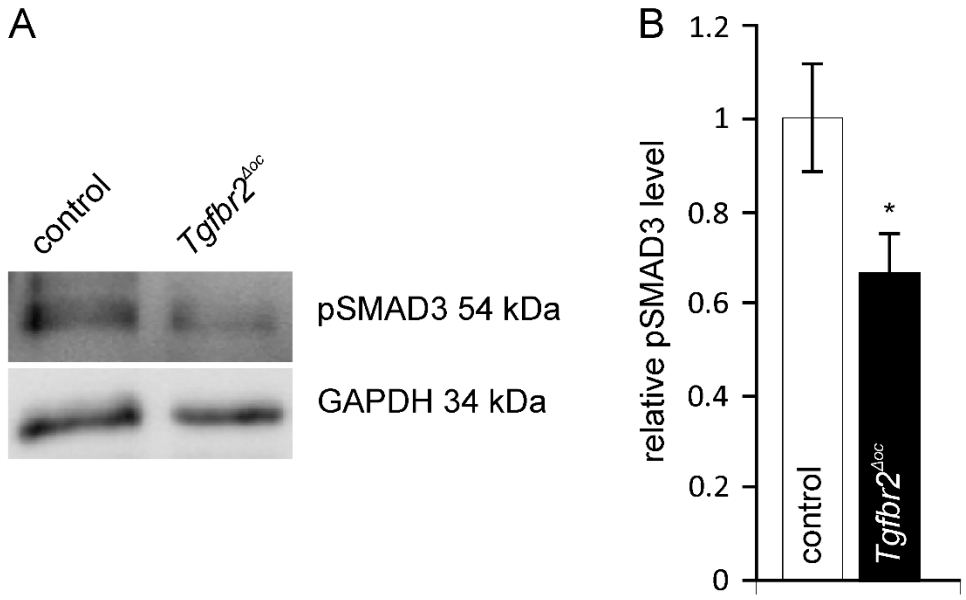


*Figure 27:* pSMAD3 Western blot analysis
A. Western blot analyses for pSMAD3 in retinal proteins of 6-8-week-old control mice and TßRII-deficient littermates. GAPDH was used as a loading control. B. Densitometric analysis of Western blots for pSMAD3 level. Data is mean ± SEM, n = 8/8 (controls to *Tgfbr2*$^{\Delta oc}$ mice), $*p = 0{,}0363$.

Taken together, these results demonstrate the successful conditional deletion of the TßRII in *Tgfbr2*$^{\Delta oc}$ mice and the consequent downregulation of TGF-ß signaling in cells, originating from the inner layer of the optic cup.

### 3.1.2 Conditional deletion of TßRII in rod photoreceptor cells

#### 3.1.2.1 Cellular expression of the Cre recombinase in the *LMOP-Cre* strain

To visualize the tissue expression pattern of the Cre recombinase enzyme in the *LMOP-Cre* strain, Rosa-LacZ reporter mice (R26R) were interbred with the *LMOP-Cre* strain and ß-galactosidase staining was performed for the progeny. Since lacZ is only expressed in tissues where Cre is expressed and active (Soriano, 1999), the eyes of wild-type

animals showed no signal (Figure 28). On the contrary, double transgenic *LMOP-Cre*/R26R mice reacted with a much more intense signal throughout outer retina (Figure 28, Figure 29), located primarily within the photoreceptor inner and outer segments layers (PIS and POS), the ONL and the outer plexiform layer (OPL).

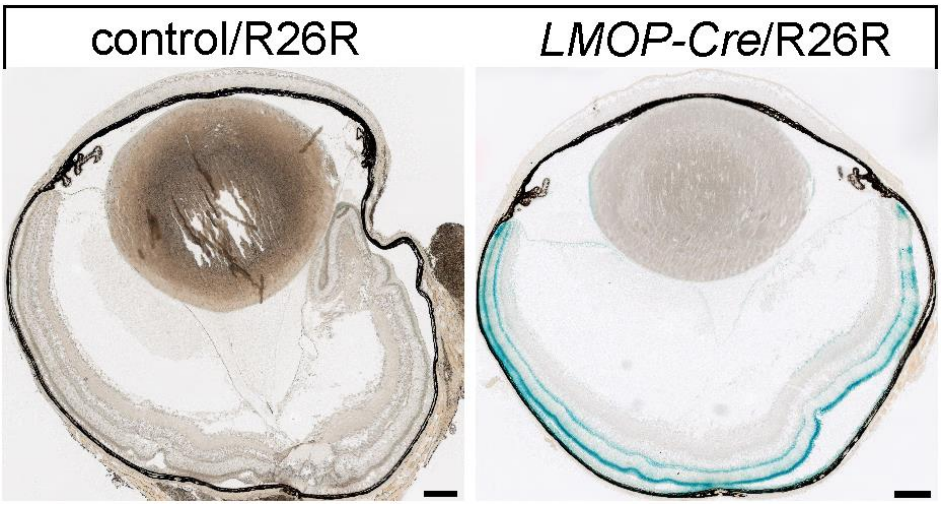


*Figure 28:* Rosa-LacZ reporter mice (R26R): panorama view of ß-galactosidase-stained eyes of 3-week-old animals

The panorama picture of the eye of a *LMOP-Cre*/R26R mouse shows a more intense reaction in its retina in comparison to the control/R26R, indicating the activity of the Cre recombinase in the ONL of the double transgenic animal. Scale bars correspond to 200 µm. Figure published in (Boneva et al., 2016).

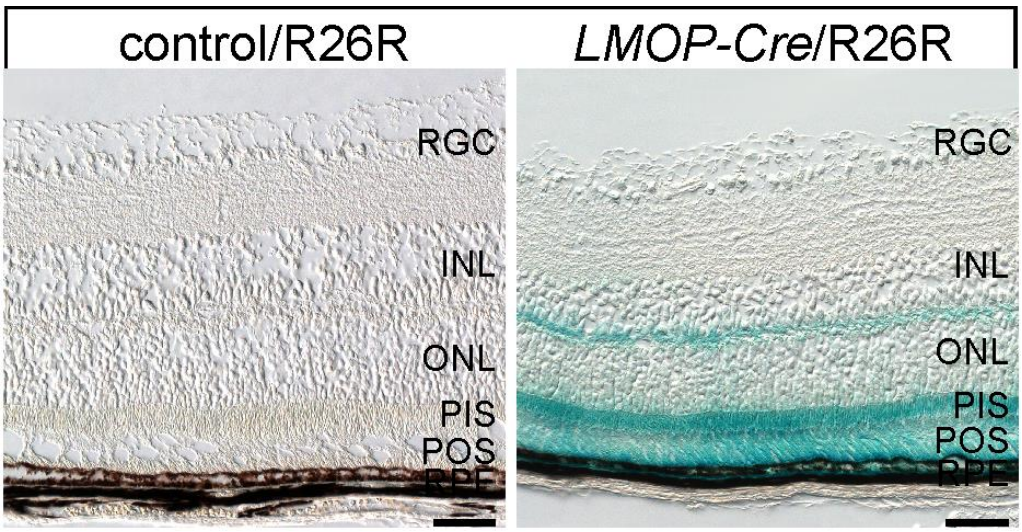


*Figure 29:* Rosa-LacZ reporter mice (R26R): detailed view of ß-galactosidase-stained eyes

The detailed magnification of the ß-galactosidase-stained *LMOP-Cre*/R26R eye from Figure 28 shows an intense reaction in the outer nuclear layer (ONL) and particularly within photoreceptor inner and outer segments (PIS and POS) and outer plexiform layer (OPL). RGC, retinal ganglion cells; INL, inner nuclear layer; RPE, retinal pigment epithelium. Scale bars correspond to 50 µm. Figure published in (Boneva et al., 2016).

3.1.2.2 *Tgfbr2* deletion PCR: characterization of a successfully occurred recombination event (*Tgfbr2*$^{\Delta rod}$ mice)

In *LMOP-Cre* mice the expression of the Cre recombinase is restricted to rod photoreceptors due to the long (4.1 kb) mouse opsin-promoter (Le et al., 2006). To confirm the recombination in rod photoreceptors, the same primer pairs were used as for the *Tgfbr2*$^{\Delta oc}$-mice, amplifying a PCR product only, if a recombination event occurred (Figure 30). Actin was used as a loading control.

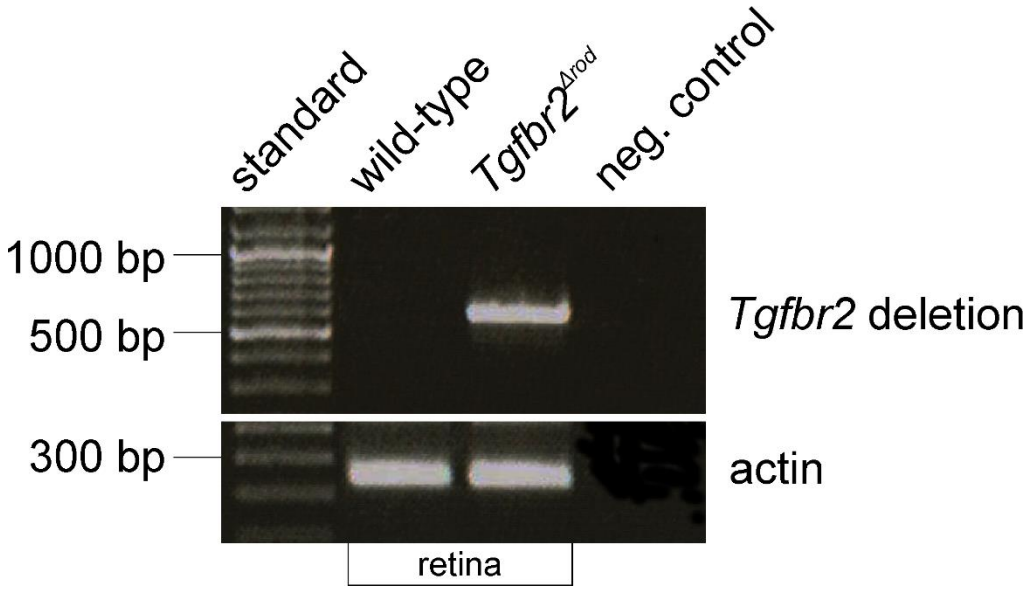


*Figure 30: Tgfbr2* deletion PCR with retinal genomic DNA of an adult 6-week-old *Tgfbr2*$^{\Delta rod}$ mouse and its control littermate

The 636 bp PCR product in *Tgfbr2*$^{\Delta rod}$ mice confirms the Cre-mediated recombination in the retina. Actin was used as a loading control.

## 3.2 Phenotype analysis

### 3.2.1 Phenotype analysis of the eyes of *Tgfbr2*$^{\Delta oc}$ mice

#### 3.2.1.1 Morphology of the retina of *Tgfbr2*$^{\Delta oc}$ mice

Semithin sections of the eyes of at least 6-week-old transgenic animals and their control littermates, stained according to the Richardson's protocol, were analyzed by light microscopy. Both genotypes did not show morphological differences (Figure 31, Figure 32): the eyes were analogous, regarding size and architecture of the retinal layers along the full circumference, from the optic nerve head (ONH) to the ora serrata (OS).

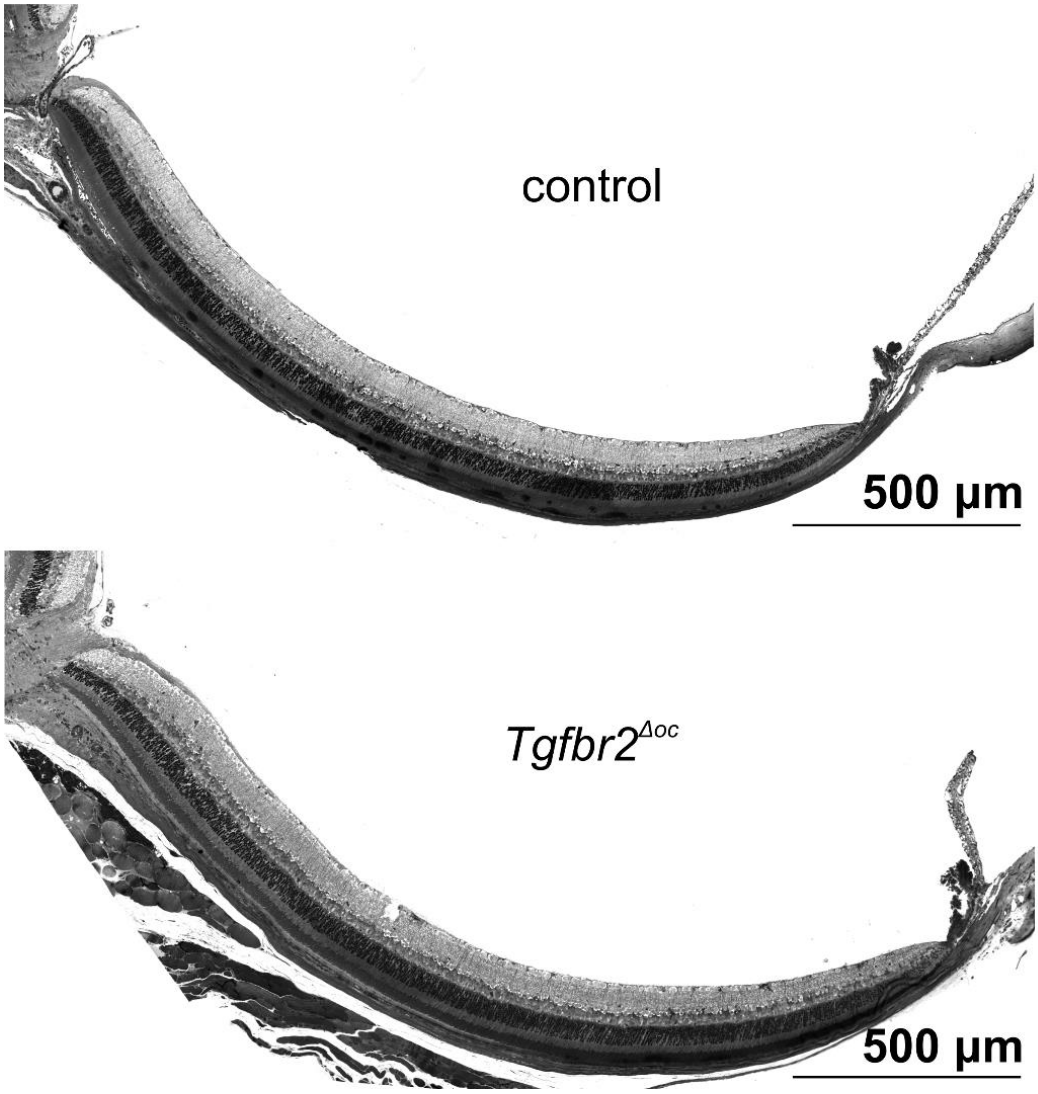


*Figure 31:* Semithin horizontal sections through the retinae of a 9.5-week-old control mouse and its *Tgfbr2*$^{\Delta oc}$ littermate

The sections (1 µm thick) present both eyes from the optic nerve head (ONH) to the periphery. A TβRII deficiency did not lead to morphological alterations in the retina.

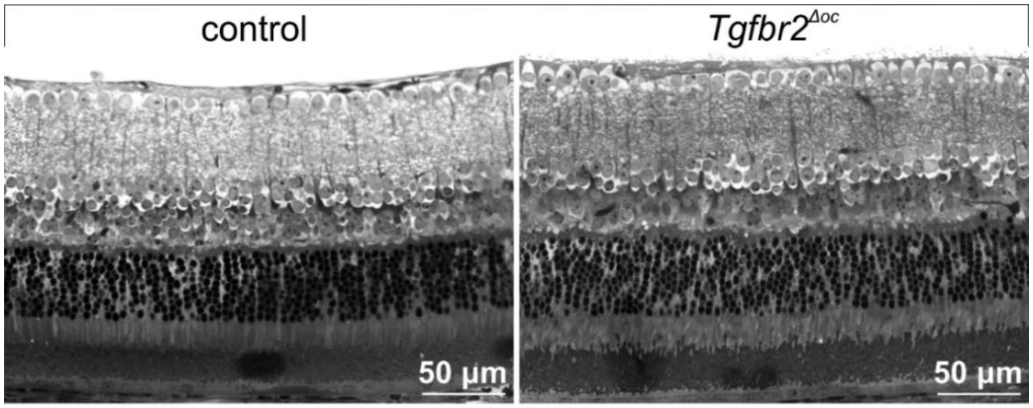


*Figure 32:* Detailed view of the central retinae of untreated animals
The retinae of a 9.5-week-old control mouse and its *Tgfbr2*$^{\Delta oc}$ littermate did not show morphological differences. Higher magnification of central retinal regions of the semithin horizontal sections from Figure 31.

To obtain statistically meaningful data, morphometric analyses were performed. To this end, the thickness of both INL and ONL throughout the entire retina was compared in untreated (no light) animals (Figure 33, Figure 34). In accordance with previously published data of our group (Braunger et al., 2013b), *Tgfbr2*$^{\Delta oc}$ animals demonstrated a reduced thickness of the INL, when compared to control littermates, with two measure points even showing a significant decrease (*$p$ = 0.043 to *$p$ = 0.048) (Figure 33).

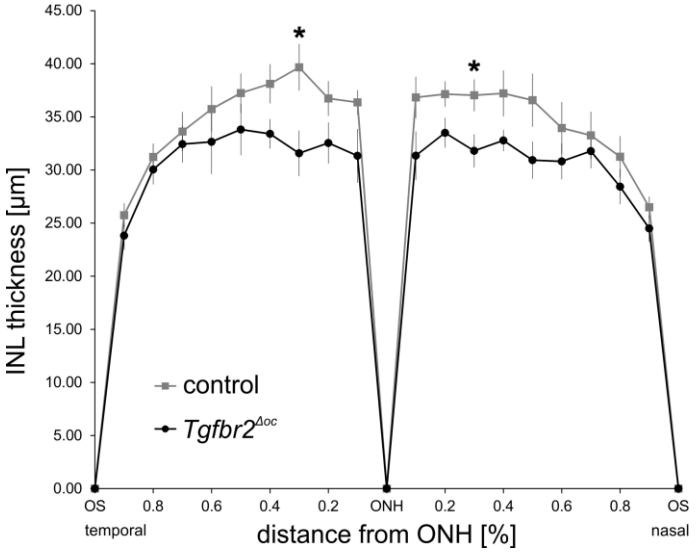


*Figure 33:* Thickness of the inner nuclear layer (INL), measured on mid-horizontal semithin sections through the eyes of untreated 7-9.5-week-old *Tgfbr2*$^{\Delta oc}$ animals and their control littermates
Throughout the circumference of the retina the thickness of the INL was uniformly reduced for the eyes of *Tgfbr2*$^{\Delta oc}$ animals, compared to control littermates, reaching a significant decrease at two measure points (*$p$ = 0.043 to *$p$ = 0.048). Mean ± SEM, $n$ = 8 each. INL, inner nuclear layer; ONH, optic nerve head.

The morphometric analysis of the thickness of the ONL (Figure 34) did not show any significant differences for the eyes of *Tgfbr2*$^{\Delta oc}$ mice in comparison to their control littermates ($n$ = 8 per each group).

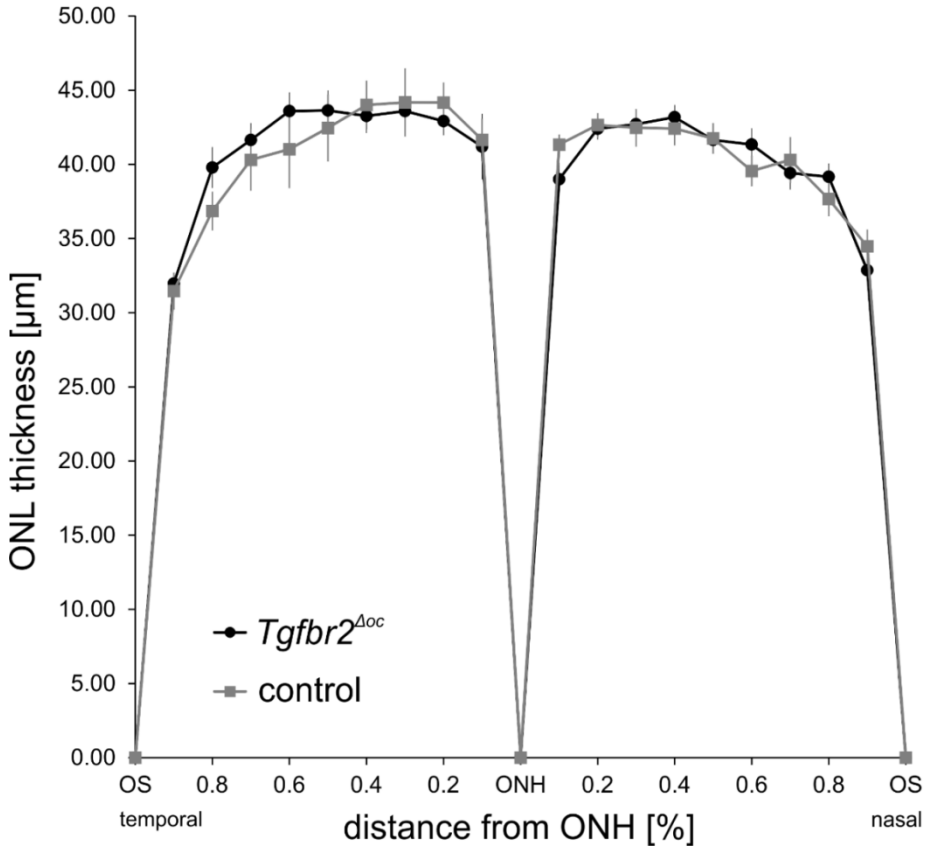


*Figure 34:* Thickness of the outer nuclear layer (ONL): eyes of untreated 7-9.5-week-old control animals and their *Tgfbr2*$^{\Delta oc}$ littermates

Throughout the circumference of the retina the thickness of the ONL did not differ between the eyes of *Tgfbr2*$^{\Delta oc}$ animals and their control littermates. Mean ± SEM, $n$ = 8 each. ONL, outer nuclear layer; ONH, optic nerve head.

### 3.2.1.2 Vascular phenotype

To detect any possible alterations in the vasculature of TβRII-deficient animals *in vivo* funduscopy and fluorescein angiography (FLA) were performed on the eyes of 6-week-old transgenic and control animals. *Tgfbr2*$^{\Delta oc}$ mice did not present any obvious morphological differences, regarding the retinal vasculature, in comparison to their control littermates (Figure 35).

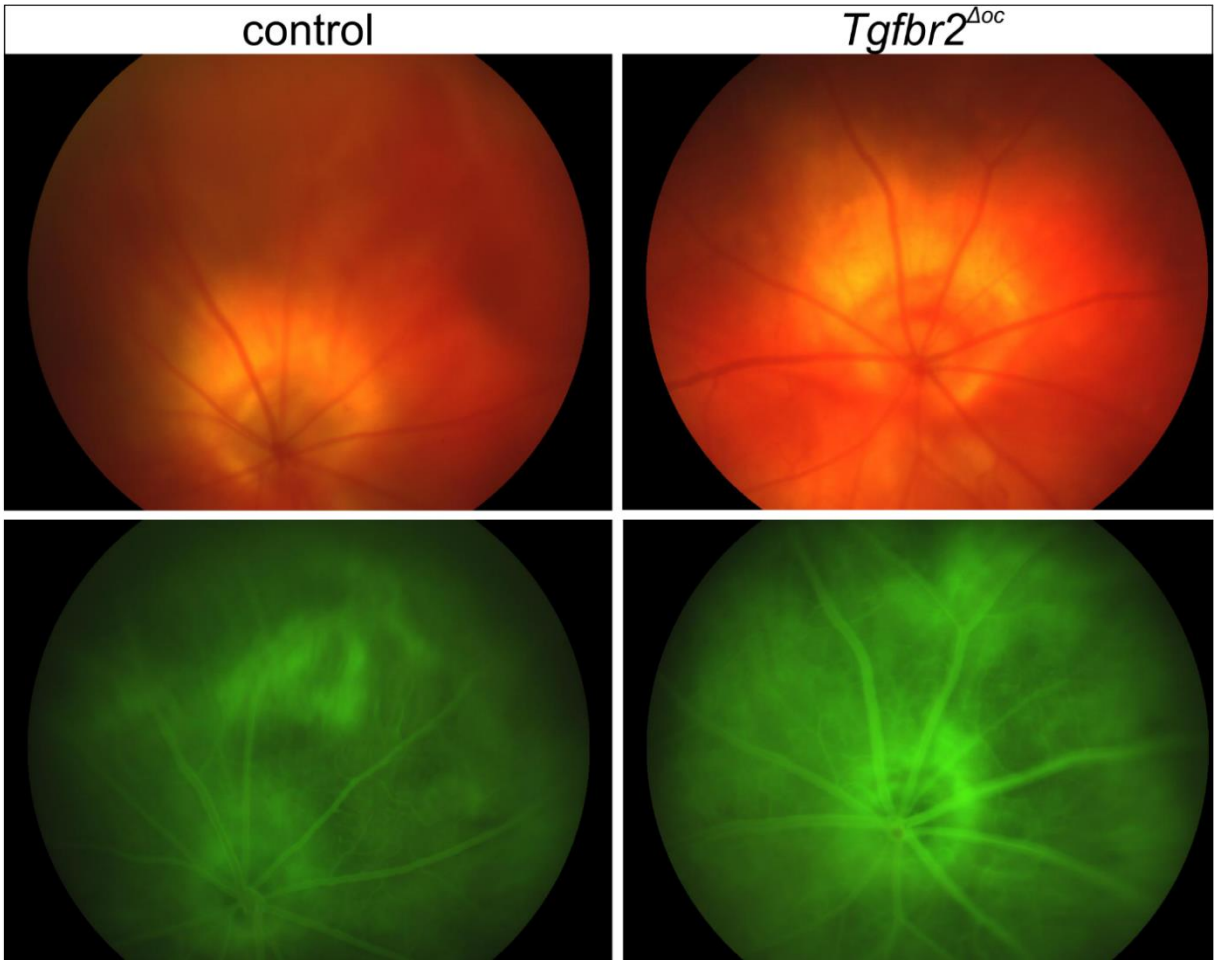


*Figure 35: In vivo* funduscopy (upper panel) and fluorescein angiography (FLA) (lower panel)

The retinal vasculature of a 1.5-month-old *Tgfbr2*$^{\Delta oc}$ animal did not show any obvious differences in comparison to the control littermate. *In vivo* funduscopy and FLA were performed in cooperation with Prof. H. Jägle.

### 3.2.2 Morphological analysis of the eyes of *Tgfbr2*$^{\Delta rod}$ mice, bearing the TβRII deficiency within the rod photoreceptors

Mid-horizontal semithin sections of the eyes of at least 6-week-old transgenic animals and their control littermates, stained according to the Richardson's protocol were analyzed by light microscopy. Both genotypes did not show morphological differences (Figure 36, Figure 37): the eyes were analogous, regarding size and architecture of the retinal layers along the full circumference, from the ONH to the periphery.

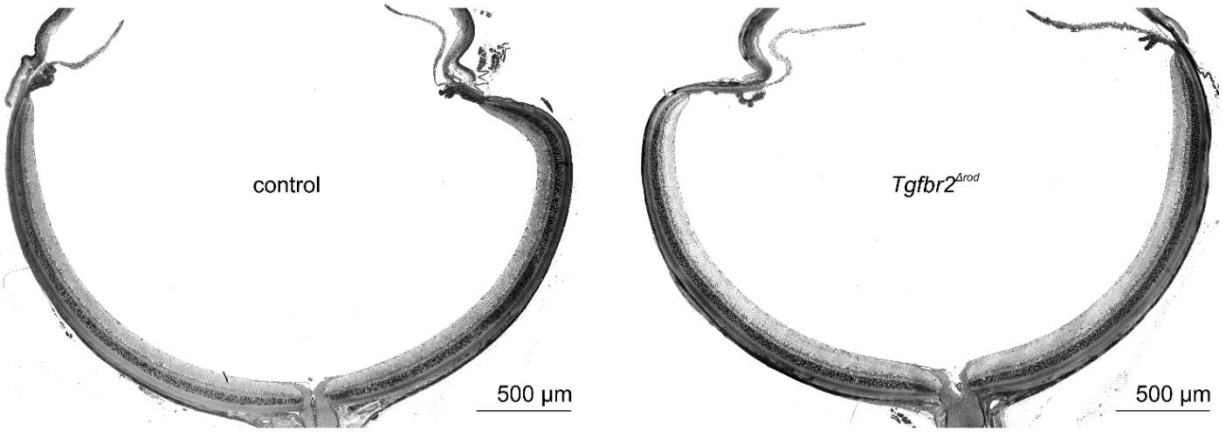


*Figure 36:* Semithin horizontal sections through the eyes of a 6-week-old control mouse and its *Tgfbr2*$^{\Delta rod}$ littermate

The sections (1 µm thick) present similar phenotypes. The size of both eyes is alike and the architecture of the retinal layers is regular: all present from the optic nerve head to the periphery.

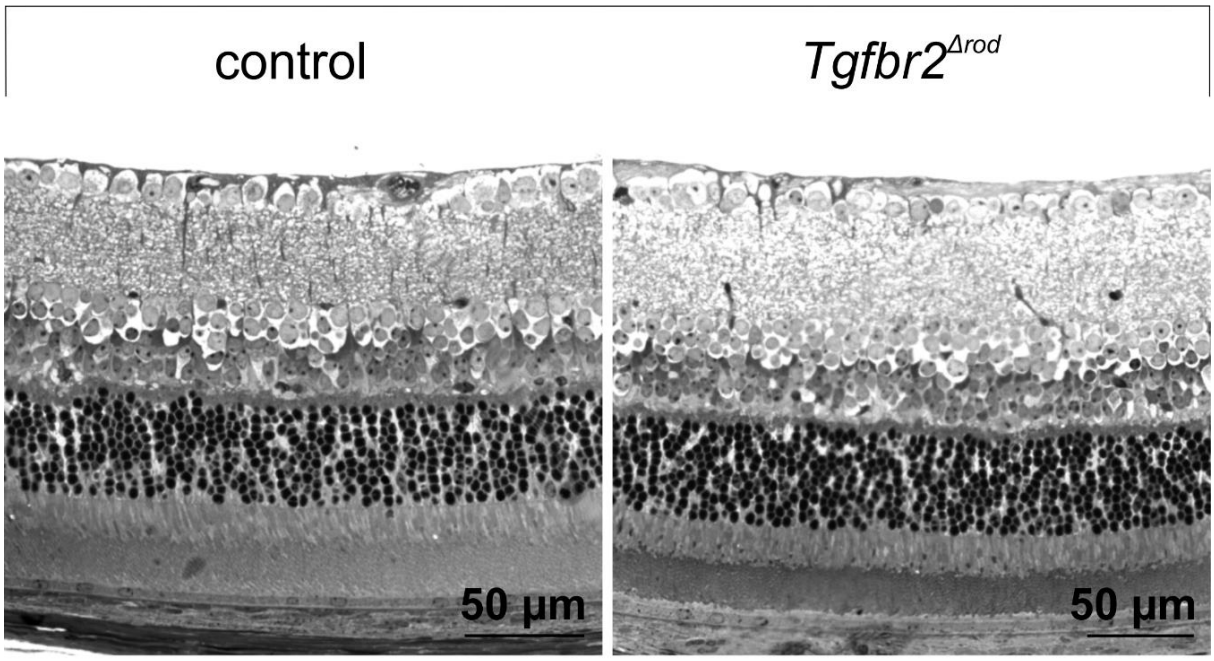


*Figure 37:* Semithin sections through the central retinae of untreated animals

The retinae of a 6-week-old control mouse and its *Tgfbr2*$^{\Delta rod}$ littermate did not show morphological differences (higher magnification of central retinal regions of the horizontal sections from Figure 36).

Prior to light damage experiments the thickness of both the INL and the ONL throughout the entire retina was compared (Figure 38 and Figure 39, respectively). Along the circumference of the retina the thickness of the INL (Figure 38) and the ONL (Figure 39) did not differ significantly between control animals and transgenic littermates.

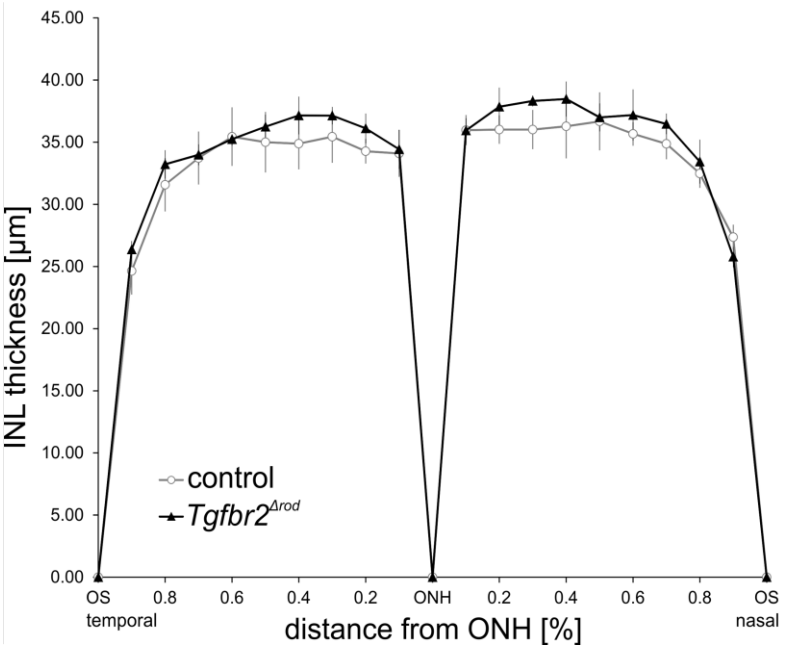


*Figure 38:* Thickness of the inner nuclear layer (INL): eyes of at least 6-week-old untreated control animals and their *Tgfbr2*$^{\Delta rod}$ littermates

Throughout the circumference of the retina the thickness of the INL did not differ significantly between the eyes of *Tgfbr2*$^{\Delta rod}$ animals and their control littermates. Mean ± SEM, $n$ = 6/4.

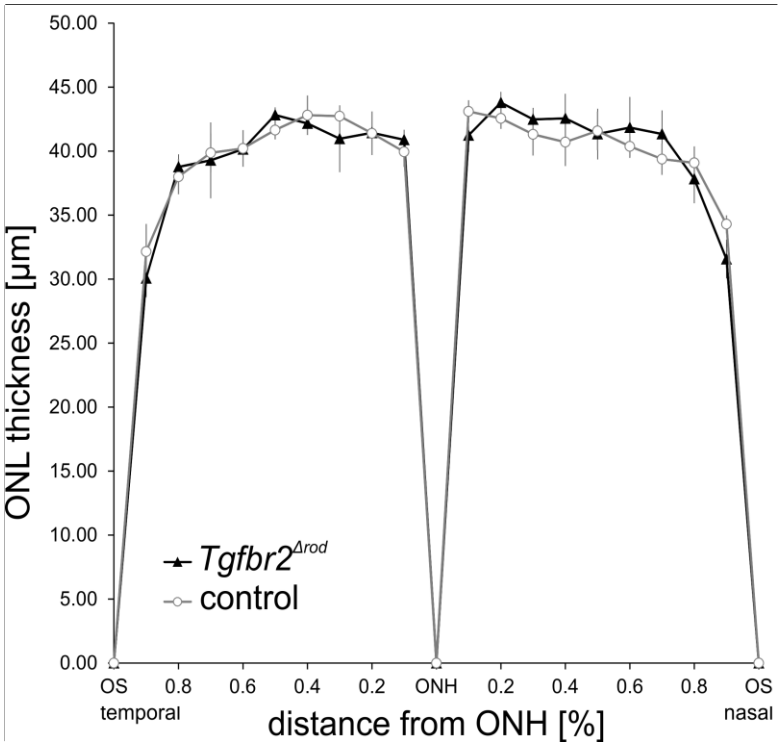


*Figure 39:* Thickness of the outer nuclear layer (ONL): eyes of at least 6-week-old untreated control animals and their *Tgfbr2*$^{\Delta rod}$ littermates

Throughout the circumference of the retina the thickness of the ONL did not vary significantly between the eyes of *Tgfbr2*$^{\Delta rod}$ animals and control littermates. Mean ± SEM, $n$ = 6/4. OS, ora serrata; ONH, optic nerve head.

## 3.3 Light damage experiments

Light damage experiments were performed in order to assess the hypothesis that the TGF-ß signaling pathway plays a neuroprotective role for photoreceptors in the adult retina.

### 3.3.1 Light damage experiments on *Tgfbr2*$^{\Delta oc}$ mice: TßRII deficiency within the optic-cup-derived cells of the neural retina

#### 3.3.1.1 Morphometric analyses of the light-exposed eyes of *Tgfbr2*$^{\Delta oc}$ and control littermates

To evaluate, whether the regular function of the TGF-ß signaling pathway in retinal neurons and Müller cells would protect photoreceptors from light- induced damage, 6-8-week-old *Tgfbr2*$^{\Delta oc}$ and control animals were treated with cool white light at an intensity of 5000 lux for 1 h. 14 days later the eyes were processed for light microscopy and semithin mid-horizontal sections were analyzed subsequently. The thickness of the outer nuclear layer (ONL) was measured at 21 equidistant loci along the nasal-temporal plane. The major portion of light damage on photoreceptors was concentrated in the central retina, around the ONH, while the peripheral retina, near the OS, was hardly concerned by light stress. However, the resulting Spider diagram did not show any significant morphometrical differences between the retinae of *Tgfbr2*$^{\Delta oc}$ mice and their control littermates (Figure 40). Although the thickness of the ONL was severely reduced in the retinae of transgenic animals, the impairment was similar for control eyes, which were not affected by the downregulation of TGF-ß signaling.

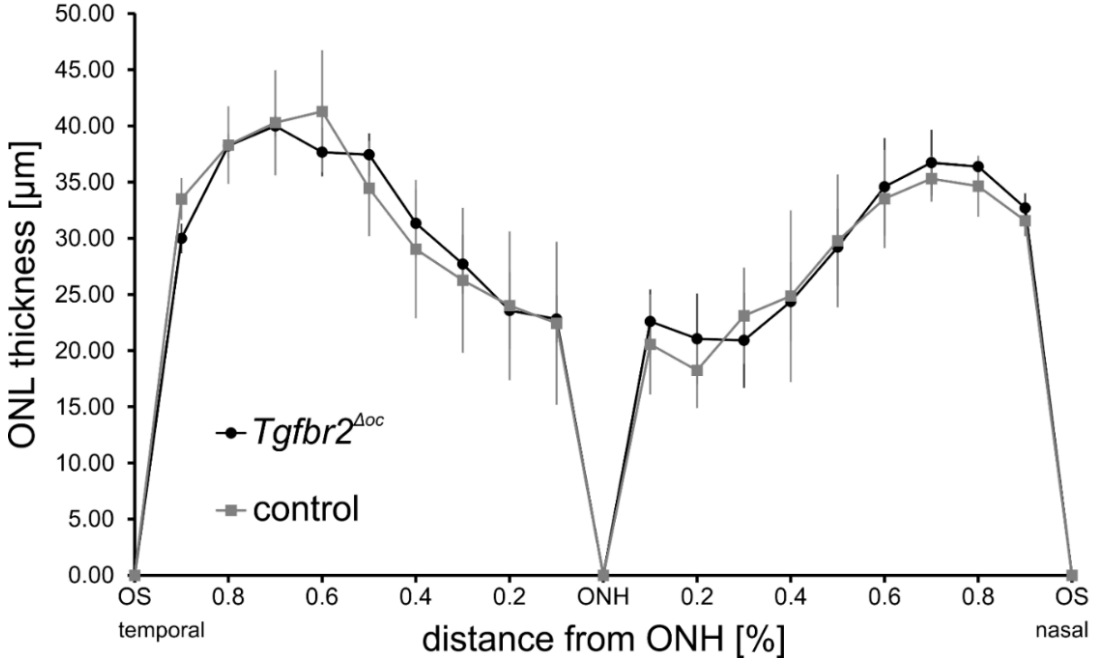


*Figure 40:* A spider diagram, visualizing the thickness of the outer nuclear layer (ONL) of 8-week-old *Tgfbr2*$^{\Delta oc}$ mice and control littermates after exposure to light for 1 h
Despite the robust diminishment of cell rows within the ONL of *Tgfbr2*$^{\Delta oc}$ animals, the damage was similar to that, observed for control littermates. Mean ± SEM, n = 5 *Tgfbr2*$^{\Delta oc}$, n = 6 controls. OS, ora serrata; ONH, optic nerve head.

Following an exposure for only half of the time – 30 min, another morphometric analysis was performed. The central part of control retinae demonstrated 6 to 8 rows of remaining nuclei in the ONL (Figure 41, upper panel; Figure 42, left-hand side panel). In contrast, in *Tgfbr2*$^{\Delta oc}$ animals, only 3 to 4 layers of nuclei were present in the ONL following damage (Figure 41, lower panel; Figure 42, right-hand side panel).

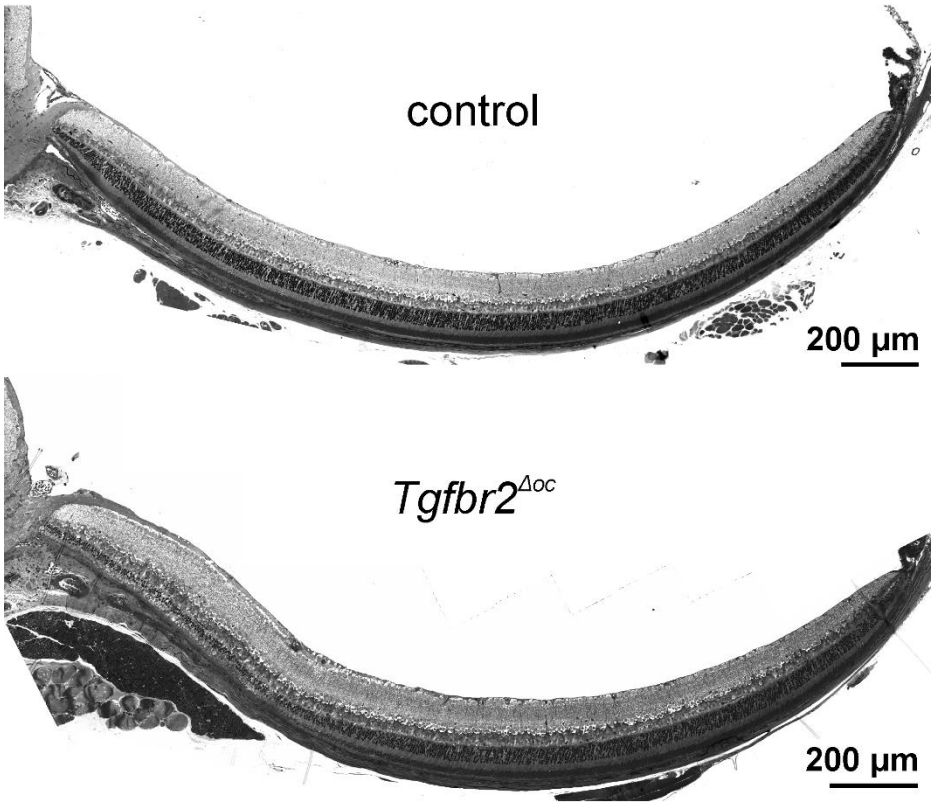


*Figure 41:* Deletion of TGF-ß signaling in neurons and Müller cells enhances photoreceptors degeneration following light damage: retinae of an 8-week-old *Tgfbr2*$^{\Delta oc}$ mouse and its control littermate 14 d after light exposure

The semithin sections are stretching through the central and peripheral retina. The outer nuclear layer (ONL) in the central part of the TßRII-deficient retina (lower panel) is considerably thinner than the respective part of the control retina (upper panel).

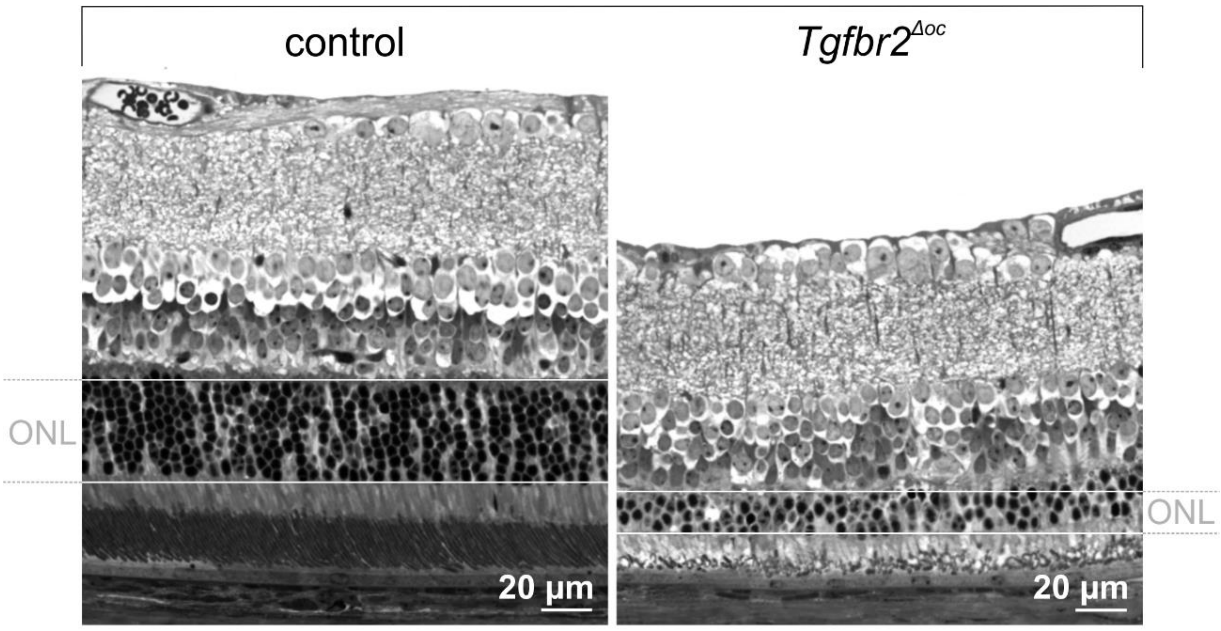


*Figure 42:* Higher magnification of the central retina following light exposure

Semithin sections of a light-exposed 8-week-old *Tgfbr2*$^{\Delta oc}$ mouse and its control littermate 14 d after light damage. The outer nuclear layer (ONL) is flanked by white bars.

To obtain statistically meaningful data, the thickness of the ONL was measured on mid-horizontal sections at 21 equidistant loci along the nasal-temporal plane. The means of the individual measure points were visualized in form of a Spider diagram (Figure 43). The subsequently performed statistical analysis showed a significantly thinner ONL in *Tgfbr2*$^{\Delta oc}$ animals, compared to control littermates – a finding, which indicates that following light exposure a higher number of photoreceptors degenerated in animals, carrying a deletion of the TGF-ß signaling pathway in retinal neurons and Müller cells.

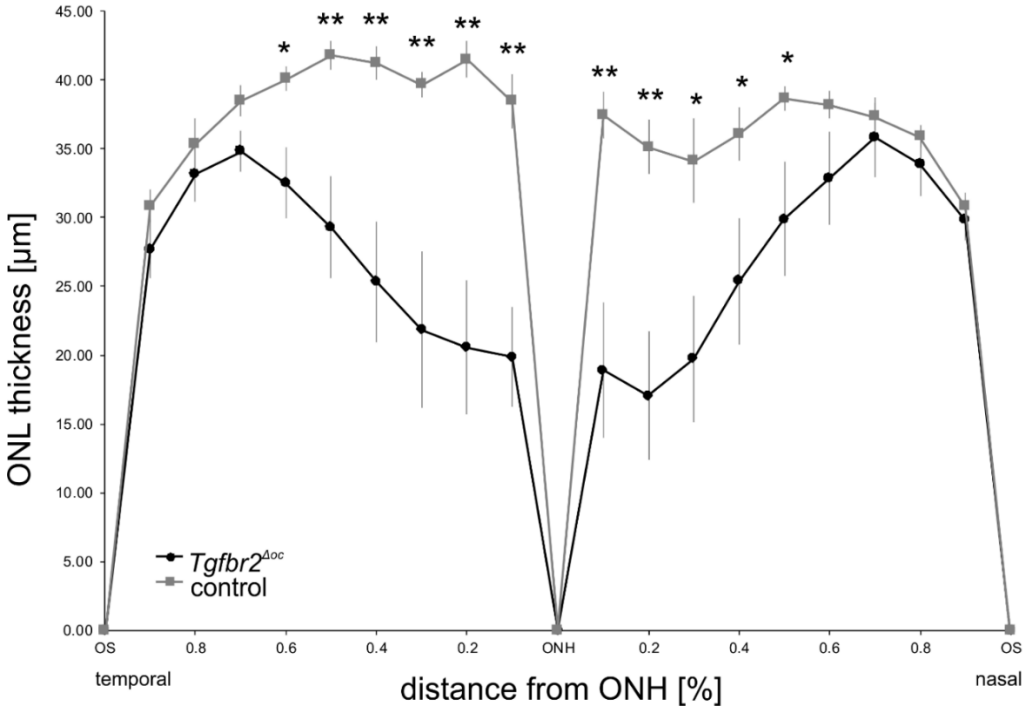


*Figure 43:* Deletion of TGF-ß signaling in neurons and Müller cells enhances photoreceptors degeneration following light damage: Spider diagram
The spider diagram reflects the thickness of the outer nuclear layer (ONL) of light-exposed 8-11-week-old *Tgfbr2*$^{\Delta oc}$ mice and control littermates. The measurements were performed at 21 equidistant loci on mid-horizontal semithin sections, stretching from the temporal to the nasal side. Mean ± SEM, n = 6 *Tgfbr2*$^{\Delta oc}$, n = 5 controls. $^{**}p < 0.01$, $^{*}p < 0.05$. OS, ora serrata; ONH, optic nerve head.

### 3.3.1.2 *In vivo* laser scanning ophthalmoscopy (SLO) and optical coherence tomography (OCT) imaging after light damage

To further validate our results, laser scanning ophthalmoscopy (SLO) and optical coherence tomography (OCT) were executed on the eyes of light-exposed control animals and their *Tgfbr2*$^{\Delta oc}$ littermates. Here, the configuration of the retinal vasculature appeared pretty regular in both control and TßRII-deficient animals. However, the fundus

of the light-exposed animals exhibited characteristic autofluorescence, when excited by blue light in the frame of SLO imaging (Figure 44A.). Light-exposed TßRII-deficient animals showed a more pronounced autofluorescence in comparison to light-exposed control animals, a fact that further indicates a thicker, less degenerated retina in the control animals and thus affirms once more the presumable neuroprotective role of TGF-ß signaling in the course of light-induced retinopathy and retinal degenerative diseases.
In addition, optical coherence tomography (OCT) experiments certified the previously acquired morphological data point, as OCT images of light-damaged control animals exposed a considerably thicker ONL in the central retinae, when compared to their TßRII-deficient littermates (Figure 44B.).

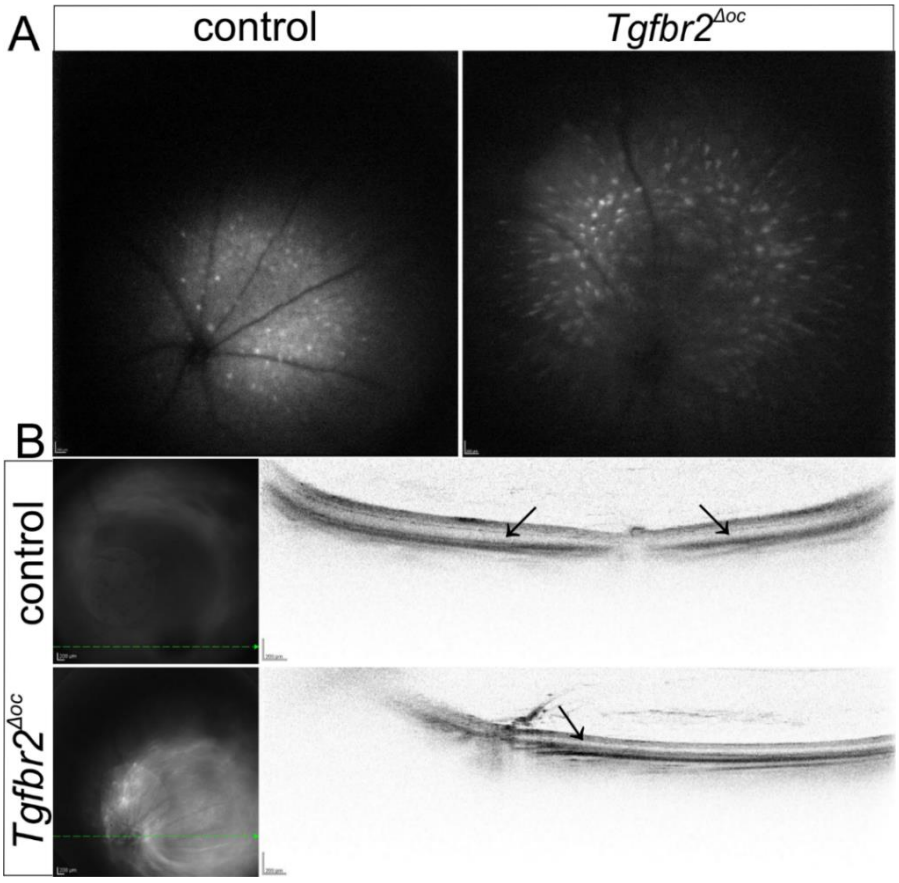


*Figure 44:* Deletion of TGF-ß signaling in neurons and Müller cells enhances photoreceptors degeneration following light damage: *in vivo* SLO and OCT imaging
A. Laser scanning ophthalmoscopy (SLO) of a 9-week-old light-exposed *Tgfbr2*$^{\Delta oc}$ animal and its control littermate. The retina of the control mouse exhibited a less pronounced autofluorescence than the one of the *Tgfbr2*$^{\Delta oc}$ littermate. B. Optic coherence tomography (OCT) of a 9-week-old light-exposed *Tgfbr2*$^{\Delta oc}$ animal and its control littermate. The thickness of the outer nuclear layer (ONL – black arrows) was considerably thinner in the retina of the *Tgfbr2*$^{\Delta oc}$ animal. The green punctured lines in the left-hand side images serve as orientation sectional planes for the right-hand side figures. Analyses were performed in cooperation with Prof. Jägle.

### 3.3.1.3 Functional analysis: Electroretinography (ERG)

Electroretinography (ERG) was applied in order to verify, whether the structural alterations in the retinae of light-exposed *Tgfbr2*$^{\Delta oc}$ would correlate with functional changes. First of all, analyses were performed on 6-8-week-old untreated controls (Figure 45, light blue line, WT-LD) and their *Tgfbr2*$^{\Delta oc}$ littermates (Figure 45, yellow line, TG-LD). Scotopic single-flash electroretinograms (ERGs) revealed similar response amplitudes (Figure 45B.) and implicit times (Figure 45C.) of the a- and b-waves for both *Tgfbr2*$^{\Delta oc}$ and control animals, which implied a comparable function of both photorececptors and bipolars for all untreated animals. 14 d upon light damage a profound loss of the b-wave component was detected for the eyes of *Tgfbr2*$^{\Delta oc}$ animals in scotopic ERGs (Figure 45A.). Prolonged implicit times and altered response amplitudes were observed in a greater extent for *Tgfbr2*$^{\Delta oc}$ animals than for control animals, for which the a- and b-wave parameters were considerably better preserved (Figure 45B.-D.).

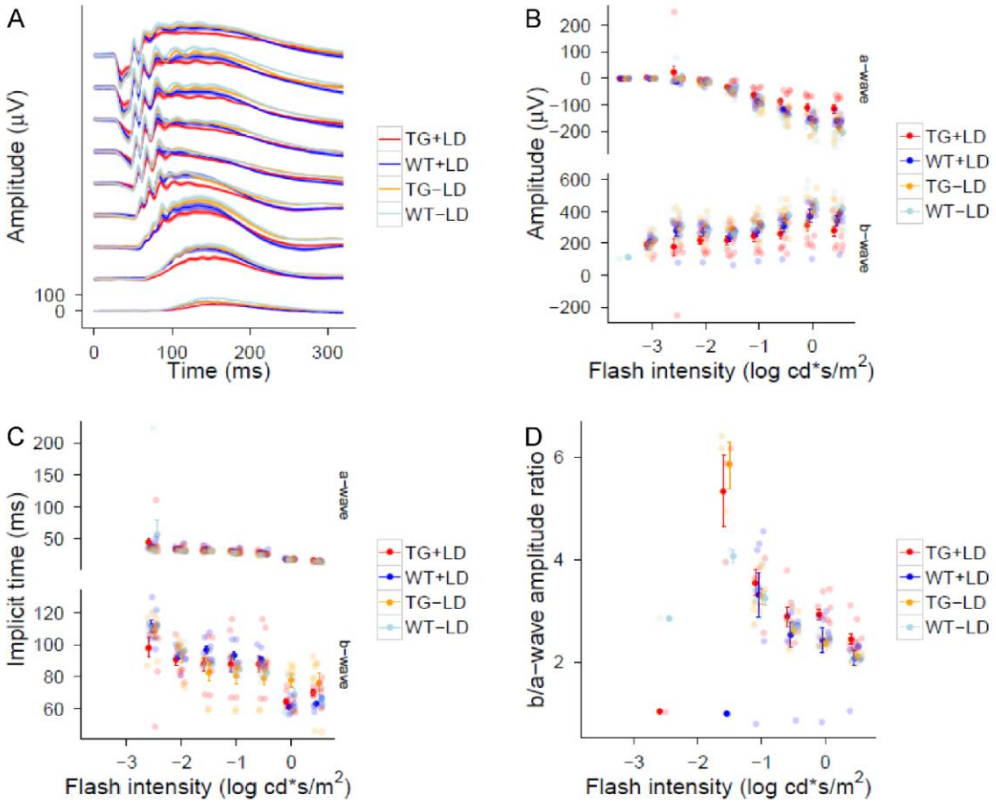


*Figure 45:* Scotopic single-flash ERG recordings for at least 6-week-old control and *Tgfbr2*$^{\Delta oc}$ animals

Untreated control (light blue line) and *Tgfbr2*$^{\Delta oc}$ (yellow line) animals revealed similar responses to single flashes, as far as amplitude of the waveform (B.) and implicit times (C.) were concerned. On the contrary, 14 d after light damage prolonged implicit times and lower b-wave amplitudes were detected for both controls (dark blue line, WT+LD) and *Tgfbr2*$^{\Delta oc}$ animals (red line, TG+LD), but in a much greater extent for the latter.

Under photopic conditions noticeable differences were detected, concerning primarily cone bipolar cells responses to single flashes of higher intensities in untreated animals: the implicit times were prolonged (Figure 46, right panel) and the b-wave amplitudes (Figure 46, middle panel) appeared to be lower for *Tgfbr2*$^{\Delta oc}$ animals (Figure 46, yellow line), when compared to control littermates (Figure 46, light blue line). In contrast to the effects, observed under scotopic conditions for light-damaged animals, no such effects were detected in light-adapted single-flash ERGs (Figure 46, left panel).

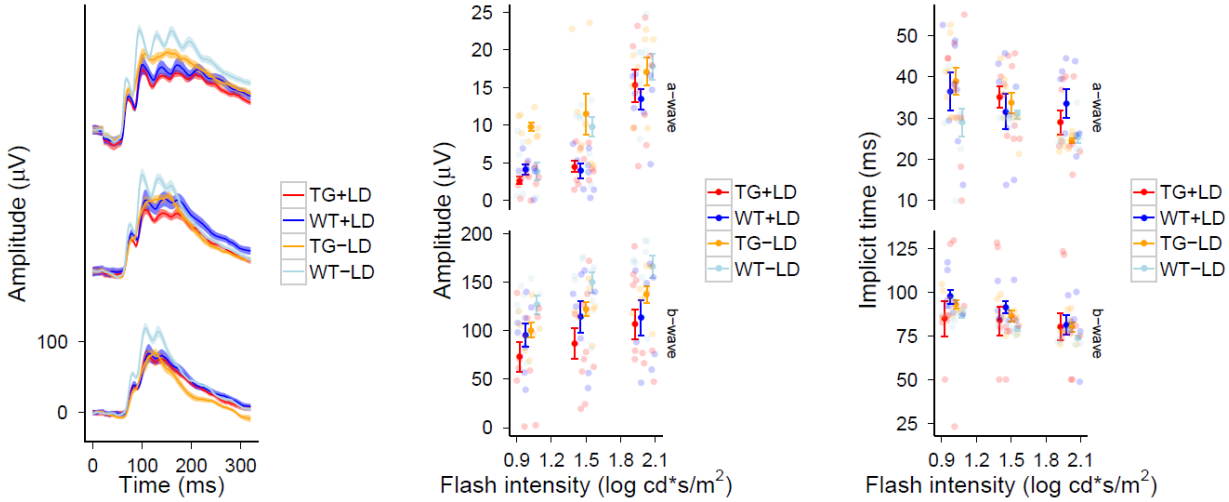


*Figure 46:* Photopic single-flash ERG recordings for at least 6-week-old control and *Tgfbr2*$^{\Delta oc}$ animals

Untreated *Tgfbr2*$^{\Delta oc}$ animals (yellow line) revealed altered responses to single flashes, when compared to control (light blue line) littermates: a lower amplitude of the waveform (middle panel) and prolonged implicit times (right panel) were detected. 14 d after light damage both tested groups (controls – dark blue line) and *Tgfbr2*$^{\Delta oc}$ animals – red line) did not exhibit significant differences, concerning implicit times or b-wave amplitudes.

### 3.3.1.4 Retinal apoptosis following light exposure

To clarify, whether the morphological and functional differences between control animals and their *Tgfbr2*$^{\Delta oc}$ littermates were due to the diverging proportion of photoreceptors, undergoing apoptosis, TUNEL labeling was performed 30 h after light damage. Here, numerous TUNEL-positive nuclei were observed in the ONL, especially in the central portions of the retinae of *Tgfbr2*$^{\Delta oc}$ and control animals (Figure 47A., right-hand side panel). To obtain statistically meaningful data, the total rate of fluorescing cells within the ONL was quantified in horizontal sections, stretching through the optic nerve head (ONH) of the retina in a temporal-nasal orientation, and the amount was normalized to the area of the ONL. The number of apoptotic cells was significantly smaller in control

animals (1 ± 0.068 cells per 1 mm² ONL), compared to *Tgfbr2*$^{\Delta oc}$ animals (1.85 ± 0.24 cells per 1 mm² ONL, $^{**}p < 0.01$) (Figure 47A., left-hand side panel).

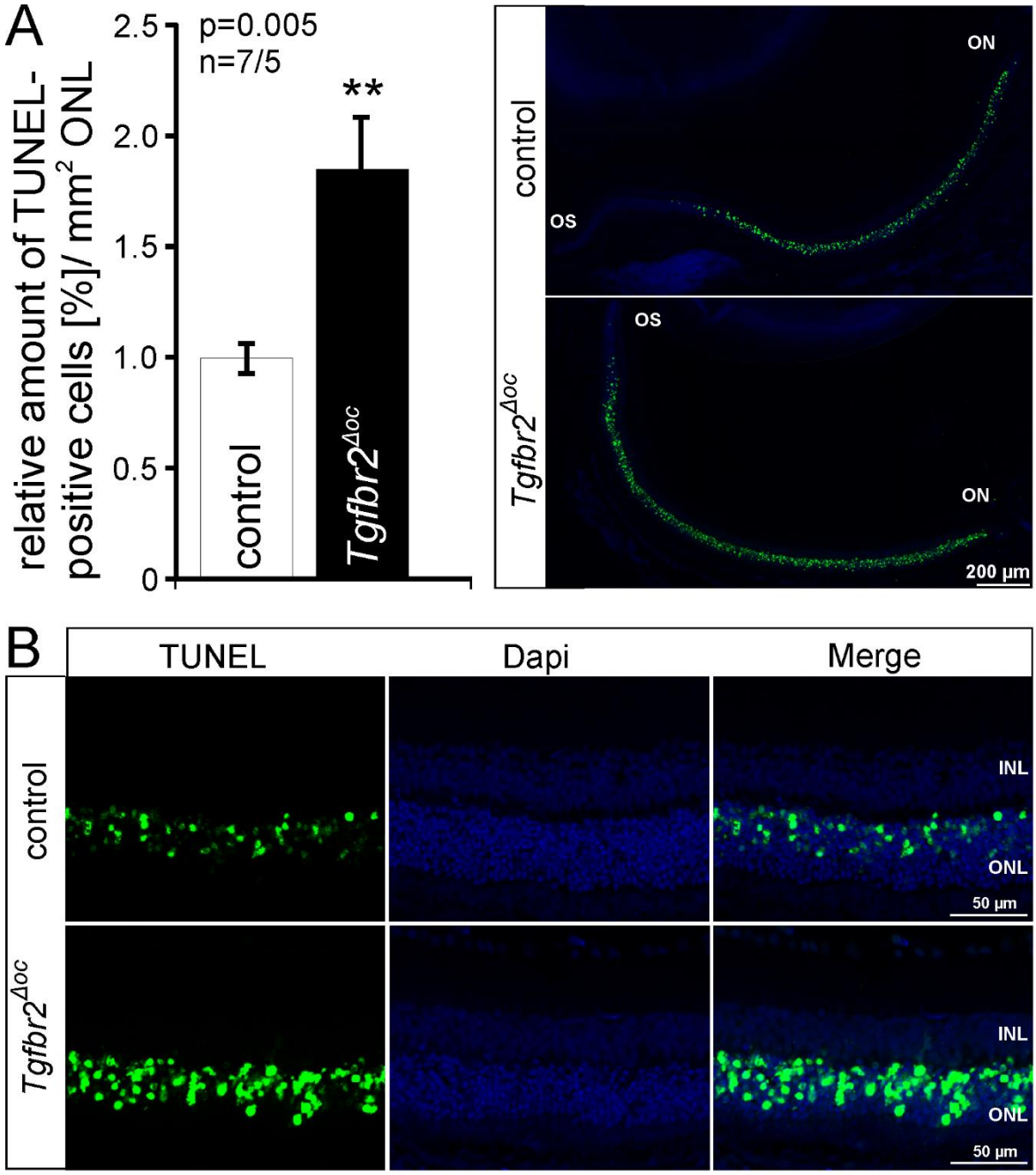


*Figure 47:* TUNEL labeling of the retinae of 6-7-week-old control mice and their *Tgfbr2*$^{\Delta oc}$ littermates, 30 h after light-induced damage

A. Right-hand side panel: fluorescing TUNEL-positive (green) nuclei were localized preferentially in the ONL, showing the characteristic distribution of a light-induced retinal damage with the major concentration of apoptotic signals in the central retina. Nuclei were stained with DAPI (blue). Left-hand side panel: statistical quantification of the TUNEL-labeled cells per 1 mm² ONL area. Data is mean ± SEM, $^{**}p = 0.00497$, n = 7/5 (controls/*Tgfbr2*$^{\Delta oc}$ mice). B. Higher magnification of the central retinae. INL, inner nuclear layer; ONL, outer nuclear layer; ON, optic nerve; OS, ora serrata.

### 3.3.1.5 Molecular mechanism of the neuroprotective effect of TGF-ß signaling

In order to investigate, whether the protective effect of the TGF-ß signaling pathway is mediated by an enhanced expression of certain neuroprotective factors, the profiles of several of them, frequently associated with light damage, were analyzed by means of quantitative real-time PCR (Faktorovich et al., 1992; Joly et al., 2008; Rattner and Nathans, 2005; Samardzija et al., 2006). To this end, the analyses were performed in retinal RNA samples, isolated from untreated and light-exposed *Tgfbr2*$^{\Delta oc}$ mice and their control littermates. The mRNA expression level of the *leukemia inhibitory factor (Lif)* was barely detectable in both untreated *Tgfbr2*$^{\Delta oc}$ animals and their controls. However, light-exposed mice from both experimental groups demonstrated a more than 130-fold increase in the expression of *Lif* upon light damage (Figure 48).

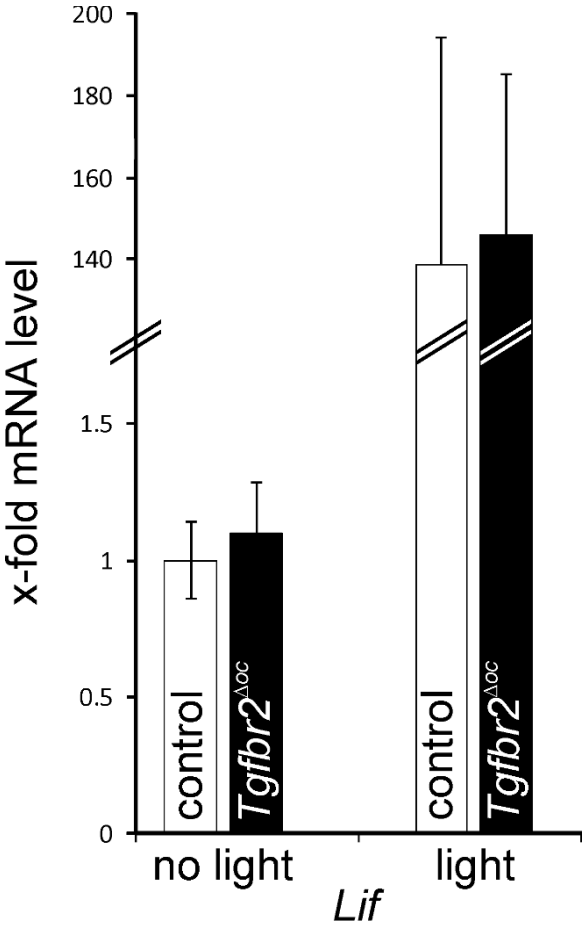


*Figure 48:* Expression level of *Lif* before and after light damage experiments

Real-time RT-PCR for *Lif (leukemia inhibitory factor)* in 6-8-week-old untreated (no light) and light-exposed (light) *Tgfbr2*$^{\Delta oc}$ animals and their control littermates before and 6 hours after light damage. The mean value, obtained with the RNA from untreated control animals, was set at 1. Data is mean ± SEM, n = 5/5 (untreated *Tgfbr2*$^{\Delta oc}$ to controls), n = 5/6 (light-exposed controls to *Tgfbr2*$^{\Delta oc}$). The y-axis was broken, in order to visualize properly the scarcely measurable *Lif* mRNA level of untreated animals.

Surprisingly, the expression levels of the other analyzed neuroprotective factors, *brain-derived neurotrophic factor (Bdnf)*, *endothelin 2 (Edn2)* and *fibroblast growth factor 2 (Fgf2)*, did not diverge significantly between the experimental groups of controls and *Tgfbr2*$^{\Delta oc}$ mice (Figure 49).

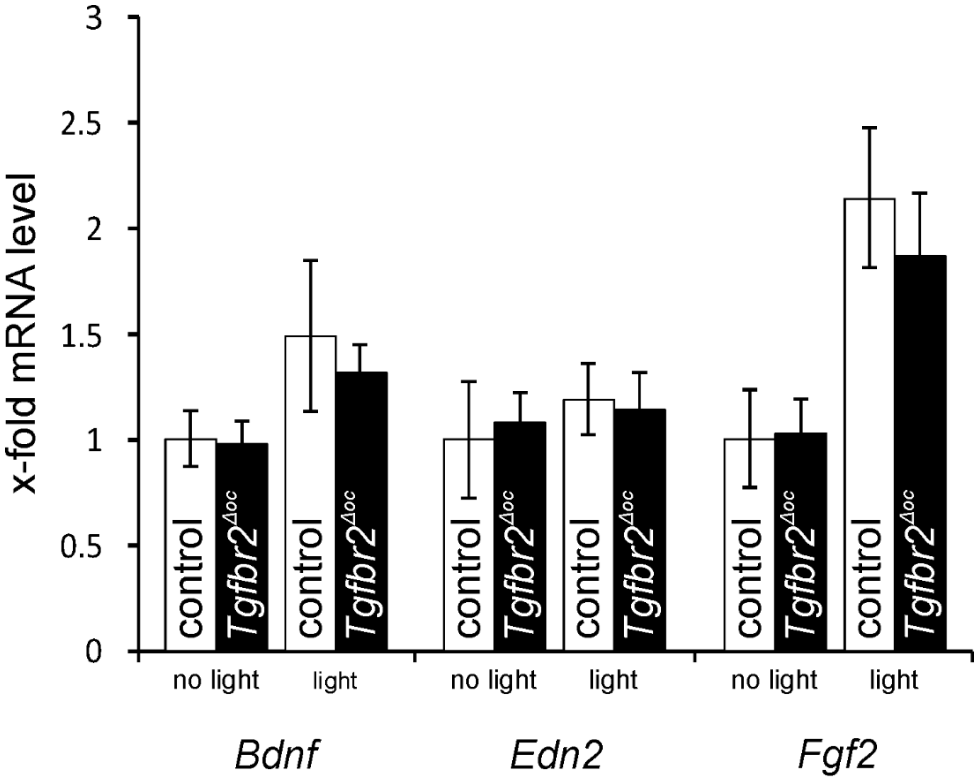


*Figure 49:* Real-time RT-PCR results for *Bdnf*, *Edn2* and *Fgf2* mRNA in 6-8-week-old *Tgfbr2*$^{\Delta oc}$ *mice* and their control littermates

The statistical evaluation of the real-time RT-PCR results for the expression levels of the neuroprotective factors *brain derived neurotrophic factor (Bdnf)*, *endothelin 2 (Edn2)* and *fibroblast growth factor 2 (Fgf2)* in untreated and light-exposed *Tgfbr2*$^{\Delta oc}$ mice and their controls did not show significant changes. Data is mean ± SEM, n ≥ 5.

The amounts of translated AKT and phosphorylated AKT (pAKT) were obtained by means of Western blot analyses of *Tgfbr2*$^{\Delta oc}$ and control retinae. First of all, the relative levels of both proteins were compared between untreated controls and *Tgfbr2*$^{\Delta oc}$ (Figure 50). The densitometric analysis of the results showed that both experimental groups did not differ with regard to the level of AKT or pAKT in their retinae (Figure 50B., C.).

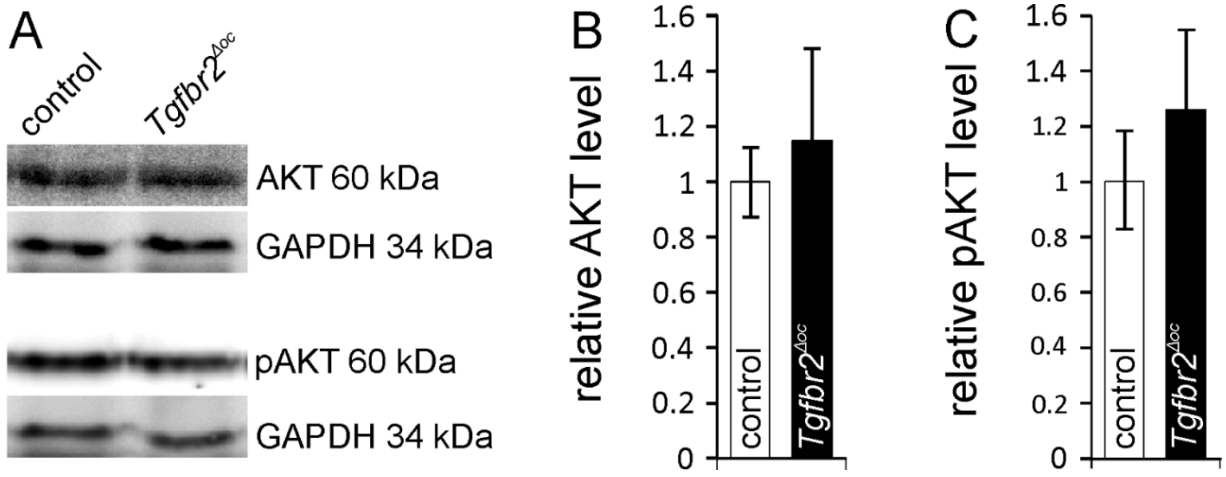


*Figure 50:* AKT and pAKT protein levels before light exposure
A. Western blot analysis for AKT and pAKT protein levels in 6-8-week-old *Tgfbr2*$^{\Delta oc}$ and their control retinae. B. Relative densitometry for AKT levels. Data is mean ± SEM. n = 4/4 (controls to *Tgfbr2*$^{\Delta oc}$). C. Relative densitometry for pAKT levels. Data is mean ± SEM. n = 7/7 (controls to *Tgfbr2*$^{\Delta oc}$).

The Western blot analysis for pAKT in retinal proteins from light-exposed mice revealed a distinct band, which migrated at the expected molecular weight of 60 kDa and was more intense in the lysates of control animals. The densitometric analysis of the relative amount of phosphorylated AKT 6 hours after light damage demonstrated a significantly higher level of the protein in control animals, when compared to their *Tgfbr2*$^{\Delta oc}$ littermates (Figure 51C.).

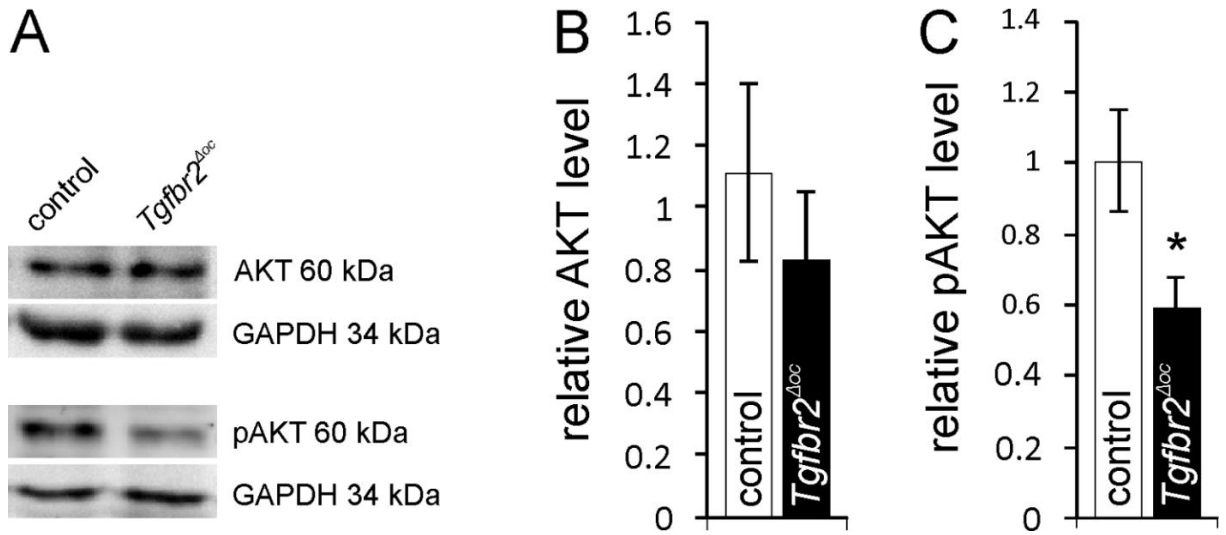


*Figure 51:* AKT and pAKT protein levels following light exposure
A. Western blot analysis for AKT and pAKT protein levels in 6-8-week-old *Tgfbr2*$^{\Delta oc}$ and their control retinae 6 h upon light damage experiments. B. Relative densitometry for AKT levels. Data is mean ± SEM. n = 8/7 (controls to *Tgfbr2*$^{\Delta oc}$). C. Relative densitometry for pAKT levels. Data is mean ± SEM. n = 8/7 (controls to *Tgfbr2*$^{\Delta oc}$), $*p < 0.05$.

### 3.3.2 Light damage experiments on *Tgfbr2*$^{\Delta rod}$ mice: TßRII deficiency within the rod photoreceptors

The Cre recombinase in *Tgfbr2*$^{\Delta oc}$ is expressed both in retinal neurons and Müller cells. Therefore, we cannot distinguish for a certainty, which cell type the neuroprotective effects, observed in this mouse line, originate from. In a final experiment we aimed to identify the very specific cell population that might be responsible for the neuroprotective effects of TGF-ß signaling. To this end, we used a second *cre* mouse line with a specific expression of the Cre recombinase in rod photoreceptors *(Tgfbr2*$^{\Delta rod}$*)* and performed light damage experiments, followed by TUNEL labeling.

#### 3.3.2.1 Retinal apoptosis following light exposure

The rate of photoreceptors, undergoing apoptosis, was assessed through TUNEL labeling, performed 30 h after light damage. Numerous TUNEL-positive nuclei were observed especially in the central parts of the retinae of both experimental groups (Figure 52A., right panel). The total number of fluorescing cells within the ONL was quantified in horizontal sections through the entire retina and the number was normalized to the area of the ONL. The following statistical analysis did not show any significant differences, when control animals (1 ± 0.21 cells per 1 mm$^2$ ONL) were compared to *Tgfbr2*$^{\Delta rod}$ littermates (1.5 ± 0.2 cells per 1 mm$^2$ ONL) (Figure 52A., left-hand side panel).

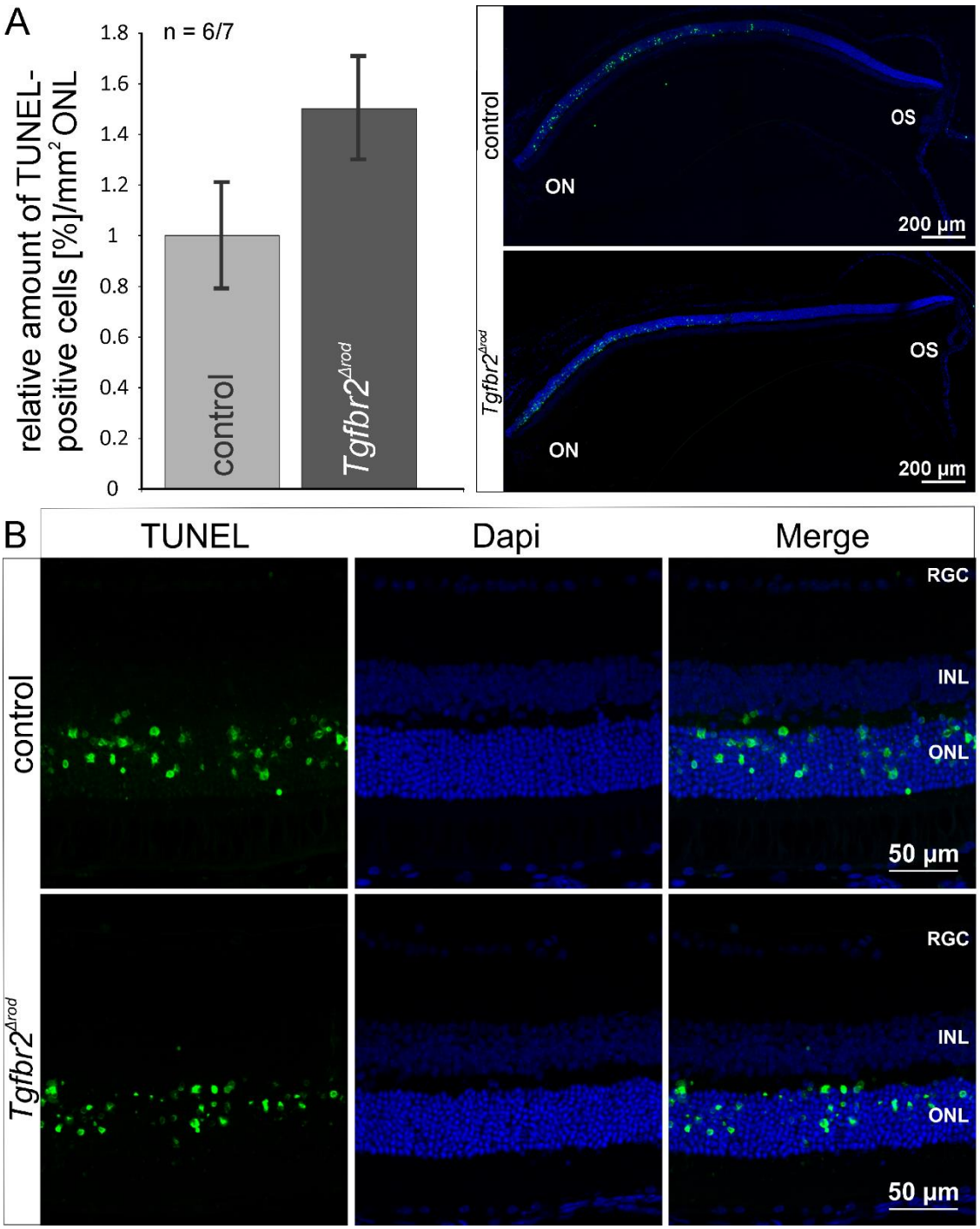


*Figure 52:* TUNEL labeling of the retinae of 6-8-week-old control mice and their *Tgfbr2*$^{\Delta rod}$ littermates, 30 h after light-induced damage

A. Right-hand side panel: fluorescing TUNEL-positive (green) nuclei are localized preferentially in the ONL, showing the characteristic distribution of a light-induced retinal damage with the major concentration of apoptotic signals in the central retina. Nuclei were stained with DAPI (blue). Left-hand side panel: the statistical quantification of the TUNEL-labeled cells per 1 mm² ONL area did not show any significant differences between the eyes of both experimental groups, concerning apoptotic cell death upon light-induced damage. Data is mean ± SEM, n = 6/7 (controls/ *Tgfbr2*$^{\Delta rod}$ mice). B. Higher magnification of the central retinal regions. ON, optic nerve; OS, ora serrata; RGC, retinal ganglion cells; INL, inner nuclear layer; ONL, outer nuclear layer.

# 4. Discussion

Given our results, we conclude that the deficiency of TGF-ß signaling in retinal neurons and Müller cells enhances the vulnerability of photoreceptors following light-induced degeneration. This effect is most likely mediated through Müller cells and involves a diminished phosphorylation of AKT, finally resulting in a higher number of apoptotic cells, a thinner outer nuclear layer (ONL) and a reduced retinal function.

## 4.1 Cre recombinase expression and neuronal vulnerability

The notion that the expression of a foreign protein, such as the Cre enzyme, might alter tissue maintenance, is a legitimate concern and arises from findings, demonstrating that the high-level endonuclease activity of Cre leads to growth arrest and chromosomal aberrations in cultured mammalian cells (Loonstra et al., 2001; Silver and Livingston, 2001). However, no similar toxicity of the protein could be detected in the frame of *in vivo* gene targeting (Pfeifer et al., 2001). Jimeno and coworkers pointed out that the expression of the Cre protein is likely to result in photoreceptors degeneration, though probably not due to the presence of the enzyme itself, but because of its overexpression (Jimeno et al., 2006). Similar findings, regarding the overexpression of other exogenous proteins in photoreceptors, for instance a wild-type human rod opsin, have also been reported (Olsson et al., 1992). Nevertheless, based on our results, we conclude that the ectopic expression of the enzyme does not interfere with the structure of the retina, at least for the investigated mouse line, included in this project – the *α-Cre* (Boneva et al., 2016). These results are in accordance with previously published conclusions, concerning the *LMOP-Cre* and the *iCre-75*, mouse strains with a less pronounced expression of the enzyme (Le et al., 2006; Li et al., 2005).

However, there is evidence that the impairment of glial cell function, for instance through expression of external proteins, such as the Cre recombinase, could make the very sensitive photoreceptor cells even more vulnerable to apoptosis (Gehrig et al., 2007; Karlstetter et al., 2010; Shin et al., 2005; Zeng et al., 2005). In order to assess this notion, we performed light damage experiments, triggering the degeneration of photoreceptor cells (Remé et al., 2003; Wenzel et al., 2005). Our results showed no significant differences, regarding the susceptibility to light, and thus demonstrated that the neuronal vulnerability in the *α-Cre* strain is not dependent on the presence of the Cre recombinase enzyme (Boneva et al., 2016).

In the light of some contradictory findings, the first task before us consisted in discarding the possibility that the sole expression of the Cre enzyme in the retinal cells might alter the conventional architecture and the vulnerability of the neural retina, since both data points were to be assessed in this study. To summarize, we conclude that the use of the Cre/LoxP system is a safe and reliable method, as far as its use in neuronal tissues is concerned.

## 4.2 The light damage model: genetic background and *Rpe65* mutation

The model of light damage was applied, in order to induce retinal lesions in form of synchronized apoptosis on the level of photoreceptors (Grimm and Remé, 2013). The short-term exposure to bright white light permits the study of molecular mechanisms of cell death in a controlled manner. The initial conditions of our light experiments included exposure to light at an intensity of 5000 lux for 1 h. Compared to the conditions other groups are using, this is still a rather mild regime that we decided to apply with regard to the intrinsic constitution of albino mice, which are known to be highly sensitive to light-induced effects (La Vail, Matthew M. et al., 1987). However, phenotypically identical strains may also vary in the severity of retinal degeneration upon light damage due to genetic background factors (La Vail, M. M. et al., 1987). In accordance, we detected a similar variance of the neuronal susceptibility to the damage model in our light experiments: animals in a mixed FVB-N/Balb-c background (*α-Cre* and wild-type littermates) displayed a much more intense rate of apoptosis in comparison to animals in a Balb-c background (*Tgfbr2*$^{\Delta oc}$ and *Tgfbr2*$^{\Delta rod}$ and their respective control littermates). The different susceptibility to light most likely originates from the FVB-N background, which is associated with the rd1 mutation (Taketo et al., 1991). The homozygous mutation is known to affect retinal development, especially by causing degeneration of rod photoreceptors (Caley et al., 1972), and was present in a heterozygous variant in the F1 generation of our FVB-N/Balb-c animals. Since we cannot exclude the option that the heterozygous rd1 mutation could mask the degenerative effects of apoptosis, obtained in light damage experiments, heterozygous animals were only compared among themselves – the progeny of an *α-Cre* mouse, in a FVB-N background, and of a Balb-c mouse served as test individuals. All other animals, included in our light damage experiments, derived from the Balb-c background. Consequently, the effect of light stress was by far not as intense, as observed for FVB-N/Balb-c animals, but still sufficient to demonstrate the significant difference between transgenic mice and control littermates.

It has been shown that a single variation in the *Rpe65* gene, causing an amino acid substitution (Leu → Met) at codon 450 accounts for an enhanced resistance against light-mediated photoreceptor degeneration (Danciger et al., 2000; Wenzel et al., 2001). Therfore, all of the illuminated animals were tested for this mutation and homozygous leucine carriers only were used in light damage experiments.

## 4.3 The TGF-β signaling pathway in the light of neuroprotection

The purpose of this study was to approach the hypothesis that the neuroprotective effect of TGF-β signaling does not unfold itself merely in the frame of developmental programmed cell death (Braunger et al., 2013b), but also during apoptotic processes in the mature mammalian retina. This notion arises from recent insights, reported by Walshe and coworkers (Walshe et al., 2009), who managed to block TGF-β in the adult mural retina by soluble endoglin, an action, which resulted in vascular and neuronal apoptosis. This finding implies the role of the TGF-β signaling pathway in maintaining the integrity of the mature retinal architecture and poses the question of the exact course of events. The presumable neuroprotective role of TGF-β in the mammalian retina would be in accordance with previous findings, indicating the preserving function of this signaling pathway throughout the CNS. Among these activities count the protective effects against hypoxic and excitotoxic degeneration of cultured neurons (Prehn et al., 1993b; Prehn et al., 1993a), the reduction of damage to hippocampal neurons, resulting from transient global ischemia (Henrich-Noack et al., 1996), the decrease of lesions in the course of spinal cord injury in a rat model (Tyor et al., 2002), the survival promoting of dopaminergic neurons (Krieglstein et al., 1995), and many others.

In quest of insight, our group investigated the impact of TGF-β signaling on the survival of light-damaged photoreceptors (Kawall, 2015). However, although the morphometrical analysis of semithin sections and the quantification of apoptotic TUNEL-positive cells in this study suggested a certain protective effect of TGF-β signaling, the differences between transgenic animals and control littermates were not pronounced enough. This fact was most likely attributable to the pigmentation of the experimental animals in a 129SV background, concomitant with a profound resistance to light-induced degeneration (Danciger et al., 2000; Wenzel et al., 2001; Wenzel et al., 2003).

## 4.4 Deletion of TGF-ß signaling in retinal neurons and Müller cells: the *Tgfbr2*$^{\Delta oc}$ model

### 4.4.1 Characterization of untreated *Tgfbr2*$^{\Delta oc}$ animals

There are controversial discussions about a lack of Cre recombinase activity in the central retina of the *α-Cre* mouse strain. To the best of our knowledge, these discrepant notions might arise from the different experiments, conducted to explore this topic. For instance, reporter gene assays, such as histochemical staining by excision of lacZ and concomitant activation of an ubiquitously expressed alkaline phosphatase (hPLAP) reporter gene (Marquardt et al., 2001), showed diminished Cre activity in the central retina. The tenuous point has been addressed by publications, showing the limitations of reporter gene expression, especially in adult transgenic animals (Cui et al., 1994; Montoliu et al., 2000). In contrast to the data, obtained in reporter mice, immunohistochemical analyses of direct target genes, for example TßRII (Braunger et al., 2013b), accounted for a distribution of the recombination in the central and peripheral retina. In this thesis, the visualization of the Cre expression and its activity was based on a *cre*-reporter mouse strain (R26R) (Soriano, 1999), featuring a loxP-flanked DNA segment, preventing the expression of a downstream lacZ gene. Consequently, when R26R mice are crossed with a *cre*-transgenic mouse line, the activity of the enzyme leads to the removal of the loxP-flanked DNA segment, driving the expression of the lacZ protein in all cells, in which Cre has been expressed. In *α-Cre*/R26R mice, we observed a weak, but still detectable staining for ß-galactosidase in the central retina. In spite of the depicted controversial insights, our further experiments, aiming to demonstrate the neuronal vulnerability of retinae, lacking the TßRII, showed significant differences in the central retinae of *Tgfbr2*$^{\Delta oc}$ animals in comparison to their control littermates. A fact that is indicative either of a sufficient activity of the Cre recombinase in the central retina of the *Tgfbr2*$^{\Delta oc}$ animals, or of potential indirect effects, originating from a lack of secreted molecular factors.

The retinal specificity of the Cre recombinase in the *Tgfbr2*$^{\Delta oc}$ mouse strain is ensured by the α-enhancer of the *Pax6* promoter. Thus, it is constitutively expressed in the cells, deriving from the inner layer of the optic cup, from the age of embryonic day 10.5 (Marquardt et al., 2001). This point in time is coincidental with the interval, when developmental programmed neuronal death in the retina begins (Farah and Easter, 2005). Hence, the *Tgfbr2*$^{\Delta oc}$ animal model includes phenomena, occurring during the development of the neuroretina and its programmed cell death (Braunger et al., 2013b). However, merely a negligible part of the photoreceptors undergoes ontogenetic,

programmed cell death during development (Cepko et al., 1996). This fact explains the slightly pronounced difference in the ONL thickness of transgenic animals, when compared to control littermates. As intensive light exposure results in the degeneration of photoreceptor cells only (Organisciak and Vaughan, 2009), we consider potential development-related pathologies that might have affected the photoreceptor cells during their differentiation as neglectable. Therefore, in our understanding, the *Tgfbr2*$^{\Delta oc}$ model constitutes an appropriate animal model to investigate the neuroprotective role of the TGF-ß signaling pathway.

Nevertheless, the restricted deletion of TßRII in retinal neurons and Müller glia provides a plausible explanation for the mild signal, observed in Western blot analyses for TßRII and pSMAD3 in *Tgfbr2*$^{\Delta oc}$ retinal samples and accounting for residual TGF-ß signaling, e.g. within astrocytes, microglia, pericytes and the vascular endothelium – cells that do not derive from the inner layer of the optic cup and consequently still express the TßRII and are thus capable of carrying out the TGF-ß signaling pathway under the conditions of a conditional knockout.

The further phenotype characterization of *Tgfbr2*$^{\Delta oc}$ mice included morphological analyses of the inner nuclear layer (INL) of transgenic animals and their control littermates, which revealed no pronounced discrepancy, as far as the arrangement and the approximate dimensions of the retinal layers were concerned. However, the morphometric and quantitative evaluations of the acquired data, illustrated in form of Spider diagrams, showed that the thickness of the INL in the eyes of transgenic animals tends to be reduced in comparison to the controls. Although the differences were not homogenously significant, a clear trend was present and consistent with previously published data (Braunger et al., 2013b; Kawall, 2015). Our group concluded that alterations of the INL thickness are due to a decrease in the number of inherent neurons, caused by deficiency in the activity of TGF-ß signaling on progenitor cells, prior to their differentiation (Braunger et al., 2013b). The findings correspond also with a theory of Young and coworkers (Young, 1984), who bring forward the argument that a great number of these cells are subjected to programmed cell death in the course of fine-tuning of neuronal networks, a process that appears to be more pronounced given a TßRII deficiency.

Another interesting aspect, addressed in this study, is the one about the functionality losses, which would correlate with the decreased number of INL cells, observed in the depicted morphometric analysis. The performed scotopic single-flash ERG experiments demonstrated similar response amplitudes and implicit times of the b-wave for both *Tgfbr2*$^{\Delta oc}$ and control animals, which suggests a comparable function of rod bipolars for all

untreated animals. According to novel insights, the scotopic b-wave is generated directly by rod bipolars (Bach and Kellner, 2000; Tian and Slaughter, 1995). However, a regular progression of the b-wave implies merely an intact manner of functioning of the rods, triggering a bipolar cells response (Bach and Kellner, 2000). While the rods' system includes just depolarizing (on-) bipolar cells, de- (on-) and hyperpolarizing (off-)bipolars exist in the cones' system. Thus, the b-wave of the photopic ERG is the residual of the almost extinguished potentials of hyper- and depolarizing bipolar cells (Bach and Kellner, 2000; Geller et al., 1992; Sieving et al., 2009). Under photopic conditions, certain differences, concerning cone bipolar cells responses to single flashes of higher intensities in untreated animals, were detected in our ERG analyses: when compared with control animals, implicit times were prolonged and b-wave amplitudes were reduced for *Tgfbr2*$^{\Delta oc}$. Bearing in mind the proximal retinal origin of the b-wave, this finding is consistent with the developmental post-photoreceptoral loss of neurons in the retinae of *Tgfbr2*$^{\Delta oc}$ mice (Braunger et al., 2013b) and with the thinner INL of adult mice of the current study. Since the functional alterations, observed under scotopic conditions, were not pronounced to a similar extent in light-adapted single-flash ERGs upon light damage, the relevance of the developmental effect in the context of retinal degeneration did not appear to be of a great relevance. These results were not surprising, considering the rod-dominated retina of the mouse (Carter-Dawson and LaVail, 1979).

### 4.4.2 TGF-ß signaling in the light damage model

To our surprise, under the initially determined light conditions (intensity of 5000 lux for 1 h) a profound light damage effect was observed to an almost equal extent for control animals and *Tgfbr2*$^{\Delta oc}$ littermates. However, there is evidence that the ocular pigmentation is numbered among the factors, capable of modulating the amount of light stress (Rapp and Williams, 1980). In our experience, light intensity of 5000 lux is sufficient to damage albino animals, while 14,500 lux are applied to pigmented animals. Obviously, the effect of the initial illumination was too severe for the eyes of the investigated mouse strain in this thesis. Consequently, we exposed a second group of animals to 5000 lux for only half of the time, 30 min. Here we observed a pronounced neurodegenerative effect for the *Tgfbr2*$^{\Delta oc}$ mouse line, which was illustrated in the resulting Spider diagrams. Further analyses of *Tgfbr2*$^{\Delta oc}$ following light exposure, such as TUNEL labeling, SLO and OCT *in vivo* imaging, ERG, confirmed the obtained results: the reduced thickness of the ONL, observed in morphometric analyses of *Tgfbr2*$^{\Delta oc}$ correlated with a boosted rate of apoptotic cells in the TUNEL assay 30 h after

illumination, a greater number of autofluorescing areas in SLO imaging, a thinner ONL in OCT and a poorly preserved retinal function in ERG. However, the question remains which cells might primarily mediate this effect? Given the acquired results for the *Tgfbr2*$^{\Delta rod}$ mouse line, the neuroprotective properties of TGF-ß signaling do not originate from rod photoreceptors, leaving Müller cells or other neurons than rods as potential candidates. Furthermore, our data show that the neuroprotective effect of TGF-ß signaling is limited to a certain extent and vanishes under extreme conditions.

## 4.5 Molecular mechanisms, mediating the neuroprotective effect of TGF-ß signaling

After providing evidence for the neuroprotective activity of TGF-ß signaling in the conducted experiments, we aimed to investigate, whether the observed effect is mediated by an enhanced expression of certain neuroprotective factors. To this end, we analyzed the expression profiles of several neuroprotective factors, commonly associated with a response to light damage (Faktorovich et al., 1992; Joly et al., 2008; Rattner and Nathans, 2005; Samardzija et al., 2006). While the mRNA expression level of the *leukemia inhibitory factor (Lif)* was barely detectable in both untreated *Tgfbr2*$^{\Delta oc}$ animals and their controls, light-exposed mice from both experimental groups demonstrated a more than 130-fold increase in the expression of *Lif*, a finding that is in accordance with previously published results (Braunger et al., 2013a; Samardzija et al., 2006).

Intriguingly, we did not detect a significant increase in the expression levels of other analyzed neuroprotective factors, *brain-derived neurotrophic factor (Bdnf)*, *endothelin 2 (Edn2)* and *fibroblast growth factor 2 (Fgf2)* between the untreated and light-exposed controls and *Tgfbr2*$^{\Delta oc}$ mice. This result is in contrast with previously published data, describing that following light exposure or genetically induced photoreceptor degeneration *Lif* becomes significantly upregulated as part of a retinal protective mechanism, including an elevated expression of *Edn2* in photoreceptors (Rattner and Nathans, 2005) and of *Fgf2* in Müller cells (Joly et al., 2008) .

The performed Western blot analyses for AKT and phosphorylated AKT (pAKT) in retinal proteins from light-exposed *Tgfbr2*$^{\Delta oc}$ and control animals, showed a significantly higher level of pAKT in the retinae of light-exposed control animals. This finding suggests that under cell stress conditions, e.g. light exposure, the deletion of the TGF-ß signaling pathway reduces the activity of the PI3K/pAKT pathway. The TGF-ß pathway mediates its signals through canonical (SMAD-dependent) and non-canonical downstream cascades in a cell context-dependent manner (Derynck and Zhang, 2003; Zhang, 2009). The MAPK, Rho-like GTPase and PI3K/pAKT pathways count among these non-canonical, i.e. non-SMAD pathways, used by TGF-ß in its numerous tasks within the cell (Zhang, 2009). Wilkes and colleagues showed that the TGF-ß-mediated activation of PI3K happens independently of SMAD2 or SMAD3 in fibroblast cultures (Wilkes et al., 2005). Findings of Yi and coworkers demonstrated in immunoprecipitation studies an indirect constitutive association of TßRII with p85, the regulatory subunit of PI3K, and a powerful enhancement of PI3K activity, induced by TßRI (Yi et al., 2005).

In the context of neuroprotection, TGF-ß1 has been shown to enhance the activity of the anti-apoptotic factor NF-κB in cultured hippocampal neurons through the PI3K/pAKT signaling pathway (Zhu et al., 2004). Caraci and coworkers demonstrated the protective role of TGF-ß1 against ß-Amyloid neurotoxicity in the rat hippocampus and the involvement of the PI3K/PAKT pathway in this neuroprotective cascade *in vitro* (Caraci et al., 2008). Our data are in accordance with these findings and highlight the importance of a TGF-ß-regulated activity of the PI3K/pAKT signaling pathway following light induced photoreceptor degeneration. Nevertheless, the diminished phosphorylation of pSMAD3 upon deletion of TßRII, might still indicate a combinatorial direct, SMAD-mediated, and indirect, non-SMAD, effect, emphasizing the notion that the activation of multiple cascades through TGF-ß might be adjusted according to the cellular context to yield neuroprotection ultimately (Caraci et al., 2011). This finding once again underscores the complexity of the role of the TGF-ß signaling pathway in the adult retina.

## 4.6 Future directions

It is worthwhile to mention that a deletion of the TGF-ß signaling pathway in retinal neurons and Müller cells, concomitant with a diminished phosphorylation of SMAD3, did not result in gross phenotypic changes of the retina and the photoreceptors in particular. Although photoreceptors express TßRII (Obata et al., 1999), this receptor does not seem to be essential for their development or maintenance in the adult, healthy retina. However, our data provide evidence for a neuroprotective role of the TGF-ß signaling pathway in the adult retina following light-induced photoreceptor degeneration. Furthermore, it elucidates the molecular mechanisms, mediating this effect. Nevertheless, further investigations are needed to identify the specific cell type, which primarily mediates this effect. Given or results, it is most likely attributable to Müller cells.

# 5. Summary – Zusammenfassung

## 5.1 Summary

The aim of this work was to demonstrate the neuroprotective role of TGF-ß signaling on photoreceptors in the adult retina and to investigate the molecular mechanisms, mediating this effect.

The assessment of this notion included the generation of transgenic mice, bearing a TßRII deficiency in different subpopulations of retinal cells. The deletion of TGF-ß signaling in retinal neurons and Müller cells, accompanied by a reduced phosphorylation of retinal SMAD3, led to an increased susceptibility to light-induced degeneration, resulting in a thinner outer nuclear layer (ONL), an attenuation of photoreceptors' responses in the frame of functional analyses and elevated rate of TUNEL-positive apoptotic cells in the *Tgfbr2*$^{\Delta oc}$ mouse model. The downregulation of the pathway in rod photoreceptors *(Tgfbr2*$^{\Delta rod}$*)* did not yield a comparable outcome, a fact, which implicates that other cells than rod photoreceptors are most likely responsible for the observed neuroprotective effect. To the best of our knowledge, the Müller cells are very likely candidates.

To identify the molecular machinery, which might convey the neuroprotective properties of the TGF-ß signaling pathway, real-time RT-PCR analyses for neuroprotective factors and Western blot analysis for AKT/pAKT were performed. We found that following light exposure, the deletion of TßRII in the *Tgfbr2*$^{\Delta oc}$ model resulted in a diminished phosphorylation of AKT, a serine/threonine-specific protein kinase, bound and activated by PI3K. Thus, the neuroprotective effect, downstream of TGF-ß, is most likely regulated through the activation of the PI3K/pAKT signaling cascade.

## 5.2 Zusammenfassung

Die Zielsetzung dieser Arbeit bestand in der Darlegung der neuroprotektiven Rolle des TGF-ß-Signalweges auf Photorezeptoren in der adulten Netzhaut und in der Erforschung der molekularen Mechanismen, welche den Effekt vermitteln.

Zu der Überprüfung dieser Hypothese gehörte das Generieren von konditionellen Knockout-Mäusen, die eine Deletion des TßRII in unterschiedlichen Subpopulationen retinaler Zellen aufwiesen. Die Inaktivierung des TGF-ß-Signals in retinalen Neuronen und Müllerzellen *(Tgfbr2$^{\Delta oc}$)* und die daraus resultierende verminderte Phosphorylierung von retinalem SMAD3 führte zu erhöhter Empfindlichkeit der Photorezeptoren gegenüber einer lichtinduzierten Degeneration. Diese äußerte sich in einer signifikant dünneren äußeren Körnerschicht, in einer reduzierten retinalen Funktion im Rahmen der ERG-Analysen und einer gesteigerten Anzahl TUNEL-positiver, apoptotischer Zellen im *Tgfbr2$^{\Delta oc}$*-Mausmodell. Die Deletion des TGF-ß-Signalweges in Stäbchen *(Tgfbr2$^{\Delta rod}$)* führte zu keinem vergleichbaren Ergebnis. Daraus schlussfolgern wir, dass andere Zellen als Stäbchen für den neuroprotektiven Effekt Verantwortung tragen und, basierend auf den Ergebnissen der *Tgfbr2$^{\Delta oc}$*-Mäuse, sehen wir die Müllerzellen als sehr wahrscheinliche Kandidaten an.

Um die genauen molekularen Mechanismen zu identifizieren, welche die neuroprotektiven Eigenschaften des TGF-ß-Signalweges vermitteln könnten, wurden quantitative RT-PCR für neuroprotektive Faktoren und Western-Blot-Analysen für AKT/pAKT durchgeführt. Die densitometrische Auswertung der Western-Blot-Analysen zeigte, dass die Deletion des TßRII im *Tgfbr2$^{\Delta oc}$*-Mausmodell zur verminderten Phosphorylierung von AKT führt, einer Serin/Threonin-Proteinkinase, die von PI3K gebunden und aktiviert wird und letztlich eine protektive, anti-apoptotische Wirkung vermittelt. Daraus ziehen wir die Schlussfolgerung, dass der dem TGF-ß-Signalweg nachgeschaltete neuroprotektive Effekt durch eine Aktivierung der pAKT/PI3K-Kaskade reguliert wird.

# Abbreviations

| | |
|---|---|
| % | percent |
| 5'-GMP | guanosine 5'-monophosphate |
| α | alpha |
| A | ampere |
| $A_{260/280}$ | 260/280-ratio of absorbance |
| AKT | Ak strain transforming; "Ak" stays for the nomenclature of a mouse, created by Jacob Furth and suffering spontaneous thymic lymphomas (Furth, 1978). The viral oncogene, encoded in the transforming retrovirus "Akt-8", was originally designated as "AKT" (Staal et al., 1977); Akt-8 itself was isolated from a thymoma cell line, originating from AKR mice. (the "t" in resemblance to its transforming nature). The later cloned human analogues were named respectively (Staal, 1987). AKT is also known as PKB (protein kinase B). |
| AMD | Age-related macular degeneration |
| AMPA receptor | α-amino-3-hydroxy-5-methyl-4-isoxazolepropionic acid |
| ANOVA | Analysis of variance |
| APS | ammoniumperoxodisulfate |
| *Bdnf* | *brain derived neurotrophic factor* |
| BMP | bone morphogenetic factor |
| BMPR-I, -II | bone morphogenetic factor receptors I, II |
| bp | base pair |
| BSA | bovine serum albumin |
| b.w. | body weight |
| °C | grade Celsius |
| Caco buffer | sodium cacodylate buffer |
| cd | candela |
| cDNA | complementary deoxyribonucleic acid |
| cGMP | guanosine 3',5'-cyclic monophosphate |
| CNS | central nervous system |
| CNV | choroidal neovascularization |
| *Cntf* | *ciliary neurotrophic factor* |

| | |
|---|---|
| *cre* | cyclization recombination (transgene) |
| Cre | cyclization recombination (enzyme) |
| d | day |
| DAPI | 4',6-Diamidion-2-phenylindole |
| DHA | docosahexaenoic acid |
| DMP-30 | 2,4,6-Tris(dimethylaminomethyl)phenol |
| DDSA | 2-Dodecenylsuccinic acid anhydride |
| DMSO | dimethyl sulfoxide |
| DNA | deoxyribonucleic acid |
| dNTP | deoxyribonucleoside triphosphate |
| DPC4 | deleted in pancreatic carcinoma locus 4 |
| Dpp | decapentaplegic, a *Drosophila* orthologue of TGF-ß (*dpp*, respective gene) |
| dUTP | 2'-deoxyuridine 5'-triphosphate |
| *Edn2* | *endothelin 2* |
| *Ednrb* | *endothelin receptor B* |
| EDTA | ethylenediaminetetraacetic acid |
| EGF | epidermal growth factor |
| eGFP | enhanced green fluorescent protein |
| ERG | electroretinography, electroretinogram |
| ERK | extracellular signal-regulated kinase |
| *Fgf2* | *fibroblast growth factor 2* |
| FITC | fluorescein isothiocyanate |
| FLA | fluorescein angiography |
| fwd | forward |
| g | gram; standard acceleration due to gravity |
| *Gapdh*/GAPDH | glyceraldehyde 3-phosphate dehydrogenase |
| GCL | ganglion cell layer |
| GDNF | glial cell line-derived neurotrophic factor |
| *Gfap* | *glial fibrillary acid protein* |
| *Gnb2l1* | *guanine nucleotide binding protein, beta polypeptide 2-like 1* |
| GTPase | a hydrolase enzyme that can bind and hydrolyze guanosine triphosphate |
| h | hour |
| HCl | hydrochloric acid |

| | |
|---|---|
| $H_2O$ | water |
| hPLAP | human placental alkaline phosphatase |
| HRP | horseradish peroxidase |
| Hz | hertz |
| ILM | inner limiting membrane |
| INL | inner nuclear layer |
| IPL | inner plexiform layer |
| k | kilo |
| $KH_2PO_4$ | potassium dihydrogen phosphate |
| $K_3[Fe(CN)_6]$ | potassium ferricyanide |
| $K_4[Fe(CN)_6] \cdot 3\ H_2O$ | potassium ferrocyanide |
| l | liter |
| LED | light-emitting diode |
| *Lif* | *leukemia inhibitory factor* |
| LMOP | long mouse opsin promoter |
| loxP | locus of X-over of P1 |
| µ | micro- |
| m | meter, milli- |
| M | molar |
| MAPK | mitogen-activated protein kinases |
| MEK | MAPK/ERK kinase = mitogen-activated protein kinase kinase (also abbreviated as MKK or MAP2K) |
| $MgCl_2$ | magnesium chloride |
| min | minute |
| MNA | methylnadic anhydride |
| mRNA | messenger RNA |
| MwoI | a restriction enzyme from an *E. coli* strain, carrying the MwoI gene from *Methanobacterium wolfeii* |
| n | nano- |
| NaCl | sodium chloride |
| NaDC | sodium desoxycholate |
| $NaH_2PO_4 \cdot H_2O$ | sodium dihydrogen phosphate monohydrate |
| $Na_2HPO_4 \cdot 2\ H_2O$ | disodium hydrogen phosphate dihydrate |
| NFκB | nuclear factor "kappa-light-chain-enhancer" of activated B-cells |
| $NH_4^+$ | ammonium |

| | |
|---|---|
| OCT | optical coherence tomography |
| OLM | outer limiting membrane |
| ONH | optic nerve head |
| ONL | outer nuclear layer |
| OP | oscillatory potential |
| OPL | outer plexiform layer |
| OS | ora serrata |
| pAKT | phosphorylated AKT |
| PBS | phosphate buffered saline |
| PCR | polymerase chain reaction |
| PDE | phosphodiesterase |
| PFA | paraformaldehyde |
| PI3K | phosphatidylinositol 3-Kinase |
| pm | plasma membrane |
| PVDF | polyvinyl difluoride |
| R26R | Rosa-LacZ reporter mice |
| Ras | rat sarcoma, in resemblance to the discovery of the first two oncogenes as loci of saroma-causing viruses in rats (Malumbres and Barbacid, 2003) |
| rev | reverse |
| RGC | retinal ganglion cell |
| Rho | Ras homologue |
| Rho-GTPases | Rho family of GTPases |
| *Rpl32* | *ribosomal protein L32* |
| RNA | ribonucleic acid |
| RP | Retinitis pigmentosa |
| RPE | retinal pigment epithelium |
| rpm | rounds per minute |
| R-SMAD | receptor-regulated SMAD |
| RT | reverse transcriptase |
| rTdT | recombinant terminal deoxynucleotidyl transferase |
| RT-PCR | real-time polymerase chain reaction |
| SDS | sodium dodecyl sulfate |
| SDS-PAGE | sodium dodecyl sulfate polyacrylamide gel electrophoresis |
| sec | second |

| | |
|---|---|
| SEM | scanning electron micrograph; standard error of the mean |
| SLO | laser scanning ophthalmoscopy |
| SMAD | SMA/MAD-related (Massagué, 2012), SMA: small size; MAD: *Mothers against dpp* (a *Drosophila melanogaster* gene) (Sekelsky et al., 1995) |
| SPSS | Statistical Package for the Social Sciences |
| STR | scotopic threshold response |
| *Stat3* | *signal transducer and activator of transcription 3* |
| Taq | a thermostable DNA polymerase, purified from the thermophilic bacterium Thermus aquaticus |
| TβRI | TGF-β receptor type I |
| TβRII | TGF-β receptor type II |
| TβRIII | TGF-β receptor type III |
| TBE | Tris-Borate-EDTA buffer |
| TBS | Tris-buffered saline |
| TBS-T | Tris-buffered saline-Tween 20 |
| TdT | terminal deoxynucleotidyl transferase |
| TEMED | N,N,N',N'-tetramethylethylenediamine |
| TGF-β | transforming growth factor beta |
| *Tgfbr2*$^{\Delta oc}$ | *Tgfbr2*$^{fl/fl}$*;α-Cre*-mice |
| *Tgfbr2*$^{\Delta rod}$ | *Tgfbr2*$^{fl/fl}$*;LMOP*-mice |
| TM | melting temperature |
| TNF-α | tumor necrosis factor-α |
| Tris | Tris(hydroxymethyl)aminomethan |
| *Trk*B | tyrosine receptor kinase B |
| TUNEL | terminal deoxynucleotidyl transferase-mediated dUTP nick end labeling |
| V | Volt |
| VEGF | vascular endothelial growth factor |
| VPP | a mouse model, characterized by a rhodopsin transgene, encoding a protein with three amino acid substitutions Val-20 → Gly (V20G), Pro-23 → His (P23H), and Pro-27 → Leu (P27L) (Naash et al., 1993) |
| W | watt |
| X-Gal | 5-bromo-4-chloro-3-indolyl-β-D-galactopyranoside |

# References

Alberts B, Johnson A, Lewis J, Raff M, Roberts K, Walter P, et al. DNA Replication, Repair, and Recombination: Transposition and Conservative Site-specific Recombination. In: Alberts B, Johnson A, Lewis J, Raff M, Roberts K, Walter P, Wilson J, Hunt T, editors. Molecular biology of the cell. New York: Garland Science Taylor & Francis; 2008. p. 316–328.

Anderson DH, Fisher SK. The photoreceptors of diurnal squirrels: Outer segment structure, disc shedding, and protein renewal. Journal of Ultrastructure Research 1976;55(1):119–41.

Anderson DH, Fisher SK, Steinberg RH. Mammalian cones: disc shedding, phagocytosis, and renewal. Investigative Ophthalmology & Visual Science 1978;17(2):117–33.

Angel P, Schorpp-Kistner M. Jun/Fos. In: Encyclopedic Reference of Genomics and Proteomics in Molecular Medicine. Berlin, Heidelberg: Springer Berlin Heidelberg; 2006. p. 928–935.

Assoian RK, Komoriya A, Meyers CA, Miller DM, Sporn MB. Transforming growth factor-beta in human platelets. Identification of a major storage site, purification, and characterization. Journal of Biological Chemistry 1983;258(11):7155–60.

Attisano L, Wrana JL. Signal transduction by the TGF-ß superfamily. Science (New York) 2002;296(5573):1646–7.

Bach M, Kellner U. Elektrophysiologische Diagnostik in der Ophthalmologie. Der Ophthalmologe 2000;97(12):898–920.

Baehr W, Wu SM, Bird AC, Palczewski K. The retinoid cycle and retina disease. Vision Research 2003;43(28):2957–8.

Baulmann DC, Ohlmann A, Flügel-Koch C, Goswami S, Cvekl A, Tamm ER. Pax6 heterozygous eyes show defects in chamber angle differentiation that are associated with a wide spectrum of other anterior eye segment abnormalities. Mechanisms of Development 2002;118(1-2):3–17.

Berson EL. Retinitis pigmentosa. The Friedenwald Lecture. Investigative Ophthalmology & Visual Science 1993;34(5):1659–76.

Bhutto I, Lutty G. Understanding age-related macular degeneration (AMD): relationships between the photoreceptor/retinal pigment epithelium/Bruch's membrane/choriocapillaris complex. Molecular Aspects of Medicine 2012;33(4):295–317.

Boneva SK, Groß TR, Schlecht A, Schmitt SI, Sippl C, Jägle H, et al. Cre recombinase expression or topical tamoxifen treatment do not affect retinal structure and function, neuronal vulnerability or glial reactivity in the mouse eye. Neuroscience 2016;325:188–201.

Bonilha V, Rayborn M, Bhattacharya S, Gu X, Crabb J, Crabb J, et al. The Retinal Pigment Epithelium Apical Microvilli and Retinal Function. In: Hollyfield J, Anderson R, LaVail M, editors. Retinal Degenerative Diseases: Springer US; 2006. p. 519–524.

Braunger BM, Boneva SK, Groß TR, Kawall D, Tamm ER. Light-induced photoreceptor degeneration in mice.

Braunger BM, Ohlmann A, Koch M, Tanimoto N, Volz C, Yang Y, et al. Constitutive overexpression of Norrin activates Wnt/ß-catenin and endothelin-2 signaling to protect photoreceptors from light damage. Neurobiology of Disease 2013a;50(0):1–12.

Braunger BM, Pielmeier S, Demmer C, Landstorfer V, Kawall D, Abramov N, et al. TGF-ß Signaling Protects Retinal Neurons from Programmed Cell Death during the Development of the Mammalian Eye. The Journal of Neuroscience 2013b;33(35):14246–58.

Bringmann A, Pannicke T, Grosche J, Francke M, Wiedemann P, Skatchkov SN, et al. Müller cells in the healthy and diseased retina. Progress in Retinal and Eye Research 2006;25(4):397–424.

Burnette W. "Western Blotting": Electrophoretic transfer of proteins from sodium dodecyl sulfate-polyacrylamide gels to unmodified nitrocellulose and radiographic detection with antibody and radioiodinated protein A. Analytical Biochemistry 1981;112(2):195–203.

Burt DW, Law AS. Evolution of the transforming growth factor-beta superfamily. Progress in Growth Factor Research 1994;5(1):99–118.

Burt DW, Paton IR. Evolutionary origins of the transforming growth factor-beta gene family. DNA and Cell Biology 1992;11(7):497–510.

Byrne C, Tainsky M, Fuchs E. Programming gene expression in developing epidermis. Development 1994;120(9):2369–83.

Caley DW, Johnson C, Liebelt RA. The postnatal development of the retina in the normal and rodless CBA mouse: a light and electron microscopic study. The American Journal of Anatomy 1972;133(2):179–212.

Caraci F, Battaglia G, Bruno V, Bosco P, Carbonaro V, Giuffrida ML, et al. TGF-ß1 Pathway as a New Target for Neuroprotection in Alzheimer's Disease. CNS Neuroscience & Therapeutics 2011;17(4):237–49.

Caraci F, Battaglia G, Busceti C, Biagioni F, Mastroiacovo F, Bosco P, et al. TGF-ß1 protects against Aß-neurotoxicity via the phosphatidylinositol-3-kinase pathway. Neurobiology of Disease 2008;30(2):234–42.

Carter-Dawson LD, LaVail MM. Rods and cones in the mouse retina: I. Structural analysis using light and electron microscopy. The Journal of Comparative Neurology 1979;188(2):245–62.

Cepko CL, Austin CP, Yang X, Alexiades M, Ezzeddine D. Cell fate determination in the vertebrate retina. Proceedings of the National Academy of Sciences 1996;93(2):589–95.

Cheifetz S, Weatherbee JA, Tsang ML-S, Anderson JK, Mole JE, Lucas R, et al. The transforming growth factor-ß system, a complex pattern of cross-reactive ligands and receptors. Cell 1987;48(3):409–15.

Chytil A, Magnuson MA, Wright, Christopher V. E., Moses HL. Conditional inactivation of the TGF-ß type II receptor using Cre:Lox. Genesis 2002;32(2):73–5.

Coons AH, Creech HJ, Jones NR, Berliner E. The Demonstration of Pneumococcal Antigen in Tissues by the Use of Fluorescent Antibody. The Journal of Immunology 1942;45(3):159–70.

Crooks J, Kolb H. Localization of GABA, glycine, glutamate and tyrosine hydroxylase in the human retina. The Journal of Comparative Neurology 1992;315(3):287–302.

Cui C, Wani MA, Wight D, Kopchick J, Stambrook PJ. Reporter genes in transgenic mice. Transgenic Research 1994;3(3):182–94.

Curcio CA. Photoreceptor topography in ageing and age-related maculopathy. Eye (London, England) 2001;15(Pt 3):376–83.

Curcio CA, Medeiros NE, Millican CL. Photoreceptor loss in age-related macular degeneration. Investigative Ophthalmology & Visual Science 1996;37(7):1236–49.

Curcio CA, Millican CL, Allen KA, Kalina RE. Aging of the human photoreceptor mosaic: evidence for selective vulnerability of rods in central retina. Investigative Ophthalmology & Visual Science 1993;34(12):3278–96.

Danciger M, Matthes MT, Yasamura D, Akhmedov NB, Rickabaugh T, Gentleman S, et al. A QTL on distal Chromosome 3 that influences the severity of light-induced damage to mouse photoreceptors. Mammalian Genome 2000;11(6):422–7.

DasGupta R, Fuchs E. Multiple roles for activated LEF/TCF transcription complexes during hair follicle development and differentiation. Development 1999;126(20):4557–68.

de Jong, Paulus T. V. M. Age-related macular degeneration. The New England Journal of Medicine 2006;355(14):1474–85.

Derynck R, Lindquist PB, Lee A, Wen D, Tamm J, Graycar JL, et al. A new type of transforming growth factor-ß, TGF-ß3. The EMBO journal 1988;7(12):3737–43.

Derynck R, Zhang YE. Smad-dependent and Smad-independent pathways in TGF-ß family signalling. Nature 2003;425(6958):577–84.

Dunaief JL. The Role of Apoptosis in Age-Related Macular Degeneration. Archives of Ophthalmology 2002;120(11):1435.

Duncan TE, O'Steen WK. The diurnal susceptibility of rat retinal photoreceptors to light-induced damage. Experimental Eye Research 1985;41(4):497–507.

Elbers, P. F., Ververgaert, P. H. J. T., Demel R. Tricomplex fixation of phospholipids. The Journal of Cell Biology 1965;24(1):23–30.

Fain GL, Lisman JE. Photoreceptor degeneration in vitamin A deprivation and retinitis pigmentosa: the equivalent light hypothesis. Experimental Eye Research 1993;57(3):335–40.

Faktorovich EG, Steinberg RH, Yasumura D, Matthes MT, LaVail MM. Basic fibroblast growth factor and local injury protect photoreceptors from light damage in the rat. The Journal of Neuroscience 1992;12(9):3554–67.

Farah MH, Easter SS. Cell birth and death in the mouse retinal ganglion cell layer. Journal of Comparative Neurology 2005;489(1):120–34.

Feng X-H, Derynck R. Specificity and versatility in TGF-ß signaling through Smads. Annual Review of Cell and Developmental Biology 2005;21:659–93.

Forbes MS, Sperelakis N. Myocardial couplings: Their structural variations in the mouse. Journal of Ultrastructure Research 1977;58(1):50–65.

Friedman DS, O'Colmain BJ, Munoz B, Tomany SC, McCarty C, Jong PT de, et al. Prevalence of age-related macular degeneration in the United States. Archives of Ophthalmology 2004;122(4):564–72.

Frolik CA, Dart LL, Meyers CA, Smith DM, Sporn MB. Purification and initial characterization of a type beta transforming growth factor from human placenta. Proceedings of the National Academy of Sciences 1983;80(12):3676–80.

Furth J. The creation of the AKR strain, whose DNA contains the genome of a leukemia virus. In: Morse, HC, III, editor. Origins of inbred mice. Academic Press Inc., New York; 1978. p. 69–97.

García M, Vecino E. Role of Müller glia in neuroprotection and regeneration in the retina. Histology and Histopathology 2003;18(4):1205–18.

Gauthier R, Joly S, Pernet V, Lachapelle P, Di Polo A. Brain-Derived Neurotrophic Factor Gene Delivery to Müller Glia Preserves Structure and Function of Light-Damaged Photoreceptors. Investigative Ophthalmology & Visual Science 2005;46(9):3383–92.

Gavrieli Y, Sherman Y, Ben-Sasson SA. Identification of programmed cell death in situ via specific labeling of nuclear DNA fragmentation. The Journal of Cell Biology 1992;119(3):493–501.

Gehrig A, Langmann T, Horling F, Janssen A, Bonin M, Walter M, et al. Genome-Wide Expression Profiling of the Retinoschisin-Deficient Retina in Early Postnatal Mouse Development. Investigative Ophthalmology & Visual Science 2007;48(2):891–900.

Geller AM, Sieving PA, Green DG. Effect on grating identification of sampling with degenerate arrays. Journal of the Optical Society of America A 1992;9(3):472.

Goumans M-J, Mummery C. Functional analysis of the TGFbeta receptor/Smad pathway through gene ablation in mice. International Journal of Developmental Biology 2000;44(3):253–66.

Grimm C, Remé CE. Light damage as a model of retinal degeneration. Methods in Molecular Biology (Clifton, New Jersey) 2013;935:87–97.

Grimm C, Wenzel A, Hafezi F, Yu S, Redmond, T. Michael, Reme CE. Protection of Rpe65-deficient mice identifies rhodopsin as a mediator of light-induced retinal degeneration. Nature Genetics 2000;25(1):63–6.

Grus F, Kottler U. Bildgebende Verfahren. In: Marion Philipp, editor. Augenheilkunde. Berlin Heidelberg New York: Springer; 2007. p. 1017–1036.

Guo F, Gopaul DN, van Duyne, G D. Structure of Cre recombinase complexed with DNA in a site-specific recombination synapse. Nature 1997;389(6646):40–6.

Hageman G. An Integrated Hypothesis That Considers Drusen as Biomarkers of Immune-Mediated Processes at the RPE-Bruch's Membrane Interface in Aging and Age-Related Macular Degeneration. Progress in Retinal and Eye Research 2001;20(6):705–32.

Hamilton DL, Abremski K. Site-specific recombination by the bacteriophage P1 *lox*-Cre system: Cre-mediated synapsis of two *lox* sites. Journal of Molecular Biology 1984;178(2):481–6.

Hao W, Wenzel A, Obin MS, Chen C-K, Brill E, Krasnoperova NV, et al. Evidence for two apoptotic pathways in light-induced retinal degeneration. Nature Genetics 2002;32(2):254–60.

Hartong DT, Berson EL, Dryja TP. Retinitis pigmentosa. Lancet 2006;368(9549):1795–809.

Henrich-Noack P, Prehn JH, Krieglstein J. TGF-ß1 Protects Hippocampal Neurons Against Degeneration Caused by Transient Global Ischemia: Dose-Response Relationship and Potential Neuroprotective Mechanisms. Stroke 1996;27(9):1609–15.

Hutchinson J, Tay W. Symmetrical central choroido-retinal disease occurring in senile persons. Royal London Ophthalmic Hospital Reports Journal of Ophthalmic Medical Surgery 1874;8:231–44.

Ito, S. and Karnovsky, M.J. Formaldehyde-Glutaraldehyde Fixatives Containing Trinitrocompounds. The Journal of Cell Biology 1968;39:168A-169A.

Itoh S, Itoh F, Goumans M-J, Dijke P ten. Signaling of transforming growth factor-ß family members through Smad proteins. European Journal of Biochemistry 2000;267(24):6954–67.

Jadhav AP, Roesch K, Cepko CL. Development and neurogenic potential of Müller glial cells in the vertebrate retina. Progress in Retinal and Eye Research 2009;28(4):249–62.

Jager RD, Mieler WF, Miller JW. Age-related macular degeneration. The New England Journal of Medicine 2008;358(24):2606–17.

Jakowlew SB, Dillard PJ, Sporn MB, Roberts AB. Complementary deoxyribonucleic acid cloning of a messenger ribonucleic acid encoding transforming growth factor beta 4 from chicken embryo chondrocytes. Molecular Endocrinology (Baltimore, Maryland) 1988;2(12):1186–95.

Jimeno D, Feiner L, Lillo C, Teofilo K, Goldstein LSB, Pierce EA, et al. Analysis of Kinesin-2 Function in Photoreceptor Cells Using Synchronous Cre-loxP Knockout of Kif3a with RHO-Cre. Investigative Ophthalmology & Visual Science 2006;47(11):5039–46.

Joly S, Lange C, Thiersch M, Samardzija M, Grimm C. Leukemia inhibitory factor extends the lifespan of injured photoreceptors *in vivo*. The Journal of Neuroscience the Official Journal of the Society for Neuroscience 2008;28(51):13765–74.

Jurklies B. Klinische Elektrophysiologie. In: Marion Philipp, editor. Augenheilkunde. Berlin Heidelberg New York: Springer; 2007. p. 1037–1100.

Jurklies B, Puls S. Grundzüge der Angiographie. In: Marion Philipp, editor. Augenheilkunde. Berlin Heidelberg New York: Springer; 2007. p. 963–1016.

Kammandel B, Chowdhury K, Stoykova A, Aparicio S, Brenner S, Gruss P. Distinct *cis*-Essential Modules Direct the Time–Space Pattern of the *Pax6* Gene Activity. Developmental Biology 1999;205(1):79–97.

Kanski JJ. Erworbene Makulaerkrankungen. In: Kanski JJ, editor. Klinische Ophthalmologie: Lehrbuch und Atlas. München, Jena: Elsevier, Urban & Fischer; 2008. p. 643–678.

Karlstetter M, Ebert S, Langmann T. Microglia in the healthy and degenerating retina: Insights from novel mouse models. EMDS Special Issue: Phenotypical Diversity of Macrophages and Dendritic Cells in Tissues and Organs 2010;215(9–10):685–91.

Karnovsky MJ. A formaldehyde-glutaraldehyde fixative of high osmolality for use in electron microscopy. The Journal of Cell Biology 1965;27:137A-138A.

Karnovsky MJ. Use of ferrocyanide-reduced osmium tetroxide in electron microscopy. Proceedings of the 11th Annual Meeting of the American Society for Cell Biology 1971:146a.

Kawall D. Der Einfluss des TGF-ß-Signalweges auf das Überleben lichtgeschädigter Photorezeptoren, 2015.

Kellner U. Hereditäre Erkrankungen von Netzhaut und Aderhaut. In: Marion Philipp, editor. Augenheilkunde. Berlin Heidelberg New York: Springer; 2007. p. 401–464.

Kerr JFR, Wyllie AH, Currie AR. Apoptosis: a basic biological phenomenon with wide-ranging implications in tissue kinetics. British Journal of Cancer 1972;26(4):239.

Kingsley DM. The TGF-ß superfamily: new members, new receptors, and new genetic tests of function in different organisms. Genes & Development 1994;8(2):133–46.

Kondaiah P, Sands MJ, Smith JM, Fields A, Roberts AB, Sporn MB, et al. Identification of a novel transforming growth factor-ß (TGF-ß 5) mRNA in Xenopus laevis. The Journal of Biological Chemistry 1990;265(2):1089–93.

Korte GE, Reppucci V, Henkind P. RPE destruction causes choriocapillary atrophy. Investigative Ophthalmology & Visual Science 1984;25(10):1135–45.

Kretzschmar M, Doody J, Timokhina I, Massague J. A mechanism of repression of TGFß/ Smad signaling by oncogenic Ras. Genes & Development 1999;13(7):804–16.

Krieglstein K, Farkas L, Unsicker K. TGF-ß regulates the survival of ciliary ganglionic neurons synergistically with ciliary neurotrophic factor and neurotrophins. Journal of Neurobiology 1998;37(4):563–72.

Krieglstein K, Strelau J, Schober A, Sullivan A, Unsicker K. TGF-ß and the regulation of neuron survival and death. Journal of Physiology (Paris) 2002;96(1-2):25–30.

Krieglstein K, Suter-Crazzolara C, Fischer WH, Unsicker K. TGF-beta superfamily members promote survival of midbrain dopaminergic neurons and protect them against MPP+ toxicity. The EMBO journal 1995;14(4):736–42.

Kritzenberger M, Junglas B, Framme C, Helbig H, Gabel V-P, Fuchshofer R, et al. Different collagen types define two types of idiopathic epiretinal membranes. Histopathology 2011;58(6):953–65.

La Vail, M. M., Gorrin GM, Repaci MA, Thomas LA, Ginsberg HM. Genetic regulation of light damage to photoreceptors. Investigative Ophthalmology & Visual Science 1987;28(7):1043–8.

La Vail, Matthew M., Gorrin GM, Repaci MA. Strain differences in sensitivity to light-induced photoreceptor degeneration in albino mice. Current Eye Research 1987;6(6):825–34.

LaVail MM, Yasumura D, Matthes MT, Lau-Villacorta C, Unoki K, Sung CH, et al. Protection of mouse photoreceptors by survival factors in retinal degenerations. Investigative Ophthalmology & Visual Science 1998;39(3):592–602.

Le Y-Z, Zheng L, Zheng W, Ash JD, Agbaga M-P, Zhu M, et al. Mouse opsin promoter-directed Cre recombinase expression in transgenic mice. Molecular Vision 2006;12:389–98.

Li S, Chen D, Sauvé Y, McCandless J, Chen Y-J, Chen C-K. Rhodopsin-iCre transgenic mouse line for Cre-mediated rod-specific gene targeting. Genesis 2005;41(2):73–80.

Li ZY, Possin DE, Milam AH. Histopathology of bone spicule pigmentation in retinitis pigmentosa. Ophthalmology 1995;102(5):805–16.

Life Technologies. TRIzol® Reagent. Manuals and Protocols, 2012. http://tools.lifetechnologies.com/content/sfs/manuals/trizol_reagent.pdf (accessed [November 07, 2016]).

Loonstra A, Vooijs M, Beverloo HB, Allak BA, van Drunen E, Kanaar R, et al. Growth inhibition and DNA damage induced by Cre recombinase in mammalian cells. Proceedings of the National Academy of Sciences 2001;98(16):9209–14.

Macias-Silva M, Abdollah S, Hoodless PA, Pirone R, Attisano L, Wrana JL. MADR2 is a substrate of the TGFβ receptor and its phosphorylation is required for nuclear accumulation and signaling. Cell 1996;87(7):1215–24.

Magalhães MM, Coimbra A. The rabbit retina Müller cell. A fine structural and cytochemical study. Journal of Ultrastructure Research 1972;39(3):310–26.

Malumbres M, Barbacid M. RAS oncogenes: the first 30 years. Nature Reviews Cancer 2003;3(6):459–65.

Marquardt T, Ashery-Padan R, Andrejewski N, Scardigli R, Guillemot F, Gruss P. Pax6 Is Required for the Multipotent State of Retinal Progenitor Cells. Cell 2001;105(1):43–55.

Masland RH. The Neuronal Organization of the Retina. Neuron 2012;76(2):266–80.

Massagué J. TGF-ß signal transduction. Annual Review of Biochemistry 1998;67:753–91.

Massagué J. How cells read TGF-ß signals. Nature Reviews Molecular Cell Biology 2000;1(3):169–78.

Massagué J. TGFß signalling in context. Nature Reviews Molecular Cell Biology 2012;13(10):616–30.

Mescher AL. The Eye and Ear: Special Sense Organs: Eyes: The Photoreceptor System. In: Mescher, Anthony L., Junqueira, Luiz Carlos Uchôa, editor. Junqueira's basic histology: Text & atlas. New York: McGraw-Hill Medical; 2010. p. 412–424.

Mescher, Anthony L., Junqueira, Luiz Carlos Uchôa, editor. Junqueira's basic histology: Text & atlas. 12th ed. New York: McGraw-Hill Medical; 2010.

Montoliu L, Chávez S, Vidal M. Variegation associated with lacZ in transgenic animals: a warning note. Transgenic Research 2000;9(3):237–9.

Morrow EM, Furukawa T, Cepko CL. Vertebrate photoreceptor cell development and disease. Trends in Cell Biology 1998;8(9):353–8.

Moses R, Claycomb WC. Ultrastructure of terminally differentiated adult rat cardiac muscle cells in culture. American Journal of Anatomy 1982;164(2):113–31.

Mullis K, Faloona F, Scharf S, Saiki R, Horn G, Erlich H. Specific Enzymatic Amplification of DNA In Vitro: The Polymerase Chain Reaction. Cold Spring Harbor Symposia on Quantitative Biology 1986;51(0):263–73.

Naash MI, Hollyfield JG, al-Ubaidi MR, Baehr W. Simulation of human autosomal dominant retinitis pigmentosa in transgenic mice expressing a mutated murine opsin gene. Proceedings of the National Academy of Sciences of the United States of America 1993;90(12):5499–503.

Nagy A. Cre recombinase: the universal reagent for genome tailoring. Genesis 2000;26(2):99–109.

Nandakumar N, Buzney S, Weiter JJ. Lipofuscin and the principles of fundus autofluorescence: a review. Seminars in Ophthalmology 2012;27(5-6):197–201.

Negoescu A, Guillermet C, Lorimier P, Brambilla E, Labat-Moleur F. Importance of DNA fragmentation in apoptosis with regard to TUNEL specificity. Biomedicine & Pharmacotherapy 1998;52(6):252–8.

Negoescu A, Lorimier P, Labat-Moleur F, Drouet C, Robert C, Guillermet C, et al. In situ apoptotic cell labeling by the TUNEL method: improvement and evaluation on cell preparations. Journal of Histochemistry & Cytochemistry 1996;44(9):959–68.

Noell WK, Walker VS, Kang BS, Berman S. Retinal Damage by Light in Rats. Investigative Ophthalmology & Visual Science 1966;5(5):450–73.

Obata H, Kaji Y, Yamada H, Kato M, Tsuru T, Yamashita H. Expression of transforming growth factor-ß superfamily receptors in rat eyes. Acta Ophthalmologica Scandinavica 1999;77(2):151–6.

Olsson JE, Gordon JW, Pawlyk BS, Roof D, Hayes A, Molday RS, et al. Transgenic mice with a rhodopsin mutation (Pro23His): A mouse model of autosomal dominant retinitis pigmentosa. Neuron 1992;9(5):815–30.

Orban PC, Chui D, Marth JD. Tissue- and site-specific DNA recombination in transgenic mice. Proceedings of the National Academy of Sciences of the United States of America 1992;89(15):6861–5.

Organisciak DT, Darrow RM, Barsalou L, Kutty, R. Krishnan, Wiggert B. Circadian-Dependent Retinal Light Damage in Rats. Investigative Ophthalmology & Visual Science 2000;41(12):3694–701.

Organisciak DT, Vaughan DK. Retinal Light Damage: Mechanisms and Protection. Progress in Retinal and Eye Research 2009;29(2):113–34.

Oshima M, Oshima H, Taketo MM. TGF-ß Receptor Type II Deficiency Results in Defects of Yolk Sac Hematopoiesis and Vasculogenesis. Developmental Biology 1996;179(1):297–302.

Pascolini D, Mariotti SP. Global estimates of visual impairment: 2010. The British Journal of Ophthalmology 2012;96(5):614–8.

Pfeifer A, Brandon EP, Kootstra N, Gage FH, Verma IM. Delivery of the Cre recombinase by a self-deleting lentiviral vector: Efficient gene targeting *in vivo*. Proceedings of the National Academy of Sciences 2001;98(20):11450–5.

Prehn JHM, Backhauß C, Krieglstein J. Transforming Growth Factor-ß1 Prevents Glutamate Neurotoxicity in Rat Neocortical Cultures and Protects Mouse Neocortex from Ischemic Injury in vivo. Journal of Cerebral Blood Flow & Metabolism 1993a;13(3):521–5.

Prehn JHM, Peruchc B, Unsicker K, Krieglstein J. Isoform-Specific Effects of Transforming Growth Factors-ß on Degeneration of Primary Neuronal Cultures Induced by Cytotoxic Hypoxia or Glutamate. Journal of Neurochemistry 1993b;60(5):1665–72.

Promega. DeadEnd™ Fluorometric TUNEL System Technical Bulletin: Technical Bulletin, 2009. https://www.promega.de/~/media/files/resources/protocols/technical%20bulletins/0/deadend%20fluorometric%20tunel%20system%20protocol.pdf (accessed [November 08, 2016]).

Rapp LM, Williams TP. The role of ocular pigmentation in protecting against retinal light damage. Proceedings of a Symposium 1980;20(12):1127–31.

Rattner A, Nathans J. The genomic response to retinal disease and injury: evidence for endothelin signaling from photoreceptors to glia. The Journal of Neuroscience the Official Journal of the Society for Neuroscience 2005;25(18):4540–9.

Redmond TM, Poliakov E, Yu S, Tsai J-Y, Lu Z, Gentleman S. Mutation of key residues of RPE65 abolishes its enzymatic role as isomerohydrolase in the visual cycle. Proceedings of the National Academy of Sciences of the United States of America 2005;102(38):13658–63.

Redmond TM, Yu S, Lee E, Bok D, Hamasaki D, Chen N, et al. Rpe65 is necessary for production of 11-cis-vitamin A in the retinal visual cycle. Nature Genetics 1998;20(4):344–51.

Reh TA. The Development of the Retina. In: Ryan SJ, Schachat AP, Wilkinson CP, Hinton DR, Sadda S, Wiedemann P, editors. Retina: Elsevier Health Sciences; 2012. p. 330–341.

Remé CE, Grimm C, Hafezi F, Iseli H-P, Wenzel A. Why study rod cell death in retinal degenerations and how? Documenta Ophthalmologica 2003;106(1):25–9.

Renart J, Reiser J, Stark GR. Transfer of proteins from gels to diazobenzyloxymethyl-paper and detection with antisera: a method for studying antibody specificity and antigen structure. Proceedings of the National Academy of Sciences of the United States of America 1979;76(7):3116–20.

Richardson, K. C., Jarett L, Finke, E. H. Embedding in Epoxy Resins for Ultrathin Sectioning in Electron Microscopy. Biotechnic & Histochemistry 1960;35(6):313–23.

Roberts AB, Anzano MA, Lamb LC, Smith JM, Sporn MB. New class of transforming growth factors potentiated by epidermal growth factor: isolation from non-neoplastic tissues. Proceedings of the National Academy of Sciences 1981;78(9):5339–43.

Roberts AB, Anzano MA, Meyers CA, Wideman J, Blacher R, Pan, Yu Ching E., et al. Purification and properties of a type ß transforming growth factor from bovine kidney. Biochemistry 1983;22(25):5692–8.

Roberts AB, Sporn MB. The Transforming Growth Factor-ßs. In: Sporn M, Roberts A, editors. Peptide Growth Factors and Their Receptors I: Springer Berlin Heidelberg; 1990. p. 419–472.

Saiki R, Gelfand D, Stoffel S, Scharf S, Higuchi R, Horn G, et al. Primer-directed enzymatic amplification of DNA with a thermostable DNA polymerase. Science 1988;239(4839):487–91.

Samardzija M, Wenzel A, Aufenberg S, Thiersch M, Remé C, Grimm C. Differential role of Jak-STAT signaling in retinal degenerations. The FASEB journal 2006;20(13):2411–3.

Sanyal S, Hawkins RK. Development and degeneration of retina in rds mutant mice: effects of light on the rate of degeneration in albino and pigmented homozygous and heterozygous mutant and normal mice. Vision Research 1986;26(8):1177–85.

Saszik SM, Robson JG, Frishman LJ. The scotopic threshold response of the dark-adapted electroretinogram of the mouse. The Journal of Physiology 2002;543(3):899–916.

Sauer B, Henderson N. Site-specific DNA recombination in mammalian cells by the Cre recombinase of bacteriophage P1. Proceedings of the National Academy of Sciences of the United States of America 1988;85(14):5166–70.

Schmidt TM, Chen S-K, Hattar S. Intrinsically photosensitive retinal ganglion cells: many subtypes, diverse functions. Trends in Neurosciences 2011;34(11):572–80.

Schmidt-Erfurth U. Netzhaut, Aderhaut und Glaskörper. In: Marion Philipp, editor. Augenheilkunde. Berlin Heidelberg New York: Springer; 2007. p. 339–400.

Sekelsky JJ, Newfeld SJ, Raftery LA, Chartoff EH, Gelbart WM. Genetic Characterization and Cloning of Mothers against Dpp, a Gene Required for Decapentaplegic Function in Drosophila Melanogaster. Genetics 1995;139(3):1347–58.

Seyedin SM, Segarini PR, Rosen DM, Thompson AY, Bentz H, Graycar J. Cartilage-inducing factor-B is a unique protein structurally and functionally related to transforming growth factor-ß. Journal of Biological Chemistry 1987;262(5):1946–9.

Shi Y, Massagué J. Mechanisms of TGF-ß Signaling from Cell Membrane to the Nucleus. Cell 2003;113(6):685–700.

Shin J-Y, Fang Z-H, Yu Z-X, Wang C-E, Li S-H, Li X-J. Expression of mutant huntingtin in glial cells contributes to neuronal excitotoxicity. The Journal of Cell Biology 2005;171(6):1001–12.

Sieving PA, Murayama K, Naarendorp F. Push–pull model of the primate photopic electroretinogram: A role for hyperpolarizing neurons in shaping the b-wave. Visual Neuroscience 2009;11(3):519–32.

Silver DP, Livingston DM. Self-Excising Retroviral Vectors Encoding the Cre Recombinase Overcome Cre-Mediated Cellular Toxicity. Molecular Cell 2001;8(1):233–43.

Sobotta J. Head, Neck, Upper Limb. In: Paulsen F, Waschke J, editors. Sobotta atlas of human anatomy. Munchen: Elsevier; 2013.

Soriano P. Generalized lacZ expression with the ROSA26 Cre reporter strain. Nature Genetics 1999;21(1):70–1.

Spilsbury K, Garrett KL, Shen W-Y, Constable IJ, Rakoczy PE. Overexpression of Vascular Endothelial Growth Factor (VEGF) in the Retinal Pigment Epithelium Leads to the Development of Choroidal Neovascularization. The American Journal of Pathology 2000;157(1):135–44.

Staal SP. Molecular cloning of the akt oncogene and its human homologues AKT1 and AKT2: amplification of AKT1 in a primary human gastric adenocarcinoma. Proceedings of the National Academy of Sciences of the United States of America 1987;84(14):5034–7.

Staal SP, Hartley JW, Rowe WP. Isolation of transforming murine leukemia viruses from mice with a high incidence of spontaneous lymphoma. Proceedings of the National Academy of Sciences of the United States of America 1977;74(7):3065–7.

Steinberg RH, Fisher SK, Anderson DH. Disc morphogenesis in vertebrate photoreceptors. The Journal of Comparative Neurology 1980;190(3):501–8.

Steinberg RH, Wood I, Hogan MJ. Pigment epithelial ensheathment and phagocytosis of extrafoveal cones in human retina. Philosophical Transactions of the Royal Society of London. Series B, Biological Sciences 1977;277(958):459–74.

Sternberg N, Hamilton D. Bacteriophage P1 site-specific recombination: I. Recombination between *lox*P sites. Journal of Molecular Biology 1981;150(4):467–86.

Stockton RA, Slaughter MM. B-wave of the electroretinogram. A reflection of ON bipolar cell activity. The Journal of General Physiology 1989;93(1):101–22.

Strauss O. The retinal pigment epithelium in visual function. Physiological Reviews 2005;85(3):845–81.

Taketo M, Schroeder AC, Mobraaten LE, Gunning KB, Hanten G, Fox RR, et al. FVB/N: an inbred mouse strain preferable for transgenic analyses. Proceedings of the National Academy of Sciences 1991;88(6):2065–9.

Tanito M, Kaidzu S, Ohira A, Anderson RE. Topography of retinal damage in light-exposed albino rats. Experimental Eye Research 2008;87(3):292–5.

Tian N, Slaughter MM. Correlation of dynamic responses in the ON bipolar neuron and the b-wave of the electroretinogram. Vision Research 1995;35(10):1359–64.

Towbin H, Staehelin T, Gordon J. Electrophoretic transfer of proteins from polyacrylamide gels to nitrocellulose sheets: procedure and some applications. Proceedings of the National Academy of Sciences of the United States of America 1979;76(9):4350–4.

Trepel M. Sinnesorgane: Auge. In: Trepel M, editor. Neuroanatomie: Struktur und Funktion. München: Urban & Fischer in Elsevier; 2012. p. 315–330.

Turner DL, Cepko CL. A common progenitor for neurons and glia persists in rat retina late in development. Nature 1987;328(6126):131–6.

Tyor WR, Avgeropoulos N, Ohlandt G, Hogan EL. Treatment of spinal cord impact injury in the rat with transforming growth factor-ß. Journal of the Neurological Sciences 2002;200(1–2):33–41.

Vosberg H-P. The polymerase chain reaction: an improved method for the analysis of nucleic acids. Human Genetics 1989;83(1):1–15.

Walshe TE, Saint-Geniez M, Maharaj ASR, Sekiyama E, Maldonado AE, D'Amore PA. TGF-ß Is Required for Vascular Barrier Function, Endothelial Survival and Homeostasis of the Adult Microvasculature. PloS ONE 2009;4(4):1–16.

Wang M, Lam TT, Tso MO, Naash MI. Expression of a mutant opsin gene increases the susceptibility of the retina to light damage. Visual Neuroscience 1997;14(1):55–62.

Welsch U, editor. Atlas Histologie: Zytologie, Histologie, mikroskopische Anatomie ; 15 Tabellen. 7th ed. München, Jena: Elsevier, Urban und Fischer; 2005.

Welsch U, Deller T. Sinnesorgane. In: Welsch U, editor. Lehrbuch Histologie. München: Elsevier, Urban & Fischer; 2010. p. 485–530.

Wenzel A, Grimm C, Samardzija M, Remé CE. The Genetic Modifier *Rpe65Leu* $_{450}$: Effect on Light Damage Susceptibility in c-*Fos*-Deficient Mice. Investigative Ophthalmology & Visual Science 2003;44(6):2798–802.

Wenzel A, Grimm C, Samardzija M, Remé CE. Molecular mechanisms of light-induced photoreceptor apoptosis and neuroprotection for retinal degeneration. Progress in Retinal and Eye Research 2005;24(2):275–306.

Wenzel A, Remé CE, Williams TP, Hafezi F, Grimm C. The Rpe65 Leu450Met Variation Increases Retinal Resistance Against Light-Induced Degeneration by Slowing Rhodopsin Regeneration. The Journal of Neuroscience 2001;21(1):53–8.

White MP, Fisher LJ. Degree of light damage to the retina varies with time of day of bright light exposure. Physiology & Behavior 1987;39(5):607–13.

Wickham H. ggplot2: Elegant Graphics for Data Analysis. New York, NY: Springer; 2009.

Wilkes MC, Mitchell H, Penheiter SG, Doré JJ, Suzuki K, Edens M, et al. Transforming Growth Factor-ß Activation of Phosphatidylinositol 3-Kinase Is Independent of Smad2 and Smad3 and Regulates Fibroblast Responses via p21-Activated Kinase-2. Cancer Research 2005;65(22):10431–40.

Wolpert K, Tsang S. Electroretinography. In: Belusic G, editor. Electroretinograms: InTech; 2011.

Wrana JL, Attisano L, Carcamo J, Zentella A, Doody J, Laiho M, et al. TGFß signals through a heteromeric protein kinase receptor complex. Cell 1992;71(6):1003–14.

Wrana JL, Attisano L, Wieser R, Ventura F, Massagué J. Mechanism of activation of the TGF-ß receptor. Nature 1994;370(6488):341–7.

Wu MY, Hill CS. TGF-ß superfamily signaling in embryonic development and homeostasis. Developmental Cell 2009;16(3):329–43.

Wyllie AH. Glucocorticoid-induced thymocyte apoptosis is associated with endogenous endonuclease activation. Nature 1980;284(5756):555–6.

Wyllie AH, Kerr J, Currie AR. Cell Death: The Significance of Apoptosis. In: Bourne GH, Danielli JF, Jeon KW, editors. International Review of Cytology: Academic Press; 1980. p. 251–306.

Wyllie AH, Morris RG, Smith AL, Dunlop D. Chromatin cleavage in apoptosis: association with condensed chromatin morphology and dependence on macromolecular synthesis. The Journal of Pathology 1984;142(1):67–77.

Yan X, Liu Z, Chen Y. Regulation of TGF-ß signaling by Smad7. Acta Biochimica et Biophysica Sinica 2009;41(4):263–72.

Yi JY, Shin I, Arteaga CL. Type I Transforming Growth Factor ß Receptor Binds to and Activates Phosphatidylinositol 3-Kinase. Journal of Biological Chemistry 2005;280(11):10870–6.

Young RW. The renewal of photoreceptor cell outer segments. The Journal of Cell Biology 1967;33(1):61–72.

Young RW. Passage of newly formed protein through the connecting cilium of retinal rods in the frog. Journal of Ultrastructure Research 1968;23(5-6):462–73.

Young RW. Participation of the retinal pigment epithelium in the rod outer segment renwal process. The Journal of Cell Biology 1969;42(2):392–403.

Young RW. Shedding of discs from rod outer segments in the rhesus monkey. Journal of Ultrastructure Research 1971;34(1-2):190–203.

Young RW. Cell death during differentiation of the retina in the mouse. The Journal of Comparative Neurology 1984;229(3):362–73.

Zeng H-y, Zhu X-a, Zhang C, Yang L-P, Wu L-m, Tso MOM. Identification of Sequential Events and Factors Associated with Microglial Activation, Migration, and Cytotoxicity in Retinal Degeneration in rd Mice. Investigative Ophthalmology & Visual Science 2005;46(8):2992–9.

Zhang YE. Non-Smad pathways in TGF-ß signaling. Cell Res 2009;19(1):128–39.

Zhu Y, Culmsee C, Klumpp S, Krieglstein J. Neuroprotection by transforming growth factor-ß1 involves activation of nuclear factor-κB through phosphatidylinositol-3-OH kinase/Akt and mitogen-activated protein kinase-extracellular-signal regulated kinase1,2 signaling pathways. Neuroscience 2004;123(4):897–906.

# Figure and Table Legend

## Figure Legend

## Table Legend

# Danksagung

Prof. Dr. med. Ernst Tamm möchte ich dafür danken, dass er mir die Durchführung dieses Projekts an seinem Lehrstuhl ermöglicht hat. Außerdem habe ich ihm meine Faszination für die Anatomie zu verdanken.

Bei Frau PD Dr. med., Dr. rer. nat. Barbara Braunger bedanke ich mich für die Ehre, in ihrer Arbeitsgruppe an meinem Dissertationsthema geforscht haben zu dürfen, für die tollste Betreuung, die ich mir vorstellen kann, und für die stets wirkungsvollen Worte der Motivation. Du hast mir nicht nur den Zugang zur Wissenschaft ermöglicht, sondern auch meine Begeisterung für die Forschung und die Augenheilkunde entfacht. Für deine Freundschaft kann ich mich an dieser Stelle nicht ausreichend bedanken, liebe Barbara!

Prof. Dr. med. Frank Schweda danke ich für die freundliche Übernahme des Zweitgutachtens.

Elke Stauber, Angelika Pach, Margit Schimmel und Silvia Babl danke ich für die immense Geduld und die unentbehrliche Unterstützung im Laboralltag.

Ebenso möchte ich mich bei allen restlichen Kollegen am Lehrstuhl für die nette Zusammenarbeit bedanken. PD Dr. med. Andreas Ohlmann und Dr. rer. nat. Marcus Koch danke ich für die Diskussionsbereitschaft und die hilfreichen Ratschläge.

Ein ganz besonderer Dank geht an meine Schicksalsgenossen Tatjana Groß und Anja Schlecht, die mit mir das Laborleben und vieles andere geteilt haben. Bei Sebastian Koschade bedanke ich mich für seine immerwährende Hilfsbereitschaft und Unterstützung in technischen Fragen.

Meinen Eltern und meiner Schwester kann ich mit Worten gar nicht genug danken. Jeden Erfolg in meinem Leben habe ich euch zu verdanken! Ohne euch hätte ich das alles nie geschafft! Meinem Freund Dennis danke ich, dass er mich bekocht, ausgehalten, unverzichtbar unterstützt, aufgeheitert und an mich geglaubt hat.

Danke schön!

# Erklärung

Ich erkläre hiermit, dass ich die vorliegende Arbeit ohne unzulässige Hilfe Dritter und ohne Benutzung anderer als der angegebenen Hilfsmittel angefertigt habe. Die aus anderen Quellen direkt oder indirekt übernommenen Daten und Konzepte sind unter Angabe der Quelle gekennzeichnet. Insbesondere habe ich nicht die entgeltliche Hilfe von Vermittlungs- bzw. Beratungsdiensten (Promotionsberater oder andere Personen) in Anspruch genommen. Niemand hat von mir unmittelbar oder mittelbar geldwerte Leistungen für Arbeit erhalten, die im Zusammenhang mit dem Inhalt der vorgelegten Dissertation stehen. Die Arbeit wurde bisher weder im In- noch im Ausland in gleicher oder ähnlicher Form einer anderen Prüfungsbehörde vorgelegt.

Regensburg, ……. …….

Unterschrift